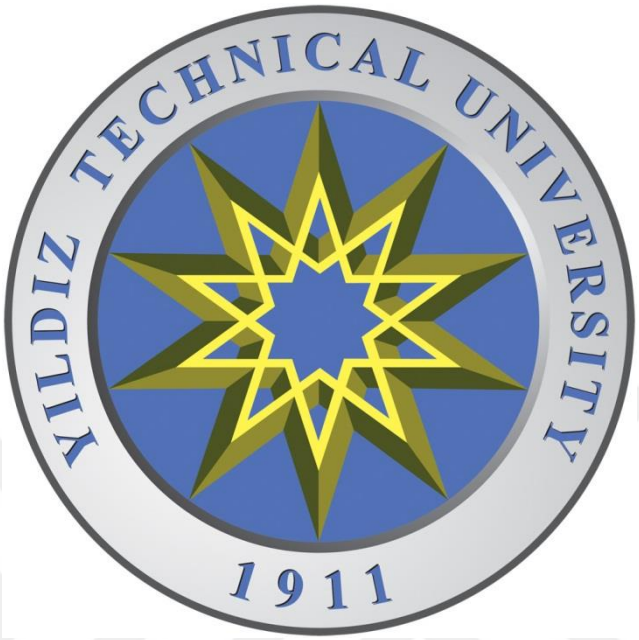

GRADUATE SCHOOL OF NATURAL AND APPLIED SCIENCES

SEPTEMBER, 2017

REPUBLIC OF TURKEY
YILDIZ TECHNICAL UNIVERSITY
GRADUATE SCHOOL OF NATURAL AND APPLIED SCIENCES

BIOACTIVITY TEST AND CELL STUDIES OF BIOCERAMICS PRODUCED FROM *CLINOCARDIUM CILIATUM* AND *TURRITELLA TEREBRA*

ZEYNEP ORMAN

MSc. THESIS
DEPARTMENT OF BIOENGINEERING

ADVISER
PROF. DR. SEVİL YÜCEL

CO-ADVISER
ASSOC. PROF. YEŞİM MÜGE ŞAHİN

İSTANBUL, 2017

REPUBLIC OF TURKEY

YILDIZ TECHNICAL UNIVERSITY

GRADUATE SCHOOL OF NATURAL AND APPLIED SCIENCES

BIOACTIVITY TEST AND CELL STUDIES OF BIOCERAMICS PRODUCED FROM *CLINOCARDIUM CILIATUM* AND *TURRITELLA TEREBRA*

A thesis submitted by Zeynep ORMAN in partial fulfillment of the requirements for the degree of **MASTER OF SCIENCE** is approved by the committee on 09.11.2017 in Department of Bioengineering, Bioengineering Program.

Thesis Adviser

Prof. Dr. Sevil YÜCEL

Yildiz Technical University

Co-Adviser

Assoc. Prof. Dr. Yeşim Müge ŞAHİN

Istanbul Arel University

Approved By the Examining Committee

Prof. Dr. Sevil YÜCEL

Yildiz Technical University _____

Assoc. Prof. Cem Bülent ÜSTÜNDAĞ

Yildiz Technical University _____

Prof. Dr. Faik Nüzhet OKTAR

Marmara University _____

This project was supported by Yildiz Technical University Projects Office. (Project No: FYL-2017-3119).

ACKNOWLEDGEMENTS

I would like to express my sincere gratitude to my thesis adviser Prof. Dr. Sevil YÜCEL for her support of my master study and related research and for her patience, motivation and knowledge. Prof. YÜCEL opened her office and laboratory to help with my researches and she was always very understanding in spite of all of the occupations. It was great pleasure and honor to work with her.

My sincere thanks also go to my thesis co-advisor Assoc. Prof. Yeşim Müge ŞAHİN for her advices and support in need.

I would also like to thank to Prof. Dr. Faik N. OKTAR for introducing me to this project, ensuring the materials for this work, and his help and advice throughout this work.

I would also like to thank to my entire friends that have worked with me in the Lipid and Biocomposite Laboratory and special thanks to Burcu KARAKUZU and Alican ÖZARSLAN for their great help with respect of determination of next steps in this research.
I would like to thank to specialist Melih Beşir ARVAS for SEM analysis.
Finally I would like to thank my mother Sümeyye ORMAN, my father İsmail ORMAN and my friend Burcu ÖZKAN for their support and continuous encouragement throughout my years of study and through the process of researching and writing this thesis.

November, 2017

Zeynep ORMAN

TABLE OF CONTENTS

Page

LIST OF SYMBOLS

μ	Micron
ml	Milliliter
μL	Microliter
J/m^2	Surface energy unit
N/m^2	Surface tension unit
°C	Celsius
g	Gram
mM	Milimolar
cm^{-1}	Wavenumber unit
λ	Wavenumber
2θ	Range of Diffraction Numbers
h	Hour

LIST OF ABBREVIATIONS

DTA/TGA	Differential thermal analyzes / Thermal gravity analyzes
EDX	Energy dispersive X-ray
FA	Fluoroapatite
FT-IR	Fourier transform infrared spectroscopy
HA	Hydroxyapatite
HCA	Hydroxycarbonapatite
JCPDS	Joint Committee on Powder Diffraction Standards
SBF	Simulated Body Fluid
SEM	Scanning Electron Microscopy
MTT	[3-(4,5-dimethylthiazol-2-yl)-2,5-diphenyltetrazolium bromide]
TCP	Tri-calcium phosphate
XRD	X-ray Diffraction
YTU	Yildiz Technical University

LIST OF FIGURES

Page

LIST OF TABLES

Page

ABSTRACT

BIOACTIVITY TEST AND CELL STUDIES OF BIOCERAMICS PRODUCED FROM *CLINOCARDIUM CILIATUM* AND *TURRITELLA TEREBRA*

Zeynep Orman

Department of Bioengineering

MSc. Thesis

Adviser: Prof. Dr. Sevil Yücel

Co-adviser: Assoc. Prof. Yeşim Müge Şahin

Hydroxyapatite and tricalcium phosphate are used in field of drug delivery and bone regeneration due to their high biocompability behaviours. Hydroxyapatite was examined since it is dispersed in a organic matrix of composite structure of bone. Hydroxyapatite and TCP have the ability to accelarate bone growth around the implant. Highly porous TCP exhibits excellent behaviour as bone implant since it dissolves after replaced by bone. Natural bioceramics can be obtained from different sources such as bone and sea shells. Most of marine structures contains calcium carbonate (calcite or aragonite) and they can be easily converted to bioceramic material.

In this study calcium phosphate nanoceramics were obtained via mechanochemical method using the sea shell *Clinocardium ciliatum* and sea snail *Turritella Terebra* as a calcium source. The characteristics of the calcium phosphate ceramics that produced from two different sources were studied in two different sintering temperature: 1000 °C and 1200 °C. The characterization of the produced materials were carried out via FT-IR, SEM, BET, XRD analysis. Biodegradability test in TRIS solution and bioactivity tests were performed for the produced materials. Fast hydroxyapatite formation occurred when the materials were immersed in simulated body fluid and proliferation of cells in cytotoxicity test was registered. As a result, hydroxyapatite, β-TCP and α-TCP were produced and their biodegradability and bioactivity behaviors were determined.

Keywords: Bioceramic material, bone regeneration, hydroxyapatite, tricalcium phosphate.

ÖZET

CLINOCARDIUM CILIATUM VE *TURRITELLA TEREBRA*'DAN ÜRETİLEN BİYOSERAMİKLERİN BİYOAKTİVİTE TESTİ VE HÜCRE ÇALIŞMALARI

Zeynep Orman

Biyomühendislik Anabilim Dalı

Yüksek Lisans Tezi

Tez Danışmanı: Prof. Dr. Sevil Yücel

Eşdanışmanı: Yrd. Doç. Dr. Yeşim Müge Şahin

Hidroksiapatit ve trikalsiyum fosfat yüksek biyouyumluluk özellikleri sayesinde ilaç salınımı ve kemik rejenerasyonu alanında kullanılırlar. Hidroksiapatit kemiğin kompozit bileşiminde organik matrikse dağılmış olarak bulunması sebebiyle araştırılmaktadır. Hidroksiapatit ve TCP implant etrafında kemik büyümesini hızlandırma yeteneğine sahiptir. Yüksek oranda gözenekli TCP, kemiğin yerini aldıktan sonra çözünmesi nedeniyle kemik implantı olarak mükemmel davranış gösterir. Doğal bioseramikler, kemik ve deniz kabukları gibi farklı kaynaklardan elde edilebilir. Deniz kaynaklarının çoğunda kalsiyum karbonat (kalsit veya aragonit) bulunur ve kolayca biyoseramik malzemeye dönüştürülebilirler.

Bu çalışmada kalsiyum fosfat nanoseramikleri, deniz kabuğu *Clinocardium ciliatum* ve deniz salyangozu *Turritella Terebra*'yı kalsiyum kaynağı olarak kullanılarak mekanokimyasal yöntemle elde edildi. İki farklı kaynaktan üretilen kalsiyum fosfat seramikleri 1000 °C ve 1200 °C olmak üzere iki farklı sinterleme sıcaklığında incelenmiştir. Üretilen malzemelerin karakterizasyonu FT-IR, SEM, BET, XRD analizi ile gerçekleştirildi. Üretilen malzemeler için TRIS çözeltisinde biyobozunabilirlik testi ve biyoaktivite testleri yapıldı. Malzemeler yapay vücut sıvısına daldırıldığında hızlı hidroksiapatit oluşumu ve sitotoksisite testlerinde hücrelerin çoğalması kaydedilmiştir. Sonuç olarak, hidroksiapatit, β-TCP ve α-TCP üretildi ve biyobozunurluk ve biyoaktivite davranışları belirlendi.

Anahtar Kelimeler: Biyoseramik malzeme, kemik rejenerasyonu, hidroksiapatit, trikalsiyum fosfat.

CHAPTER 1

INTRODUCTION

1.1 Literature Review

Bone diseases and disabilities such as joint pathologies, fractures related to osteoporosis affect many people worldwide. These problems currently are treated with bone grafts, in particular autografts and allografts or on replacement with prostheses and fixation devices using metal, polymer and ceramic material systems. Nowadays a variety of fast-resorbing, slow-resorbing and injectable ceramics have found their place in promoting bone healing in the clinical practice. Most used ceramics in orthopedic surgery and traumatology as bone tissue substitutes are mainly calcium phosphate ceramics such as hydroxyapatite, tricalcium phosphate (TCP), and certain bioglasses and glass-ceramics due to their osteoconductivity properties.

Calcium phosphate ceramics are biocompatible and biodegradable biomaterials that can be in different combinations. Calcium phosphate ceramics such as hydroxyapatite and TCP are used for metallic implants coatings for bone grafts, drug delivery and bone regeneration. Hydroxyapatite is very attractive calcium apatite since it is in the bone itself. It is highly bioactive and biocompatible with bone and it helps to bone growth surrounding of the implant. Calcium phosphate ceramics have various advantages such as their resistance to corrosion, low electrical and thermal conductivity and high compressive strength. Calcium phosphate ceramics are used as bone filler material in the repair of bone fractures, cracks or defects by forming hydroxyapatite layer between implant and surrounding tissue. Clinical applications require various shapes of bioceramics from thin films and nano-sized powders to porous or dense bodies.

Calcium phosphate ceramics can be obtained from different resources. In this study, Sea shell *Clinocardium ciliatum* and sea snail *Turritella terebra* were used as a source of calcium and converted to calcium phosphate apatites by mechanochemical method. In

the literature various sea shells, sea snails and different natural resources were used as a source of calcium and converted to calcium phosphate via different methods. Among these methods mechanochemical method takes attention due to it is economical and easy method to obtain calcium apatites.

1.2 Objective of the Thesis

In this study, sea shell *Clinocardium ciliatum* and sea snail *Turritella terebra* were used as a source of calcium to form calcium phosphate ceramic. Their conversion to calcium phosphate apatites by mechanochemical method and investigation of their physical, bioactivity and biodegradation properties are aimed.

1.3 Hypothesis

Sea shell *Clinocardium ciliatum* and sea snail *Turritella terebra* can be reliable source to form calcium apatite ceramics. Produced calcium phosphate ceramics can perform bioactivity properties.

CHAPTER 2

GENERAL INFORMATION

2.1 The Structure and Mechanical Properties of Bone

Bone contains 60–70% w/w of calcium phosphate mineral, ~20–30% w/w of organic matrix and 10% of water. Also there are negative ions such as citrate, carbonate, fluoride and hydroxyl in the bone. Bone structure protects and supports the human body and produce white and red blood cells and minerals. Collagen protein provides toughness while calcium phosphate provides the elasticity to tissue [1]. The structure of the bone is shown in the Figure 2.1 and Figure 2.2.

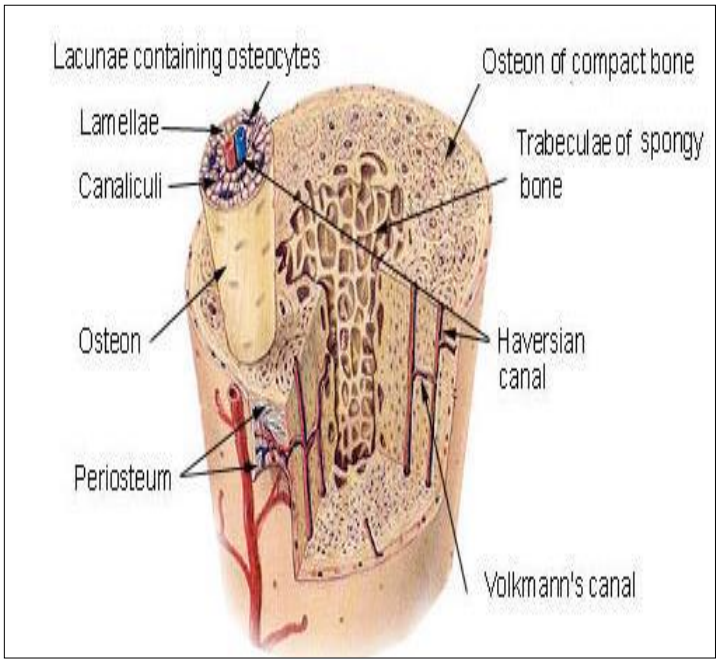

Figure 2.1 Structure of the bone

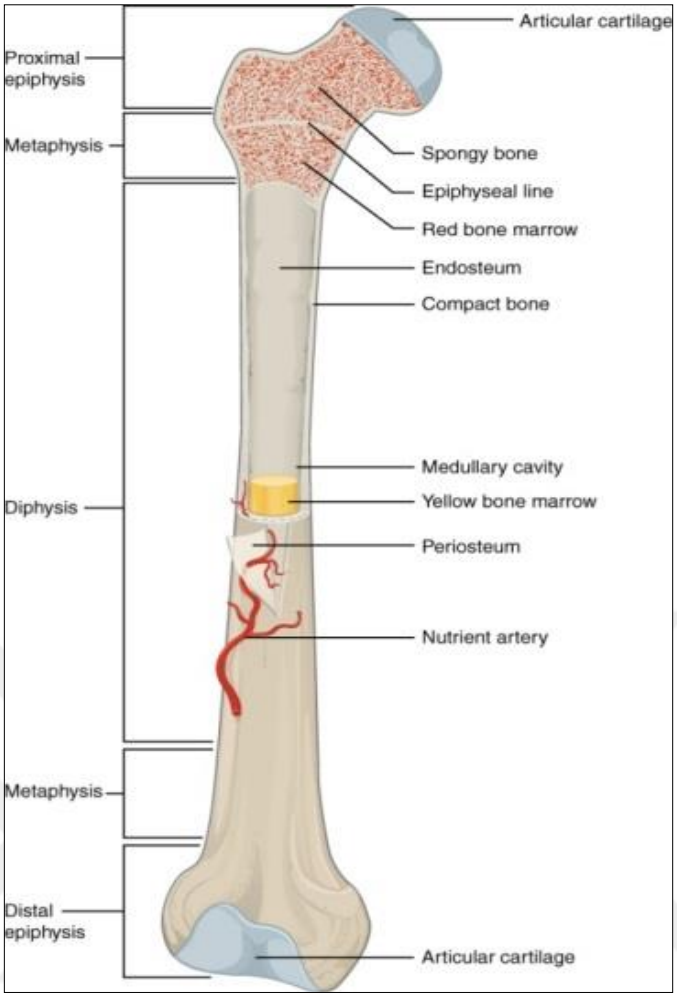

Figure 2.2 Structure of long bone [2]

The organic material of the bone is 90% of w-w mass collagen type I and there are other organic materials such as non-collagenous proteins and glycoproteins. These organic components have different functions. For instance, bone sialoprotein and bone morphogenetic protein controls the mineralization and glycoprotein has a role in determining apatite nucleation sites [1].

The inorganic material of the bone is hydroxyapatite and its crystals are impure. In particular about 4–6% of carbonate replaces the phosphate, making the mineral more of a carbonate apatite. The shape of the crystals varies in different tissues. The crystals are about 40 nm wide and sometimes their size is less than 5 nm [5].

Osteoblasts and osteoclasts take role in bone formation. They are distributed on bone surfaces and within bone narrow. Osteoblasts are basophilic, cubical cells have roles in producing bone matrix and arranging bone mineralization. They are also responsible for

synthesis of type 1 collagen, glycosaminoglycan, alkaline phosphatase, and phosphoprotein (osteonectin).

Bone reconstruction is a process that osteon bone mineral is produced and after microdamage is repaired. Typical characteristic of hard tissues in natural bone are the haversian lamellae, which are composed of columnar osteons and it is connected into a concentric circle shape around a central axis. Fabricating artificial bone and imitating natural bone is difficult due to this complex microstructure of natural bone. Latest researches focused on producing and improvement of critical-sized defect sites however using artificial bone within load-bearing region or replacing a whole bone is challenging. Researches focused on imitating human bone and fabricating HA/collagen composites [3], [4].

Stem cells are examined to produce artificial bone as a new method however the robustness of the bone and the load-bearing ability is still on the research. A combination of sponge replica and electrospinning method addressed the unidirectional structure and cortical trabecular combined approach, but this too was devoid of significant load-bearing ability and scope for further improvement [5].

2.2 Biomaterials

Biomaterial is a material can be used for part of the body as augment or replacement of tissue, organ or any function and it can be synthetic or natural in origin. In other words they are biocompatible materials that are designed to restore, replace and heal the any tissue, organ or function of the body. Through the history metal, polymer and ceramic materials and their combinations have been used as biomaterials [6]. For instance, ceramics such as alumina and zirconia are used in dental applications and used as heads and inserts of hip joint prostheses due to their resistance to corrosion. Metals such as stainless steel, cobalt-chrome alloys and titanium are used for dental implants, hip and knee joint prostheses. Polymers such as ultra-high-molecular-weight polyethylene (UHMW PE) and polymethylmethacrylate (PMMA) found application in acetabular cups, patellar prostheses, and as cements for fixing hip and joint prostheses and fillers in dentistry [7].

In biomaterial study, main object is to obtain a material that can be used in bone treatment. Calcium phosphate ceramic materials attract special interest due to their

bioactive and biocompatible properties in biomaterials. They are mostly used in order to replace diseased or damaged parts [8].

Through the years biomaterials were used in different medical applications. For instance:

- Joint replacements
- Bone plates
- Bone cement
- Artificial ligaments and tendons
- Dental implants for tooth fixation
- Blood vessel prostheses
- Heart valves
- Skin repair devices
- Cochlear replacements
- Contact lenses [9]

Furthermore they were applied in different fields such as wastewater treatment, biosensors, immobilization of bioactive materials. Figure 2.2 shows the applications of biomaterials in the human body [10].

Properties of biomaterials can be considered from different aspects including optimal nutrient and waste transport, delivery of bioactive molecules, material degradation rate, cell-recognizable surface chemistry, mechanical unity, and the ability to promote signal transduction pathways. These properties are important due to they can eventually dictate cell adherence, nutrient/waste transport, cell differentiation, cell viability, matrix synthesis and organization. Most of the biomaterials can be chemically or physically modified to control all these important parameters, and a variety of synthetic and natural materials have been used for investigating biomaterials behavior by specifically manipulating these properties [11].

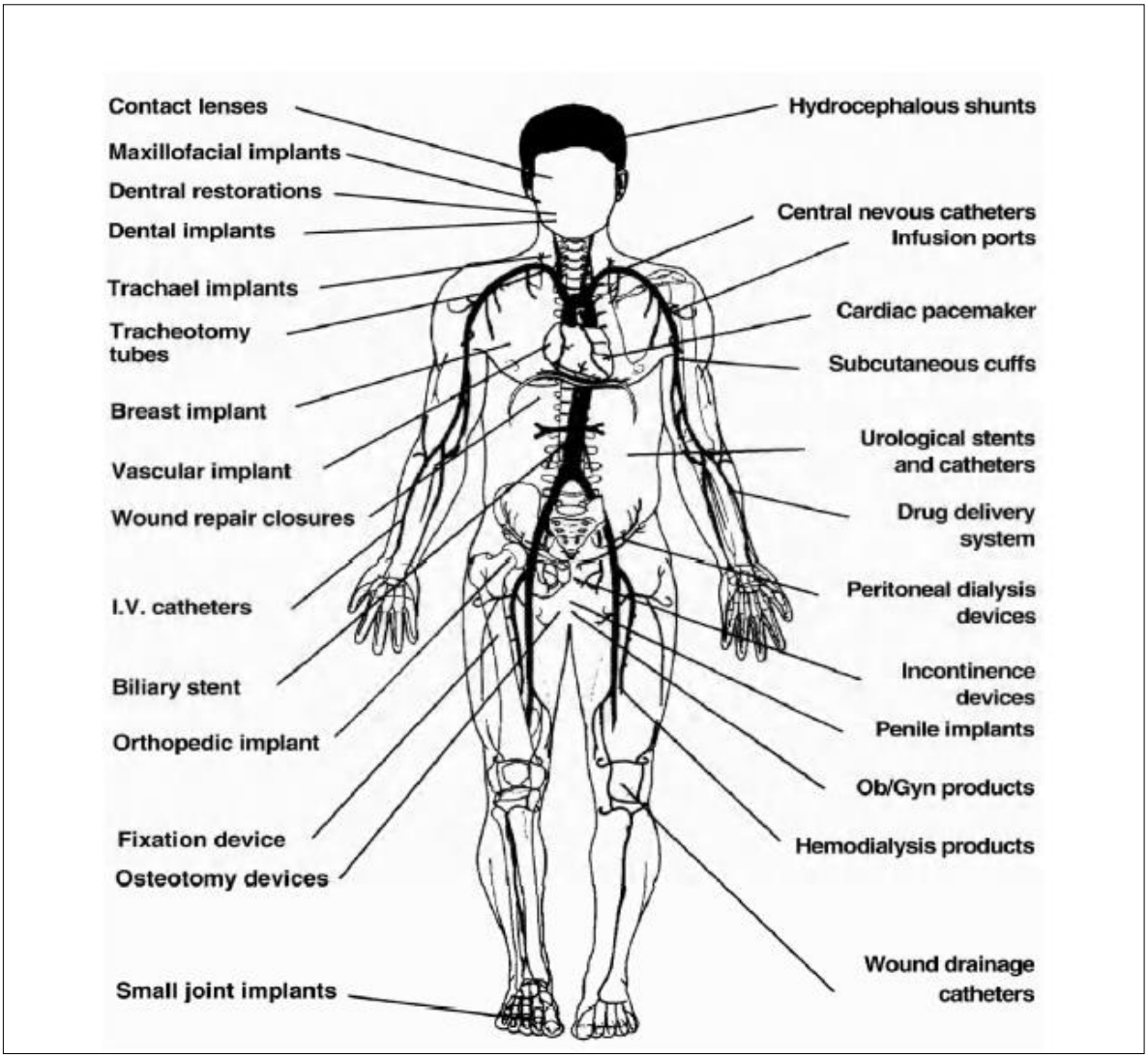

Figure 2.3 Applications of biomaterials in the human body [12]

2.2.1 Properties of Biomaterials

Biomaterials should have some properties in order to integrate with human body for a long-term usage without causing any toxic or allergic reaction with the tissue. They should be selected considering the following properties:

- Biocompatibility
- Biofunctionality
- Toxicology
- Appropriate design and manufacturability
- Mechanical properties of biomaterials
- High corrosion resistance
- High wear resistance

- Long fatigue life
- Adequate strength
- Modulus equivalent to bone

Biocompatibility

Biocompability is compability with the living systems which means ability of material to exist in the contact with tissue without damaging the body [13]. The material should not be toxic and cause any adverse reactions with body. It should be non-carcinogenic, non-pyrogenic, non-toxic, non-allergenic, blood compatible, noninflammatory [14].

Biofunctionality

Biofunctionality means that function of the material should perform with the tissue and the design of the material should provide:

- Load transmission and stress distribution (e.g. bone replacement)
- Articulation to allow movement (e.g. artificial knee joint)
- Control of blood and fluid flow (e.g. artificial heart)
- Space filling (e.g. cosmetic surgery)
- Electrical stimuli (e.g. pacemaker)
- Light transmission (e.g. implanted lenses)
- Sound transmission (e.g. cochlear implant) [15]

Toxicology

Toxicology is related to ions that cause negative results in body. There should not be any mass decreasing unless the biomaterial is designed for drug releasing applications [15].

Appropriate Design and Manufacturability

Biomaterials should be easy to process to be qualified for the required application [15].

Mechanical Properties of Biomaterials

Mechanical properties such as tensile strength, yield strength, elastic modulus, corrosion and fatigue resistance, surface quality, creep, and hardness of biomaterials should provide the conditions of targeted body application. Properties such as brittleness and

optical properties of intraocular lenses or permeability of dialysis membranes should be optimized [15].

High corrosion resistance

Corrosion resistance of biomaterial is important since body fluid is corrosive and implants should be resistant enough to be stable with body fluid. Low corrosion resistant implants can release metal ions and this may decrease the lifetime of the implant and need additional operation. Furthermore metal ions cause toxical effect in the body and decrease the life-time of the body because the metal ions accumulate in different areas in the body [16].

High wear resistance

The low wear resistance can cause implant loosening. Wear parts can interact with the bone and can be inflammatory and toxic. Friction can result corrosion and it can lead to release of metallic ions. Also mechanical loading can cause corrosion of implant which results of wear [17].

Long fatigue life

Fatigue strength can result implant loosening or implant failure and it is mostly associated with hip prostheses. The microstructures of metal biomaterials is affective in fatigue characteristics [18].

Adequate Strength

Adequate strength is important because when it is less than required amount, the bone implant inner face develops a new fibrous tissue and it can result pain due to relative motion between the implant and the bone and it leads to implant replacement [17].

Modulus equivalent to that of bone

Implant and the interacted bone should have close young modulus otherwise the large difference of Young modulus can weaken the natural bone and result of implant loosening and eventually failure of the implant [19], [20].

2.2.2 Classification of Biomaterials

Biomaterials can be classified based on tissue-implant interaction, tissue or body part they are used in, type of the material they are produced from, material source they are

produced from, type of the problem they are used for and there are other classifications are suggested [21].

Biomaterials are classified based on tissue-implant interaction as bioinert, bioactive, bioresorbable materials. Bioinert material refers to a material that does not interact with its surrounding tissue and usually tissue forms a fibrous capsule around the material. For instance stainless steel, titanium, alumina, partially stabilized zirconia, and ultra-high molecular weight polyethylene are bioinert materials. Bioactive material refers to material that interact with its surrounding tissue when it is implanted to body part and generally it results in the formation of carbonate apatite (CHA) on the implant due to ion exchange between the implant and surrounding body fluid. Bioglass® and synthetic hydroxyapatite are most common bioactive materials. Biodegradable material refers to a material that slowly dissolves and is resorbed from body and replaced by surrounding tissue. Tricalcium phosphate and polylactic–polyglycolic acid copolymers are biodegradable materials.

Classification based on material source is natural and synthetic materials. Natural sources are autograft, allograft, xenograft, isografts.

Autograft is tissue transplanted from another part of the body of the same individual, *Allograft* is transplation from a donor of the same species,

Xenograft is transplation from a donor of a different species,

Isograft is transplation from an identical twin [22].

Biomaterials can be investigated based on the material that is produced from in four classifications. These are:

- Metallic biomaterials
- Polymeric biomaterials
- Composite biomaterials
- Ceramic biomaterials

CHAPTER 3

CERAMIC BIOMATERIALS

Ceramic biomaterials used for the repair and remodeling of diseased or damaged parts of the musculo-skeletal system, termed bioceramics, may be bioinert such as alumina and zirconia), bioactive such as hydroxyapatite, bioactive glasses, and glass-ceramics, resorbable such as tricalcium phosphate, or porous for tissue ingrowth such as hydroxyapatite-coated metals [23].

Alumina and zirconia have been successfully used since 1960s in orthopedic and dental applications. They show high hardness, low friction coefficient and corrosion resistance properties and while they are under load, microstructures are controlled to inhibit static fatigue and slow crack growth.

Calcium phosphate bioceramics take attention due to their bioactivity and biocompability behaviors in the body. Hydroxyapatite, tricalcium phosphate, bioglass, octacalcium phosphate are most common calcium phosphates. They are suggested to use as an alternative or additive to autogenous bone for orthopedics and dental applications, scaffolds for tissue engineering, vectors for gene therapy, and as a drug delivery system. Hydroxyapatite has been used as thin film coatings on metallic alloys due to it can not be used under load bearing purposes [24].

Bioactive glasses and glass-ceramics are bioactive ceramics that has been used since Hench and Wilson proposed it with a composition of 45% SiO_2, 24.5% CaO, 24.5% NaO_2, and 6% P_2O_5 by weight [25]. Kokubo et al. in 1982 fabricated a glass-ceramic containing oxyfluorapatite $Ca_{10}(PO_4)_6(OH,F_2)$ and wollastonite ($CaO.SiO_2$) in a MgO-CaO-SiO_2 glassy matrix that called A-W glass ceramic[26]. They are suggested for orthopedics due to their osteoblastic activity.

Bioceramics can be in different phases:

- Crystal (sapphire),
- Polycrystalline (alumina and hydroxyapatite),
- Glass (Bioglass®),
- Glass-Ceramics (AAV glass ceramics)
- Composites (polyethylene-hydroxyapatite)

Phases are determined for required properties and functions. For instance crystal form is used in dental applications due to its tough structure. Glass-ceramics are used in backbone implants due to its ability to combine with bone. Bioglass® is used in bone defects treatments due to its fast bonding mechanism to the bone [27].

Ceramic-polymer composites are developed to overcome the low mechanical properties of ceramics. There are many composites are produced to provide optimal mechanical properties and bioactivity such as ceramics with polyethylene [28], collagen [29], [30], polysaccharide[31], poly(lactide-co-glycolide)(PLGA) [34],[35], fibrin [34]. Furthermore hydroxyapatite and clickable biodegradable polymers are proposed for novel bone tissue engineering applications [37].

Hydroxyapatite-metal composites such as HA with titanium and hydroxyapatite-metal oxide (ZrO_2, TiO_2, Al_2O_3) are also developed to obtain better mechanical properties with biocompability. Composite design should be well-designed due to obtain optimal properties. Bioactivity of the hydroxyapatite can be hidden in the composite matrix. For this reason hydroxyapatite coating methods are developed.

Bioceramics are studied for their properties, their role in the body and their biocompability performance so that the best biomaterial can be proposed for the bone and tooth defects. They are used for pacemakers, kidney dialysis machines, respirators, coating joint replacements to decrease the inflammatory response.

Autogenous bone grafts are widely used in implantation. However they have some disadvantages such as the need for an additional surgical site, increased donor site morbidity, insufficient volume of (intraorally) harvested bone, and the need to use general anesthesia for extraoral bone harvesting. TCP has taken attention as alloplastic bone graft materials and maxillary sinus floor augmentation to be used in dental implantation because of its biodegradability rate [36].

Medical ceramics market value was about U.S. $9.8 billion in 2010 and it is estimated that it will grow to U.S. $18.5 billion by 2018 [37].

Ceramic biomaterials have various medical applications:

- Orthopedic
- Coatings for bioactive bonding
- Bone space fillers
- Dental implants
- Artificial tendon and ligament
- Alveolar ridge augmentation
- Maxillofacial reconstruction
- Spinal surgery
- Therapeutic treatment of tumors
- Artificial heart valves [23]

Bioceramics can be classified as 3 main groups based on tissue-implant interaction:

- Bioinert ceramics
- Bioactive ceramics
- Biodegradable ceramics

3.1 Bioinert Ceramics

Bioinert ceramics (alumina and zirconia) are polycrystalline ceramics that consist O_2 ions dispersed in the metal ions and they can not bond to tissue due to their inert structure. They do not react with the tissue when they are implanted to human body. Bioinert ceramic implants are isolated from tissues by a non-adherent fibrous capsule which is formed after few weeks of implantation. In some cases the implant should be replaced due to the occurrence of micromovements [38]. Figure 3.1 shows the comparison between bioinert material which forms fibrous capsule and bioactive material which directly bond to bone in vivo environment.

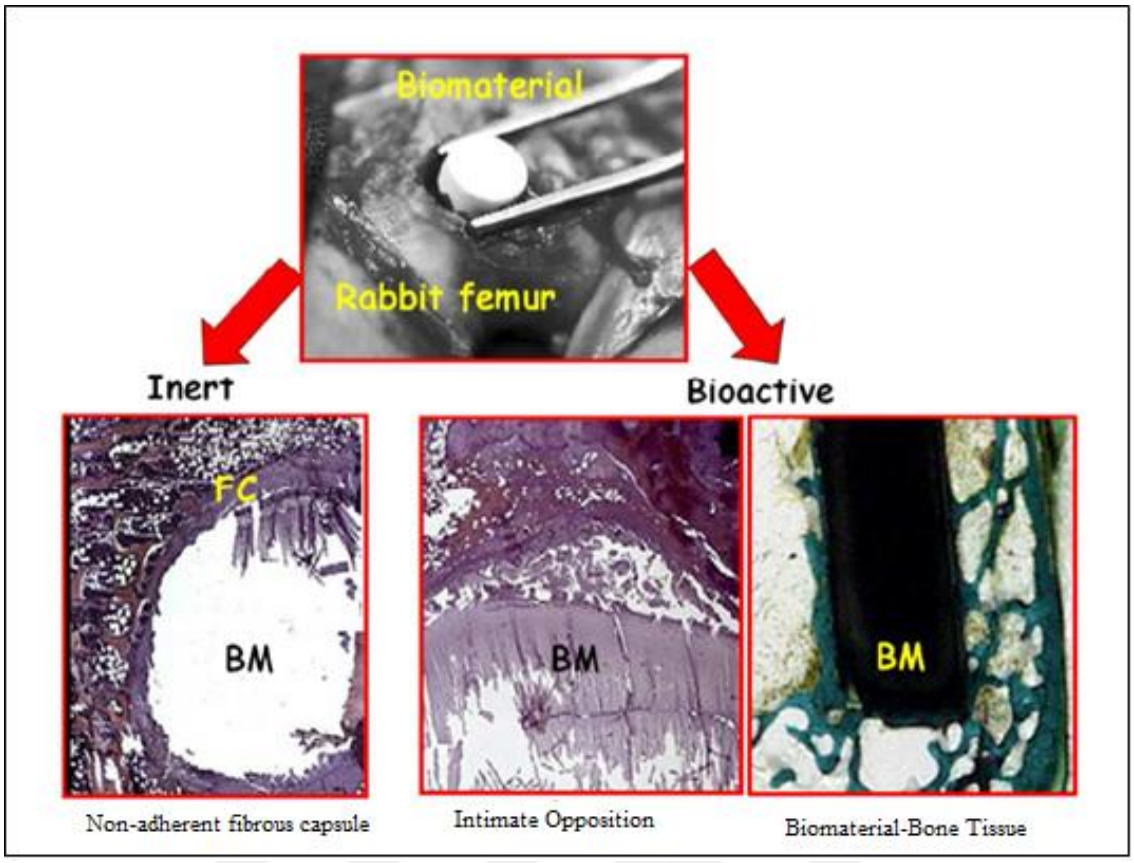

Figure 3.1 After 4 weeks implanted in a rabbit femur on the left there is a fibrous capsule formation in the middle and right bioactive material directly bond to bone [38].

Alumina (Aluminum oxide:Al_2O_3) has high hardness and surface wettability due to its strong ionic-covalent bonds. It has low electric and thermal conductivity high melting point, hardness, and resistance to attack of strong inorganic acids. These properties make alumina the ideal material for arthroprostheses joints. Zirconia (zirconium dioxide:ZrO_2) could apply many fields after it is discovered that its stabilization of the tetragonal phase to room temperature. To eliminate phase changes in zirconia; it is composed with small percentage of other materials such as its composition with yttria results component that has higher thermal, mechanical, and electrical properties. In medical applications it is stabilized by CaO, MgO and CeO [39].

3.2 Bioactive Ceramics

Bioactive ceramics such as bioglass®, hydroxyapatite, glass-ceramic A-W are produced to induce or modulate the biological activity which when they are implanted to the bone they form a layer to induce the chemical activity of bone tissue. Thus it helps to healing process in the bone defects. Due to this biological properties bioactive ceramics inspired

new bioactive materials. For example, tough bioactive materials essential for load-bearing bone repairs have been developed by subjecting titanium metal and titanium alloys to simple NaOH and heat treatments, which produce a bioactive surface layer of sodium titanate in situon the surfaces of the metals. Soft bioactive materials have been developed by copolymerizing bioactive silica or titania with polymers through sol–gel process [40].

Bioactive ceramics are capable of supporting osseointegration. In non-bearing as when the bone regeneration is aimed they are used for formation of new bone and fillings of defects. They have some drawbacks such as brittleness and low strength to fatigue. For this reason they do not show good features in large bone defects particularly in cases with high porosity percentages [38].

Nowadays metal such as titanium and stainless steel coated with bioceramic materials so the implant exhibits high mechanical properties and can be bioactive where it is interact with the bone. For this reason plasma-sprayed coating and electro deposition methods are used for coating the bioactive ceramic on the surface [38].

The bioactive ceramics are more brittle than bone but their bending strength is similar and compressive strength is higher. Comparison of mechanical properties of bioactive ceramics and bones are shown in the Table 3.1.

Table 3.1 Comparison of mechanical properties of bioactive ceramics and bones [1]

	Bending strength (MPa)	Compressive strength (MPa)	Young's modulus (GPa)
Bioglass®	42	–	35
Sintered hydroxyapatite	115–200	500–1000	80–110
Glass-ceramic A-W	215	1080	118
Cortical bone	50–150	100–230	7–30
Cancellous bone	10–20	2–12	0.05–0.5

Bioactive glass-ceramics: Bioactive glasses have been investigated since Larry Hench discovered that it is capable of the formation of hydroxy-cabonated apatite (HCA) layer between the material and bone. These glasses contain Ca^{+2}, PO_4^{3-}, Na^{2+} and Si^{4+} ions which are also exist in the human body. Low silica content makes the glass easy to melt and gives low chemical durability and calcium phosphate on the surface leads to bonding between the glass and surrounding tissue so it dissolves and be replaced by the new tissue by the time. Different bonding mechanisms are proposed by Hench [23], Kokubo [41], Salinas et al [42], Vallet-Regi [43] et al, Izquierdo et al [44] through years. These mechanisms are compared in the Figure 3.1. Kokubo indicated that in vitro formation HCA on $CaO{-}P_2O_5{-}SiO_2$ glasses occurs once Ca^{2+} ions leaches which support the formation of extra Si─OH and increase the saturation of solution, both factors favoring the HCA formation. After the new layer forms collagen fibers reach the implant and encapsulate it, HCA layer initiates to form new bone. Vallet-Regi explained the strong effect of variations in the composition of conventional sol-gel glasses on the new layer formation mechanism. In this way formation of ACP occurs in few hours and HCA forms in 7 days [38]. Figure 3.2 shows the various methods of HCA formation on the surface of bioceramics.

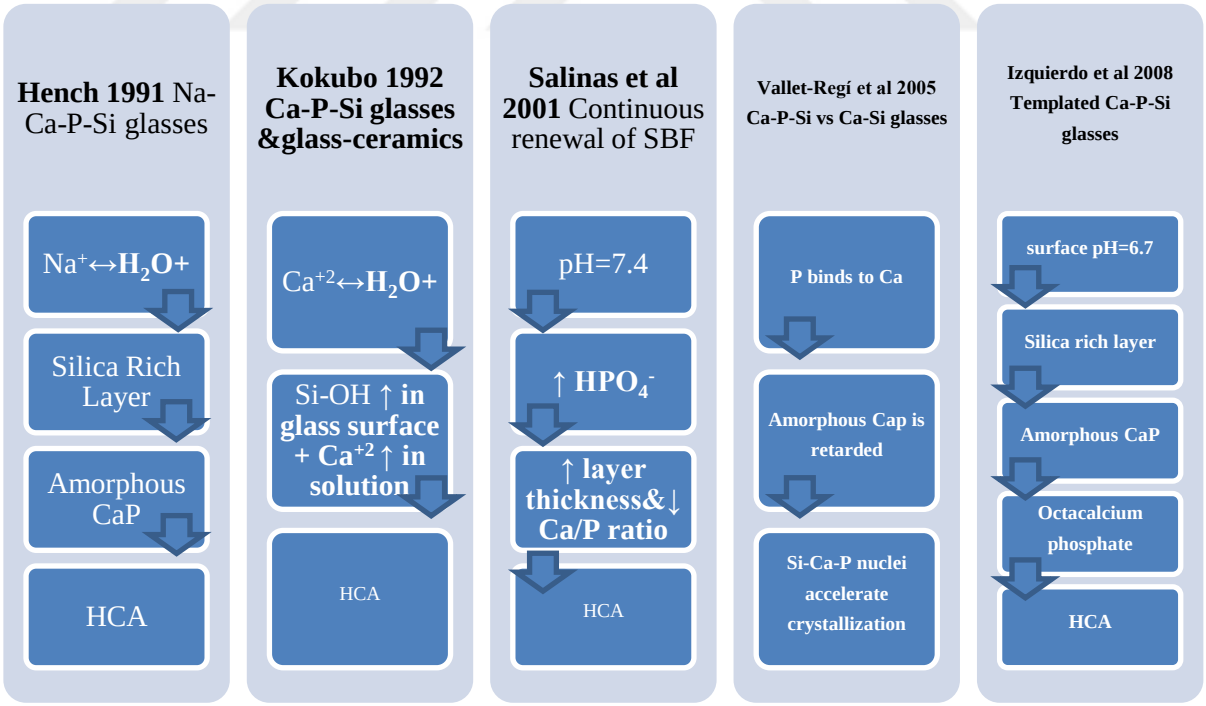

Figure 3.2 Through the years there has been various methods are suggested for the new HCA formation on the surface of bioceramics [38]

Bonding performance of the bioactive glass varies with its composition. For instance it is indicated that bonding takes a week with silica content of the range of 42–53 wt% while it takes 2-4 weeks with silica content of the range of 42-53 wt% and glass lose its bioactivity with the silica content of higher than 60 wt% [45].

The researches focused on sol-gel derived bioactive glass 45S5 and its compositions when Li et al. documented that 45S5 bioactive glass with composition of 45 wt% SiO_2, 24.5 wt% Na_2O, 24.5 wt% CaO and 6 wt% P_2O_5 has higher bioactivity than melt-derived glasses [45], [46].

3.4 Biodegradable (Bioresorbable) Ceramics

Biodegradable ceramics attract special interest since once bone healed after the implantation; they degradate and it does not require a second surgery for removing the implant. Biodegradable ceramic should degradate non-toxic materials in the body, it can be removed by body fluid completely and it should heal the tissue duration of implant in the body. The degradation should be controlled and it should transfer from the implant to body gradually by avoiding the stress shield effect [47].

Solution-driven and cell-mediated processes are considered to responsible for degradation of bioresorbable ceramics. Lamellar bone replacement occurs after cellular degradation of the ceramic matrix has taken place. The biological behavior of bioceramics is dependent on the physical characteristics and chemical composition [47].

Biodegradable ceramics are determined with dissolution of the implant material in vivo conditions without toxicity and rejection. Calcium phosphate ceramics such as hydroxyapatite (HA), TCP and bioactive glass have bioresorbable properties. Calcium phosphate ceramics were utilized for dental studies since 1970s and orthopedics applications since 1980s [48].

Hydroxyapatite is arranged by a combination of passive dissolution and osteoclast mediated resorption. The bioresorption of HA occurs slowly and heavily related to its properties. Minimal degradation and slow resorption was reported after implantation for 12 weeks in rabbit femoral bone. HA doped with manganese and/or zinc as bone substitute resulted in a faster resorption kinetics [30].

The chemical composition and crystallinity of tricalcium phosphate (TCP) $Ca_3(PO_4)_2$ is similar to mineral phase of bone. The crystalline form varies as α-TCP and β-TCP. It resolves faster than HA [48].

Dissolution and osteoclastic resorption initiate degradability. TCP implants have been utilized for two decades as bone void fillers in orthopedic and dental studies. It is been proposed that the small particle size and the sponge like microporosity improves osteoconductive abilities and support timely resorption with the remodeling process.

Zhang et al. [49] suggested the bone formation with bone marrow stromal cells (BMSCs) and β-tricalcium phosphate (β-TCP) as the bone graft implanted in rat dorsal muscles.

Cutright et al. [50] reported tricalcium phosphate ceramic implants in rat tibias 48 days results 95% absorption with extensive bone growth and marrow reformation. Cameron et al. [51] found that when TCP is implanted in cancellous it does not cause any bone untoward tissue or systemic reaction. They observed that it was slowly resorbed. Resorption of these TCPs was compromised by osteoclastic activity and resorption time varying between 6 and 24 months [52].

Based on the performances above, bioactive and resorbable ceramics are used in all types of bone reconstruction, in particular for the production of implants which densely combine with bone (for example in skull restorations after operations or trauma), tooth-root implants, biological tooth fillings, cure of diseases of the periodontal (tissue around teeth), maxillofacial reconstruction, grafting and stabilizing skull bone, joint reconstruction, for the endoprosthesis of hearing aids, cosmetic eye prostheses, etc. Biodegradable ceramics was also used in the restoration of tendons, ligaments, small blood vessels, and nerve fibers [53].

Among these products, bone graft substitutes are widely used. Reports on clinical applications are found for Depuy Spine Conduit_ (TCP), Medtronic MasterGraft_ (HA, TCP), Stryker Vitoss_ (TCP), Synthes ChronOS_, Norian_ SRS_ (calcium phosphate), Stryker Cortoss_ (bioactive glass), etc [48].

CHAPTER 4

CALCIUM PHOSPHATE CERAMICS

Calcium orthophosphates are bioactive chemical compounds and they can be used as bone scaffolds due to they release ions when they interact in the body fluid and they can precipitate apatite on the surface. Osteoblastic cells create a bone extracellular matrix due to this layer that formed in the process. Thus calcium orthaphosphate helps bone to heal in the process of osteoconduction. In this way bioactive material can create a new bone tissue around the body cells [7].

Calcium phosphates attract special interest in many fields due to large quantity of their presence in living organisms. Atomic structure of $CaPO_4$ is made of the orthophosphate (PO_4) groups and this allows to balance the structure. In this way $CaPO_4$ can be soluable in water. All chemically pure $CaPO_4$ powders are white and in structure they are colorless crystals. However natural mineral of $CaPO_4$ are always colorless due to the impurities in the material [54]. Properties of calcium orthophosphates are shown in the Table 4.1.

Fluoroapatite, hydroxyapatite and chlorapatite are natural apatites that occur naturally. They are found in different regions as deposits of apatites mostly as ion-substituted fluoratite(igneus rocks) and phosphorites(sedimentary rocks) [54]. Figure 4.1 displays the superposition of PO_4 tetrahedral for fluorapatite, hydroxyapatite, and chlorapatite. Each overlay is a superposition of the analogous polyhedra from the fluorapatite, hydroxyapatite, and chlorapatite end-members, drawn to the same scale and with coincident central cations [55].

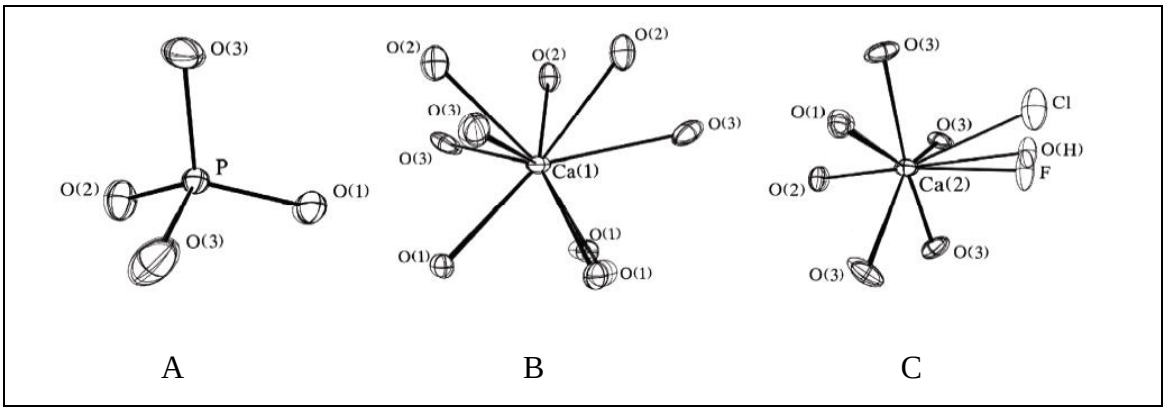

Figure 4.1 Drawings of PO_4 tetrahedron (left) and Ca(1) and Ca(2) polyhedra for the three apatite structures: A) fluorapatite B) hydroxyapatite C) chlorapatite [55].

Calcium phosphates have low mechanical properties and resistance to high pressure. Furthermore the mechanical properties decrease significantly with increasing content of an amorphous phase, microporosity, and grain sizes, while a high crystallinity, a low porosity and small grain sizes tend to give a higher stiffness, a higher compressive, and tensile strength and a greater fracture toughness[54]. In addition, ceramics strength appears to be very sensitive to a slow crack growth [56]. Table 4.1 shows common calcium phosphate ceramics and their properties.

Crystallization dissolution, and phase transformation processes of different $CaPO_4$ under various experimental conditions have been reviewed [57]. The solubility order can be seen below:

MCPM > MCPA > TTCP > α-TCP > DCPD > DCPA > β-TCP > ACP > HA in 25°C water at a pH of 7.4 [58].

HA is the least soluble one comparing to the other calcium apatites [59]. HA can be sparingly solved since their biodegradability is poor and it does not degradate by cellular activity such as the action of macrophages or bone-resorbing cells such as osteoclasts. As a result the biodegradation ratio is slow comparing to bone ingrowth and it can still be found in the body after years. To solve this inconvience biomimetic materials that similar to biological apatite's properties are produced and biomimetic materials that does not occur at the high temperatures preferred as bioceramics [7]. Figure 4.2 displays the solubility phase diagrams of the calcium phosphate ceramics as a function of pH.

Table 4.1 Chemical compositions, Ca/P molar ratio, solubility, pH and temperature stability range in aqueous solutions of some synthetic and biological calcium orthophosphates [7]

Orthophosphate	Abbreviation	Chemical Formula	Ca/P	Solubility-($\log(K_s)$[1]	pH and temperature(°C) stability
Monocalcium phosphate monohydrate	MCPM	$Ca(H_2PO_4)_2.H_2O$	0.5	1.14	0.1–2.0
Monocalcium phosphate, anhydrous	MCPA	$Ca(H_2PO_4)_2$	0.5	1.14	25°C
Dicalcium phosphate dihydrate(brushite)	DCPD	$CaHPO_4.2H_2O$	1.00	6.59	0.1–2.0
Dicalcium phosphate, anhydrous(monetite)	DCPA	$CaHPO_4$	1.00	6.90	> 80°C
Octacalcium phosphate	OCP	$Ca_8(HPO_4)_2(PO_4)_4.5H_2O$	1.33	96.6	2.0–5.5
Calcium-deficient apatite	CDA	$Ca_{10-x}[]_x(HPO_4)_x(PO_4)_{6-x}(OH)_{2-x}[]_x^2$ $(0 < x < 2)$	Variable 1.33–1.66	~85.1	6.5–9.5 25°–37 °C
Amorphous calcium phosphate	ACP	$Ca_x(HPO_4)_y(PO_4)_z \cdot nH_2O$ n=3.0–4.5; 15–20 wt% H_2O	Variable 1.2–2.2	25.7–32.7	5–12 4°–37°C
β -Tricalcium phosphate	β –TCP	β-$Ca_3(PO_4)_2$	1.50	28.9	[3]
α -Tricalcium phosphate	α –TCP	α-Ca3(PO4)2	1.50	25.5	[3]
Biphasic Calcium Phosphate	BCP	β-$Ca_3(PO_4)_2$ + $Ca_{10}(PO_4)_6(OH)_2$	Variable 1.55–1.65	ND[4]	[3]
Hydroxyapatite	HA	$Ca_{10}(PO_4)_6(OH)_2$	1.67	116.8	9.5–12.0 > 80°C
Fluoroapatite	FA	$Ca_{10}(PO_4)6F_2$	1.67	120.0	7–12 > 80°C
Tetracalcium phosphate	TTCP	$Ca_4(PO_4)_2O_2$	2.0	38–44	[3]

[1] The solubility at 25 °C in water is given as the logarithm of the ion product of the given formulas with concentrations in mol/l

[2] Represents a lacuna in the crystal lattice of hydroxyapatite

[3] These compounds cannot be precipitated from aqueous solutions and form only at elevated temperatures (β -TCP > 800°C, α-TCP > 1125°C, TTCP> 1300°C)

[4] Not determined.

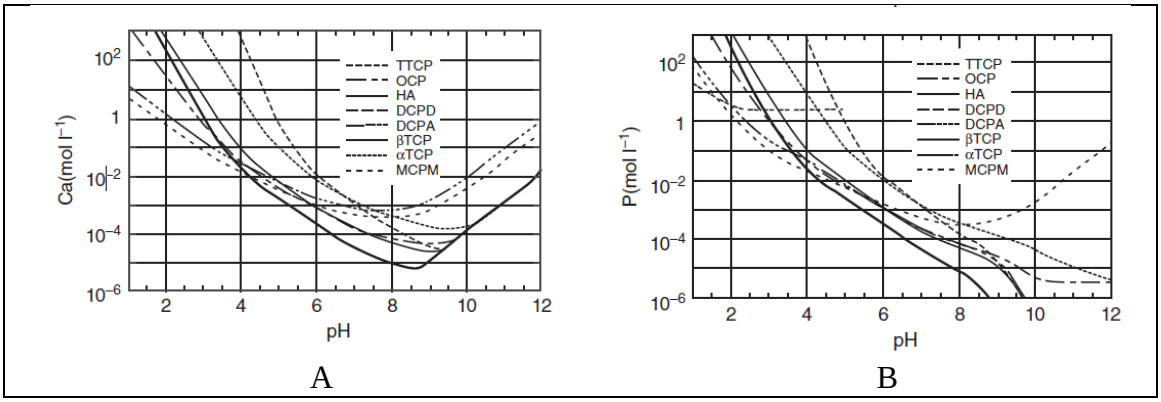

Figure 4.2 Solubility phase diagrams of A)calcium and B)orthophosphate ions as a function of the pH in solutions saturated with various salts [54]

4.1 Hydroxyapatite (HA)

Hydroxyapatite (HA) is the form of calcium apatite and its formula is $[Ca_{10}(PO_4)_6(OH)_2]$. Figure 4.3 shows the unit cell of the hydroxyapatite crystal. It has been studied in last decades due to it is the main component of human bone and teeth. It is highly biocompatible with hard and soft tissues thus it has been used as coatings on surface of Ti–6Al–4V alloy and scaffolds. Many methods have been developed to produce hydroxyapatite. Some of them are sol–gel method, solid-state reaction, hydrothermal method and microemulsion techniques, wet chemical precipitation method [60]. It has been examined that processing conditions (particularly, temperature and duration) affects the crystallinity and solubility of the material.

HA is osteocompatible and osteoconductive but stoichiometric HA is unable to bioresorbe and its toughness is less than bone tissue due to it does not remain organic component such as collagen [61].

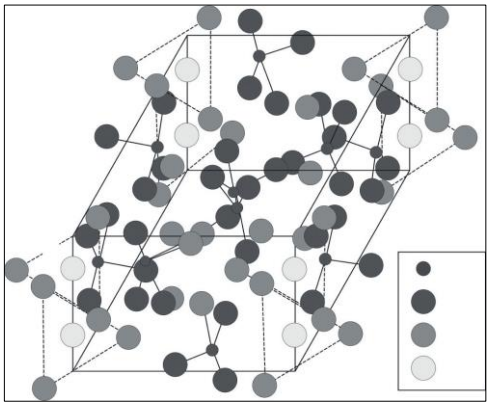

Figure 4.3 Unit cell of hydroxyapatite (HA) crystal [59].

High-temperature-type HA occur over 1200 °C with a calcium-phosphate (Ca/P) ratio of 1.67. Above this temperature heat dense hydroxyapatite can be obtained. However below this temperature heat porous hydroxyapatite can be produced. The difference between synthesized two hydroxyapatite is low temperature type of HA tend to be absorbed by the osteoclast cells which is present in the bone [59].

Synthetic HA sintered at high temperatures are characterized and the results showed that: (i) Synthetic HA with a ratio of 1.67 does not change to TCP (tricalcium phosphate) and this indicates that it is a stable form of HA. (ii) Over 1200 °C temperatures HA turns to different form which is called oxyapatite $CaO(PO_{10})_4$, $_6$ (iii) at 1450 °C different forms of calcium apatites are observed such as α-$Ca(PO_3)_4$, $Ca_2P_2O_2$, and $Ca_7P_4O_{29}$ [62]. It is studied that when the temperature and holding times increase, the structural integrity of HA decreases [63].

It was reported that the Knoop indentation study reveals that the hardness of HA exhibits a linear dependence on the inverse square root of the grain diameter, consistent with the Hall–Petch relationship, suggesting the grain-size dependence of the HA hardness [64].

Low temperature type of hydroxyapatite can be synthesized in the room temperature. It is a bioresorbable material that is resorbed by the body by transforming to bone structure by time and integrate to the bone indirectly.

This low-temperature HA is a nanocrystal-size HA and is gradually resorbed by acetic acid, which is produced by osteoclasts, so that, after resorption by osteoclasts, it can be used as a source for bone formation by osteoblasts [59].

Solubility of the biological HA occur as it is interacted to biological fluids in tissues [65]. HA is stable in the body due to it is supersaturated inside of the body. HA crystal is not precipitated from supersaturated body fluid due to proteins such as proteoglycan, metaphosphates and pyrophosphoric acid inside the body inhibits the HA precipitation [66], [67].

Hydroxyapatite can connect to the tissue by forming bonelike apatite. Niwa et. al. indicated that when the sintering temperature increases the ability to connect to tissue of HA decreases so HA has different kinetics of apatite formation process. HA with different sintering temperatures exhibit different kinetics of the apatite formation [40].

Porous HA is produced to imitate trabecular bone and successfully utilized for bone replacement implants. It is beneficial since its features such as light weight and its

porous nature and the pore spaces helps ingrowth of the bone and support favorable cell–material interaction. However HA has lower elastic modulus relatively to bone. Since HA and bone has different elastic modulus and HA shows lower inelastic abilities it cause fractures and stress concentration in the interface of bone-HA [68]. Mechanical properties of hydroxyapatite is shown in Table 4.2

Table 4.2 Mechanical properties of hydroxyapatite

Elasticity Module(GPa)	4.0-217
Compression Strength(MPa)	294
Bending Strength(MPa)	147
Toughness(Vickers, MPa)	3.43
Poisson Ratio	0.27
Density(theoretical, g/cm^3)	3.16

4.2 Tricalcium Phosphate

β-tricalcium phosphate [β-$Ca_3(PO_4)_2$]; is one of the most bioresorbable material and it is been successfully utilized for bone substitutes due to it does not remain in the bone tissue after the implantation although in some studies there was evidence of β-TCP remains in the bone tissue. It has some disadvantages such as poor osteogenic activity [61].

It has been reported that there are some ways to improve TCP's activity in the body such as adding osteoprogenitor cells on the graft material and using bone morphogenetic protein-2 (BMP-2) [61].

TCP has three forms: β-TCP is stable from sintering temperature of room temperature to 1125 °C, α-TCP is stable from 1125 °C to 1470 °C, α'-TCP is stable from 1470 °C to the melting point 1810 °C. Among these β-TCP is most bioresorbable and has taken the attention due to this property. It is utilized for oral surgeries or polymer composites

in the form of granules and rods. But in a bulk form it is hard to use in clinical applications since the powder form can not fully densify [69].

β - α phase transition is avoided to keep the high mechanical properties by controlling sintering temperature below 1125°C [69]. It is claimed that spontaneous massive microcracking in the sintered body due to the expansion-contraction cycle generated by the differences in density between β-TCP (3.07 g/cm^3) and α -TCP (2.86 g/cm^3). On the other hand there is no proof of microcracking in the transition of β – α transition.

Figure 4.4 shows partial $CaO–P_2O_5$ equilibrium phase diagram. The following notation is adopted to identify the phase composition: CHP:heptacalcium phosphate ($Ca_7(P_5O_{16})_2$), CPP: calcium pyrophosphate ($Ca_2O_7P_2$), TCP: tricalcium phosphate ($Ca_3(PO_4)_2$), and TTCP: tetracalcium phosphate ($Ca_4(PO_4)_2O$). The gray vertical line marks the composition of the starting powders and the circles indicate the sintering temperatures analyzed in this work [69].

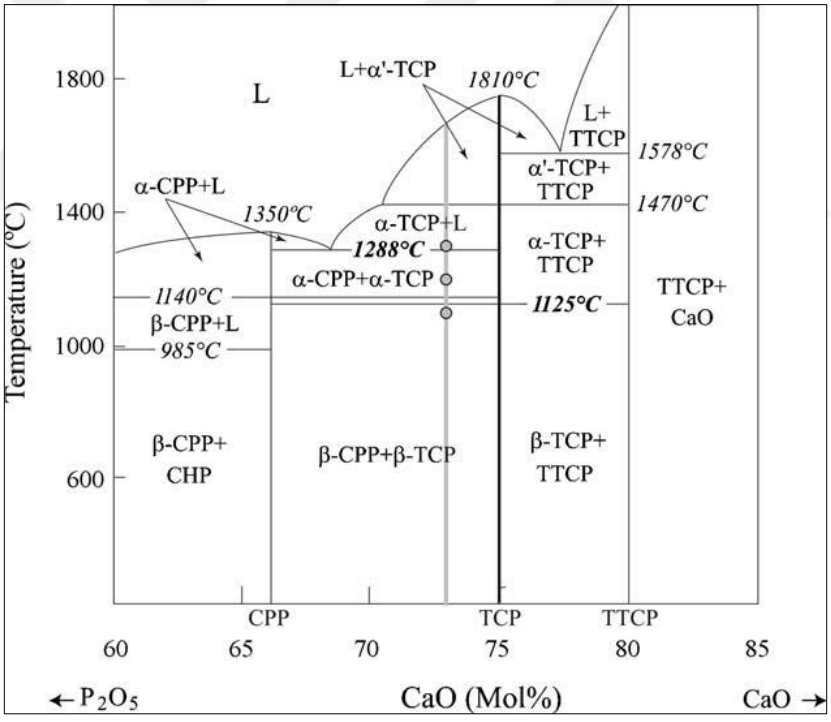

Figure 4.4 Partial $CaO–P_2O_5$ equilibrium phase diagram [19].

4.3 Fluorapatite

Fluorapatite is the formula of $Ca_5(PO_4)_3F$ and the the IUPAC name is pentacalcium fluoride tris(orthophosphate). It is the hardest (Mohs scale is 5), the most stable, least soluble among in calcium phosphates. It is guessed that these properties can be

associated to position of F^- in the center of Ca triangles in the chemical composition. Due to its properties it can naturally forms large deposits suitable for the commercial use [70].

Chemically pure FA is suggested for grafting purposes. This is attributed to the material's low solubility, good chemical stability and toxicity of high quantity of fluorides. However, attempts to test FA-containing formulations, ion-substituted FA, FHA, and porous FA bioceramics are kept performing [24]. FA is also used for fluorescent light tubes, laser materials (in both cases dopants are necessary), as well as catalysts.

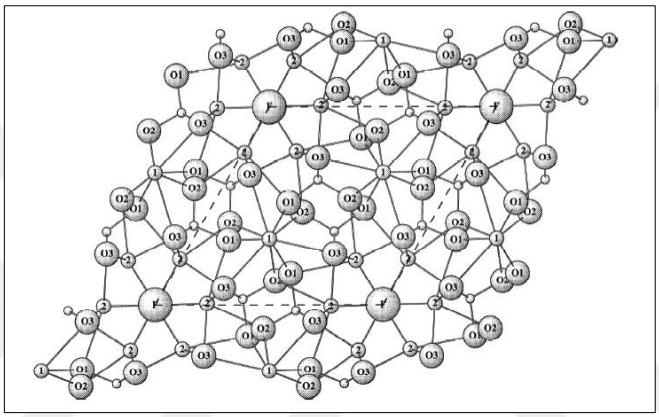

Figure 4.5 The atomic structure of fluorapatite [55].

F release stimulated by the fluoridation can be used in dental applications due to F ions can inhibit the dental caries. Besides F ions at appropriate rates induce the bone cell responses so it can lead to bone formation. These findings suggested that FHA nanofibers with HA can be used in different biomedical applications such as bone augmentation and defect filling. Moreover their composites with degradable biopolymers or proteins being hybridized can be promising for biomedical applications [71].

Moreover, the apatite nanofibers can be used as biocatalysts, biosensors, and ion-exchange filters as well as for the protein purification in the field of nanobiotechnology [71].

4.4 Biphasic, Triphasic, and Multiphasic Calcium Phosphate Formulations

Calcium phosphate materials might be in different formulations such as HA-TCP or FA-TCP and each components can not be separated. Probably they are mixed

homogeneously at a far submicron (<0.1 μm) and they are strongly bonded still their phases can be seen by X-ray diffraction method [24].

Calcium phosphate materials have different properties and in multiphasic phases sum property can be adjusted by changing each component's ratio. These can provide new benefits such as bioactivity, bioresorbability, osteoconductivity and osteoinductivity. For instance HA is more stable phase than TCP phases since it exhibits slower resorption kinetics and less biodegradation properties. It can be suggested that when the TCP/HA ratio in biphasic phase increases biodegradation increases as well. In this way in vivo bioresorbability can be modified [24]. Biphasic calcium phosphates (BCP) bioceramics main advantage is their biodegradability can be adjusted by changing its composition.

4.5 Fabrication Processes of Hydroxyapatite

Hydroxyapatite can be produced from organic and inorganic resources via various methods. Generally HA that synthesized from organic resources is not stoichiometric and it is thought to be it is the result of ions in natural resources. Major problem associated from inorganic Ca and P based resources is the high cost of the synthesis process. HA characteristics that synthesized from natural resources are related to yield, phase purity and size distribution, extraction technique, calcination temperature, structure of bone [72].

Bones should be subjected to deproteinization and then calcinated at high temperatures. Calcination is essential for removing organic components and pathogens. This extracted HA contains valuable ions which they play crucial role in bone regeneration process and increase bone formation rate. Addition of ions to synthetic hydroxyapatite and consequently the ion containing HA is several times more expensive than the simple HA [73].

HA granules are particular interest because they have the potential to be used in jaw and face surgery and in implantable drug delivery systems. HA granules can be obtained by hydrothermal reaction of corals, by crushing sintered blocks, by means of vibration and rolling, by dripping and drip casting procedures with irregular or spherical geometry. Spherical granules are preferred in order to avoid inflammation and to be easy to integrate into the bone [74], [75].

Common techniques used in the preparation of HA particles are categorized by five main methods which are dry methods, wet methods, high-temperature processes, synthesis form biogenic sources, combination procedures. Fabrication processes for bioceramics is shown in the Figure 3.3 [76].

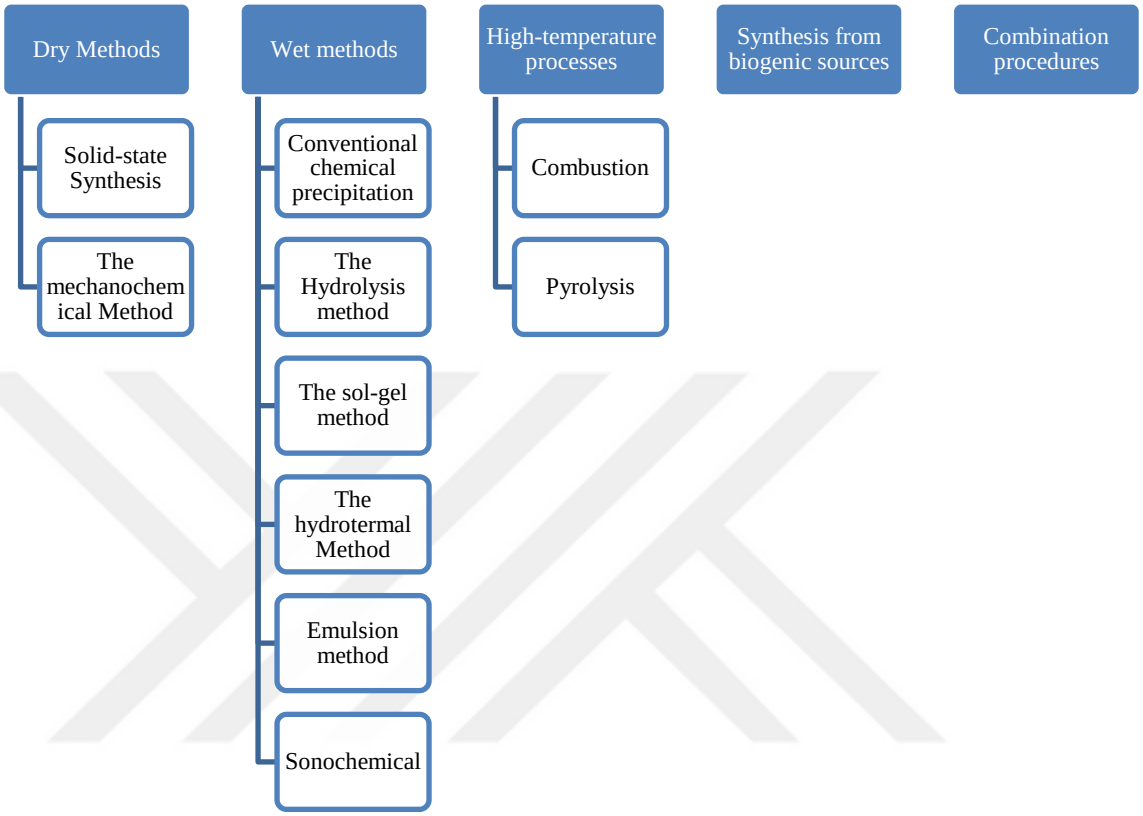

Figure 4.6 Bioceramic synthesis methods [76]

4.5.1 Dry Synthesis Method

Stoichiometric and well crystallized HA can be obtained by solid state reactions at stoichiometric Ca/P ratio of the calcium orthophosphates to calcium oxide or similar salts such as $Ca(OH)_2$ to provide HA formation at high temperatures (generally above 700 °C). Heat treatment of natural materials such as bovine bones, fish bones, corals and egg shells results in non-stoichiometric HA. The morphological properties of the product at nano-scale can be controlled by changing the parameters of the solid state reactions [77].

4.5.2 Wet Chemical Synthesis Method

Among the wet synthesis methods wet chemical precipitation is commonly used because of its simplicity.

When calcium and orthophosphate are mixed in aqueous solutions at pH> 7 oversaturated HA solution occurs which helps nanoparticles to precipitate fastly. Some researchers have conducted this precipitation in simulated body fluid (SBF) to obtain biomimetic apatite nanoparticles [78].

Precipitation in an aqueous solution produces calcium-deficient HA (CDHA): amorphous calcium phosphate (ACP) occurs in a wide range of conditions, and octacalcium phosphate (OCP) occurs in some cases[79]. Production of HA nanoparticles by the wet chemical precipitation has advantage of controlling particle size effectively. Studies have shown that the size of HA nanoparticles increases with temperature.

3.5.3 Homogeneous Precipitation Method

Homogeneous precipitation starts with a homogeneous and acidic calcium phosphate solution followed by urea or acetaminin thermal degradation (hydrolysis) results HA nucleation and development. The resulting NH_3 raises the pH of the solution (and the degree of HA saturation), thus causing the HA particles to precipitate. Slow hydrolysis of molecules at high temperature causes large size and well-crystallized HA particle formation. Hydrolysis of urea can be accelerated at the end of the urease enzyme addition, especially at 37 °C [80].

3.5.4 Sol-Gel Method

The sol-gel method has been widely used for a long time in the production of small particle size ceramics in wet conditions. The metal alkoxide is a typical precursor which is subjected to hydrolysis and polycondensation reactions to form a solid phase. In this process, the sol dissolving precursors evolves slowly becomes of a gel-like network of the solid phase. This solid phase can also be deposited on a substrate to obtain a film layer. The solid phase can be obtained as nanoparticles dispersed in the solution by changing the reaction parameters [78].

The sol-gel method is also a useful method for obtaining multiple substrate coating layers containing nanostructured HA sintered ceramics and various combinations of precursors (calcium alkoxide and phosphorus alkoxide).

The solid phase obtained in the sol-gel method for HA preparation is usually amorphous Ca-P intermediates. Therefore a thermal treatment (typically at 400–500 °C, which is lower than the sintering temperature of HA powder, 800–1000 °C) is essential to obtain well-crystallized HA. Grinding is necessary to obtain HA nanoparticles since the products are in sintered polycrystalline structure [77].

3.5.5 Emulsion Method

Emulsion process of HA is prepared with inverse (water-in-oil type) emulsion droplets, inverse microemulsion droplets or inverse micelles and it is a crystal nucleation/growth in a limited space. Restriction of crystal growth provides controlling HA nanoparticles. This method is useful for refining the clustering and restricting the formation of hard agglomerates. Nanocrystalline material can be obtained without precipitation but surfactant contamination is one of the disadvantages. It has been discovered that the microemulsion method is significantly more refined in terms of particle size and degree of particle clustering compared to particles obtained by a direct reaction in the absence of the emulsifiers and oil in wet chemical synthesis method [76], [77].

3.5.6 Mechanochemical Method

Among all the methods mechanochemical method takes attention because it is simple, environmental, low-cost method. It is dry method for producing different materials such as nanocrystalline alloys and ceramics. The reaction of calcium and phosphate resources with different Ca/P ratios in liquid medium results calcium phosphate ceramics. Ca resources can be calcium phosphates ($CaHPO_4$, $Ca_8(HPO_4)_2(PO_4)_4 \cdot 5H_2O$,$Ca_3(PO_4)_2$ [82]–[84]) or poorly soluble calcium salts ($CaCO_3$) [85], [86] and $CaSO_4.2H_2O$ [87], [88]).

CHAPTER 5

APATITE FORMATION MECHANISM

5.1 Apatite-Forming Ability in Simulated Body Fluid

Kokubo et. al. discovered that in vivo studies A-W glass ceramic bonds to bone in vivo conditions however they did not observe any formation of HCA layer in TRIS buffer studies. These discoveries lead them to produce a solution that can mimic human blood plasma which is called simulated body fluid. SBF is a solution that contains almost same inorganic ionic composition equal to human blood plasma and buffered with TRIS buffer at physiological pH. Table 5.1 indicates the inorganic ionic composition of simulated body fluid. Table 5.2 shows nominal ion concentrations of SBF in comparison with those in human blood plasma.

Table 5.1 Composition of SBF [89]

Order	Reagent	Amount	Formula Weight
1	NaCl	8.035 g	58.4430
2	$NaHCO_3$	0.355 g	84.0068
3	KCl	0.225 g	74.5515
4	$K_2HPO_4.3H_2O$	0.231 g	228.2220
5	$MgCl_2.6H_2O$	0.311 g	203.3034
6	1 M HCl	39 ml	-
7	$CaCl_2$	0.292 g	110.9848

Table 5.1 (cont'd)

8	Na_2SO_4	0.072 g	142.0428
9	TRIS	6.118 g	121.1356
10	1.0 M HCl	0–5 ml	-

Table 5.2 Nominal ion concentrations of SBF in comparison with those in human blood plasma

	Blood plasma(mM)	SBF(mM)
Na^+	142.0	142.0
K^+	5.0	5.0
Mg^{2+}	1.5	1.5
Ca^{2+}	2.5	2.5
Cl^-	103.0	147.8
HCO_3^-	27.0	4.2
HPO_4^{2-}	1.0	1.0
SO_4^{2-}	0.5	0.5
pH	7.2–7.4	7.4

A detailed research about how bonelike apatite form occurs on bioactive ceramics is important to improve the bioactive material with better properties. By forming groups such as Si–OH and Ti–OH groups these materials induce the bonelike apatite. These functional groups reveal a negative charge to positive calcium ions in the body fluid so they initiate a reaction to compound amorphous calcium silicate or calcium titanate. These amorphous calcium compounds reveal positive charge to combine the negative ions in the fluid so these reaction chains form amorphous calcium phosphate and these leads to form bonelike apatite [40].

Bonelike apatite after implantation forms in following steps:

1. HA surface starts to dissolve

2. Equilibration of body fluids and HA surface (On the surface, composition of HA can change but it does not indicate a new form of DCPA or DCPD)
3. Proteins and other organic compounds are adsorbed.
4. Cell adhesion
5. Cell proliferation
6. New bone form occurs [54].

When sintered hydroxyapatite interacts with SBF, it is negatively charged on the surface and it connects to positively charged Ca^{+2} ions in the SBF fluid. This leads to formation of Ca-rich amorphous calcium phosphate. Ca^{+2} ions are collected on the surface and it makes the hydroxyapatite positively charged so the phosphate ions in hydroxyapatite react to them. It initiates the Ca-poor amorphous calcium phosphate formation. Later, this form transit to more stable form which is crystalline bonelike apatite. The mechanism is the same in vivo conditions and it can give an idea to predict the bone-bonding ability of the material. The mechanism of apatite formation on the sintered hydroxyapatite in SBF is shown in the Figure 5.2 and hydroxyapatite surface after implantation is shown in the Figure 5.3 [1].

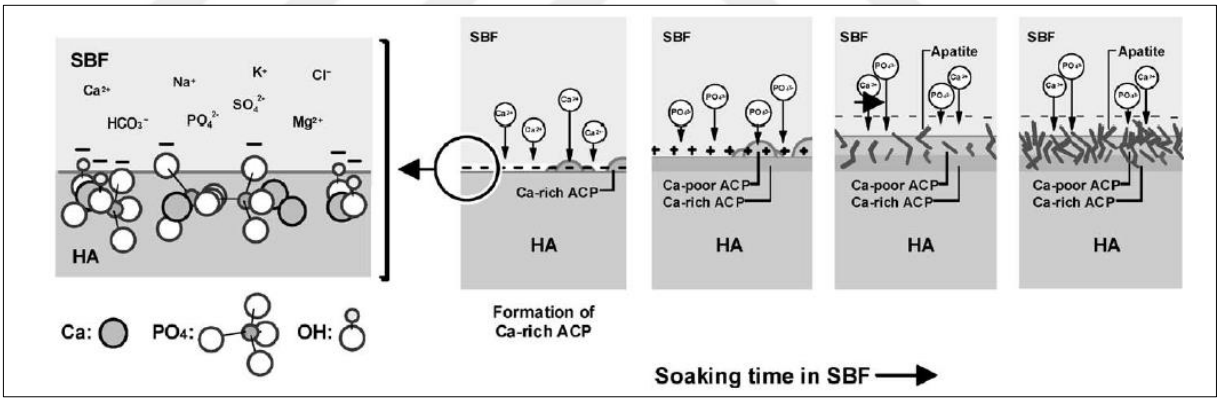

Figure 5.1 Mechanism of bonelike apatite formation on the sintered hydroxyapatite in SBF [1]

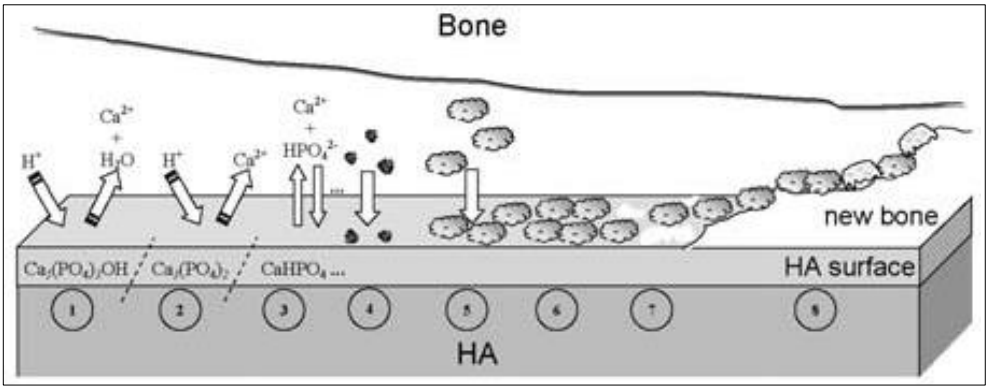

Figure 5.2 HA surface after the implantation [54]

CHAPTER 6

BIOCERAMICS FROM NATURAL ORIGIN

Hydroxyapatite can be easily obtained from natural bone with extraction process as it is already contains in bone naturally. Other sources for hydroxyapatite are bovine, tooth dentine, enamel, fish wastes, egg shells [90]. These natural materials should be treated with high temperature to avoid all prion diseases. This treatment is safer in comparison to the dilute HCl treatment of freeze-dry method, in which some prions can still survive subsequent to the treatment. It is reported that fish scales can be utilized as cheap source of bioceramics and can reduce the undesirable environmental impact by recycling [91]. Furthermore bioceramics can be obtained from corals and sea shells. Their structure contains calcium carbonate(calcite or aragonite) so it can be converted to calcium phosphate ceramics with the addition of phosphorus source [92].

The pore structure of calcium phosphate produced from certain coral species is similar to human cancellous bone, provide suitable material for bone graft applications. Since 1980s hydroxyapatite is converted from coral and has been successfully used as bone graft as it allows in-growth of blood vessels after implantation. In 1974, Roy and Linnehan produced hydroxyapatite from coral via hydrothermal method. It was reported that produced hydroxyapatite is less than 533 K and 103 MPa [93]. In 1996, HA was fabricated from Indian coral via hydrothermal method. It was reported that produced material was required to further forming and sintering process [94]. During the hydrothermal treatment aragonite converts to hydroxyapatite whilst porous structure preserves. In 2001, microwave was successfully applied to hydroxyapatite derivation from coral and higher extends of conversion was reported [95]. Hu et al, successfully produced hydroxyapatite from Australian coral via two stage process where the hydrothermal method was followed by a patented hydroxyapatite sol-gel coating process based on alkoxide chemistry. It was reported that they obtained 120% increase

in the biaxial strength of the double-treated coral in comparison to only is converted one [96].

It is investigated that natural origins such as Mediterranean Mussel (Mytilus galloprovincialis) shells [97], Sea Snail *Cerithium vulgatum* [90], Cypraea Tigris [98], sea urchin *Paracentrotus lividus*[99], Atlantic Deer Cowrie Shells (Cypraea cervus Linnaeus) [100] and many marine resources are successfully converted to calcium phosphate ceramics via mechanochemical method [101], [102].

6.1 *Clinocardium ciliatum* as Resource of Bioceramic

Clinocardium ciliatum or the Iceland cockle, is a species of bivalve mollusc in the family Cardiidae. It can be found along the Atlantic coast of North America, ranging from Greenland to Massachusetts [103]. It is displayed in Figure 6.1 and its habitat is shown in the Figure 6.2.

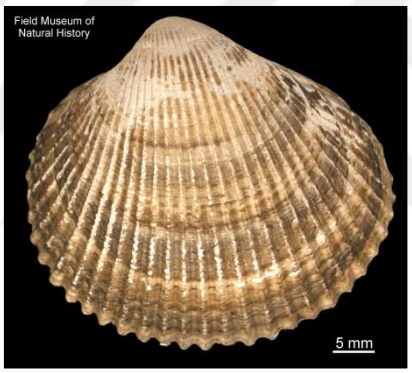

Figure 6.1 *Clinocardium ciliatum* [104]

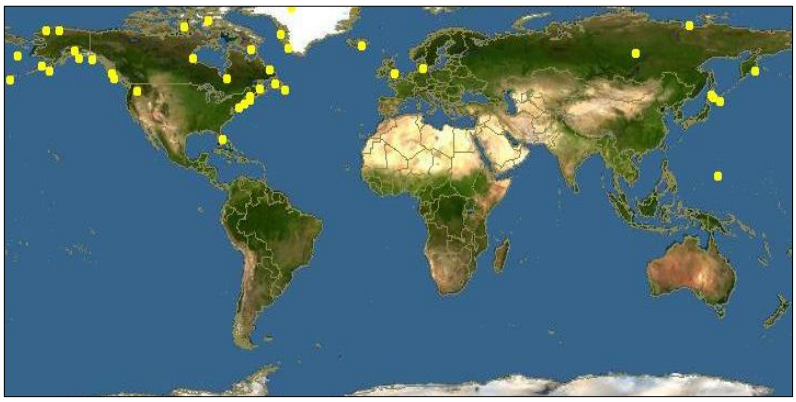

Figure 6.2 Habitats of *Clinocardium ciliatum* [105]

6.2 *Turritella terebra* as Resource of Bioceramic

Turritella terebra is a species of sea snail that can be found in Indo-West Pacific: from East Africa, including Red Sea, to Melanesia; north to Taiwan Province of China and south to central Queensland [106]. It is displayed in Figure 6.3 and its habitat is shown in the Figure 6.4.

Figure 6.3 *Turritella terebra* [107]

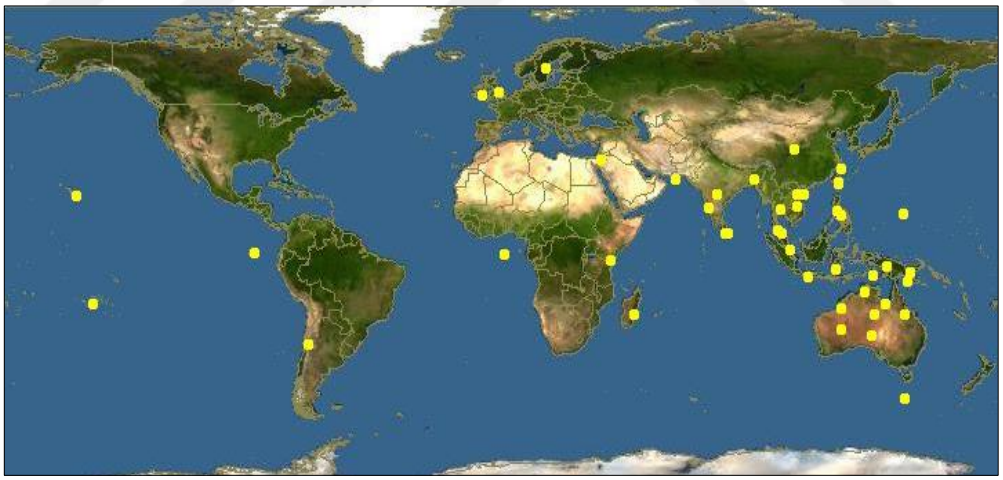

Figure 6.4 Habitats of *Turritella terebra* [108]

CHAPTER 7

EXPERIMENTAL WORK

7.1 Materials

Clinocardium ciliatum and *Turritella terebra* were obtained from Marmara University Advanced Nanomaterials Research Laboratory.

7.1.1 Chemicals

All chemicals and solutions used in this study were supplied by Lipid and Biocomposite Laboratory of Bioengineering Department at Yildiz Technical University.

7.1.2 Laboratory Equipment

Table 7.1 and Table 7.2 show general laboratory equipment list and labrotary analysis equipment list.

Table 7.1 General Laboratory Equipment List

Equipment	Brand
Vacuum furnace	Binder
pH Meter	WTW pH 3110
High Energy Ball Mill	Retsch Planetary Ball Mill PM 400
Sieve	Kapder Analysis Sieve
Heating Magnetic Stirrer	Heidolph MR 3001
Water Purification Systems	GFL Water Still for Single distillation 2004

Table 7.2 Labrotary Analysis Equipment List

Fourier Transform Infrared	Perkin Elmer Spectrum One
High Temperature Furnaces	Protherm MoS-B
BET Analyzer	Tristar II 3020
DTA/TGA Analyzer	SII6000 Exstar TG/DTA 6300
Scanning Electron Microscopes	Zeiss EVO® LS 10
Pellet Preparation Device	Manfredi OL 57
ICP-OES Device	Shimadzu ICPE 9000

7.2 Methods

Materials were washed and cleaned from the dust and other different materials (Figure 7.1).

A B

Figure 7.1 A) *Clinocardium ciliatum* B) *Turritella terebra*

They were dried in the vacuum furnace for a day at 100 °C. They were milled in an agate mortar and processed in a milling machine to obtain the size of less than 100 μm. They were sieved with a 100 μm and 100 mesh sieves and powders less than 100 μm size samples are obtained.

To evaluate the $CaCO_3$ amount in the shells the powders were processed in Differential thermal analysis. So the exact $CaCO_3$ amount was provided at 750 °C temperature in the process. The amount of H_3PO_4 was calculated for the HA stoichiometry ratio which is Ca/P is 10/6.

The chemical reaction equation to obtain HA is below:

$$10CaCO_3 + 6H_3PO_4 \rightarrow Ca_{10}(PO_4)_6(OH)_2 + 8H_2O + 10CO_2 \quad (7.1)$$

Figure 7.2 Synthesis in the hotplate under a cooler

Bioceramics were synthesized after the reaction in mechanochemical method and sintering processes for HA ratio in the sintering temperatures of 1000 °C and 1200 °C sintering temperatures for two different materials. As a result different bioceramics were obtained.

The powders are weighted 2 grams and added on 50 mL distilled water in the reaction balloon. It was put on the hotplate under a cooler and the mixture temperature was set to 80 °C for 10 minutes. H_3PO_4 with calculated ratio was added dropwise to the mixture. The reaction was left for 2 and a half hours. The precipitation was removed from the liquid by filtration and was dried at 100 °C for 24 hours in a vacuum furnace. Dried powder samples were obtained and weighted. Drided powders were sintered in an oven with a 5 °C of increase per minute and held in that temperature for 4 hours. Two different powders were sintered at 1000 °C and 1200 °C. Fabrication process can be seen in Figure 7.3.

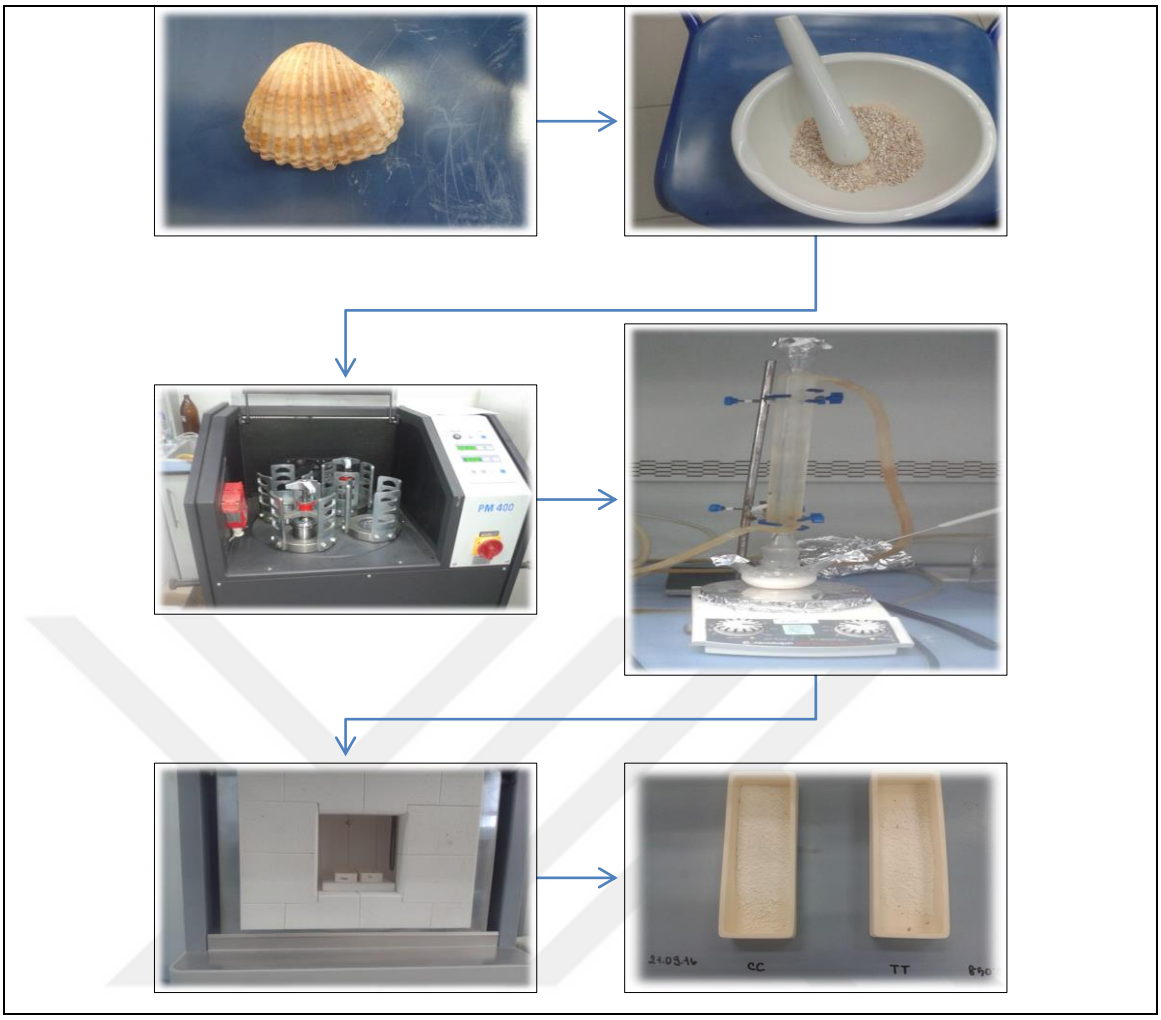

Figure 7.3 Fabrication process

7.3 Characterization of Produced Materials

Physical, morphological properties and their behaviors in simulated body fluid of calcium phosphate ceramic samples were analyzed. Samples were soaked in simulated body fluid for 7, 14 days to analyze their biological properties. Analyses show the hydroxyapatite amount on the surface of the samples so it gives information about their bioactivity properties. FT-IR, XRD, SEM analyses were investigated after soaking 7 days and 14 days in simulated body fluid. Biodegradation of the samples were investigated after they were soaked in TRIS solution for 7 days

7.3.1 FT-IR (Fourier Transform Infra-Red Spectroscopy) Analysis

Prepared samples were analyzed by FT-IR before soaking in SBF and after soaking in the SBF after 7 days and 14 days. FT-IR device is based on the principle of absorption

of infrared energy at specific frequencies or wavelengths of chemical bonds. Absorbance value was set to 650-4000 cm^{-1} and functional groups of the samples before and after soaking SBF solution were determined from the literature.

7.3.2 X-Ray Diffraction Analysis

Prepared samples molecular structure was determined by X-ray diffraction analysis. Copper Kα radiation (λ = 1.5406 nm) produced at 30 kV and 25 mA scanned. The range of diffraction angles (2θ) between 10° and 80° with a 2θ step of 0.02°/s. Identification of the phases was performed by comparing the experimental XRD patterns to standards complied by the Joint Committee on Powder Diffraction Standards (JCPDS) using the cards 71–2396 for aragonite, 09–0432 for hydroxyapatite and 09–0169 for whitlockite (TCP).

7.3.3 SEM/EDX Analysis

Morphological properties of the prepared samples before soaking in SBF and after soaking in the SBF 7^{th}, 14^{th} and 21^{th} days were performed by SEM device. Samples were coated with gold do to reduce charging which can prevent visualization. The Elemental composition of the samples was carried out with Energy Dispersive X-ray Spectroscopy (EDX). 500x, 1000x, 5000x, 10000x, 15000x magnifications of the samples visualized in 10 kV.

7.3.4 Brunauer–Emmett–Teller (BET) Theory Analysis

Specific surface area of the prepared samples was carried out with BET analysis. BET device is based on the principle of absorption of gas molecules on a solid surface. The samples were degassed at 100 °C for 2 h under nitrogen purging prior to BET measurements. Pore size and pore volume were calculated using BJH adsorption method.

7.3.5 Simulated body Fluid (SBF) Analyses

Kokubo [89] prepared a solution that its ion concentration is equal to human blood plasma. In this study SBF was prepared according to SBF that Kokubo indicated. Table 7.2 shows the ion concentrations of SBF and human blood plasma.

Table 7.2 shows the chemicals and their amounts. These chemicals were added to 800 ml distilled water. First 5 chemicals were added, then 39 ml 1M HCl solution was added and the temperature of the solution was set to 36.5 °C. After the number 7 and number 8 solutions were added last chemical $(CH_2OH)_3CNH_2$ (Hydroxymethylaminamethane) was added little by little due to it changes the pH value quickly. 1M HCl was titrated if the pH was over 7.4. When pH was set to 7.4 it was cooled and distilled water added until 1000 ml.

Table 7.3 Chemicals used for SBF with the quantity and addition order

Addition Order	Chemical	Amount(g/l)
1	NaCl	8.035
2	$NaHCO_3$	0.355
3	KCl	0.225
4	$Na_2HPO_4.2H_2O$	0.231
5	$MgCl_2.6H_2O$	0.311
6	1 M HCl	39 ml
7	$CaCl_2.2H_2O$	0.292
8	Na_2SO_4	0.072
9	$(CH_2OH)_3CNH_2$	6.118

Samples were pelleted to prepare for bioactivity test. Sample powders were pressed under 100 bar pressure for 60 seconds. Prepared pellet samples were sintered for the second time due to reach tougher pellet structure. Sintering temperature was increased 10 °C per minute until 1000 °C and 1200 °C and was kept at the sintering temperature for 2 hours. The samples were sintered at the first time sintering temperature as the second time they were pelleted.

The volume of SBF that is used for testing is the following Eq. 3.1:

$$Vs / Sa = 10 \quad (7.2)$$

where V_s is the volume of SBF (ml) and S_a is the apparent surface area of specimen (mm^2).

Samples were kept in the oven at 37 °C and SBF solution was refreshed after every 7 days. Samples in the SBF were characterized after 7 and 14 days period. To obtain the ion concentration change data in the SBF solution for each sample they were analyzed in ICP (Inductively Coupled Plasma). Hydroxyapatite formation on the pellet samples were analyzed with FT-IR, SEM and XRD devices. pH changes were also measured after every 7 days.

7.3.6 ICP-OES Analysis of SBF Solution

Ion releases during certain periods in SBF solution were analyzed with Inductively Coupled Plasma/Optical Emission Spectrometry.

7.3.7 TRIS Solution Preparation for Biodegradation Studies

TRIS solution was used to obtain in vitro biodegradation. TRIS is buffered solution and it does not contain ions so it gives an environment that calcium phosphate samples can dissolve in maximum level.

For preparation of TRIS solution 6.1 gram TRIS (Hydroxymethylaminamethane) were dissolved in the ultra-pure distilled water when the temperature was set to 36.5 °C. pH was set to 8 with drop by drop addition of 1 M HCl.

Sample powders were pressed under 100 bar pressure for 60 seconds. Prepared pellet samples were sintered for the second time due to reach tougher pellet structure. Sintering temperature was increased 10 °C per minute until 1000 °C and 1200 °C and was kept at the sintering temperature for 2 hours. The samples were sintered at the first time sintering temperature as the second time they were pelleted.

Pellet samples were soaked in the volume of TRIS that is used for testing using the following Eq. 3.1:

$$Vs / Sa = 10 \quad (7.3)$$

7.3.8 Cell Viability Studies

It is necessary to prepare a sample ion medium for cell studies. To prepare the sample-containing medium has concentration of 20 mg / ml (powder / DMEM-F12); 0.1 g of material was placed in 5 ml DMEM-F12 and left at 37 ° C for 24 hours. After 24 hours, the mixture was centrifuged; the supernatant was collected and then passed through a 0.2 μm filter for sterilization.

Cell culture, cell viability and cytotoxicity were examined in the following procedure:

Saos-2 osteoblast-like cells were cultured in DMEM-F12 supplemented with 10% FBS (fetal bovine serum) at 37 ° C in 5% CO_2. The culture medium was changed every two days. Cell viability was measured by MTT assay according to the manufacturer's protocol (Sigma USA). Cells were seeded in a 96-well culture plate to be $1x10^3$ cells for per well. After 24 hours of incubation, the sample extracts prepared with DMEM-F12 were added in different concentrations. After 7 days, 20 μl MTT solution (5 mg / ml) was added to each well. 100 μl of DMSO was added after additional incubation for 4 hours. Absorbance was measured at 540 nm with a microplate reader.

CHAPTER 8

RESULTS AND DISCUSSION

In this study, sea shell *Clinocardium ciliatum* and sea snail *Turritella terebra* were used as a resource of $CaCO_3$, H_3PO_4 was used as phosphate resource. Ca/P ratio was calculated as 10/6 for stoichiometric molar of hydroxyapatite so necessary H_3PO_4 volume was obtained.

$CaCO_3$ amount of powder samples were determined by Differential thermal analysis. % mass loss data obtained from DTA analysis to calculate the mass percentage of CaO. DTA analysis graphics are shown in the Figure 8.1 and Figure 8.2. DTA results are shown as percent mass loss in Table 8.1. In this study, 85% concentrated H_3PO_4 solution is used and the required volume is calculated for 2 grams of raw materials. Table 8.2 shows the necessary H_3PO_4 volume for 2 grams of raw material sample.

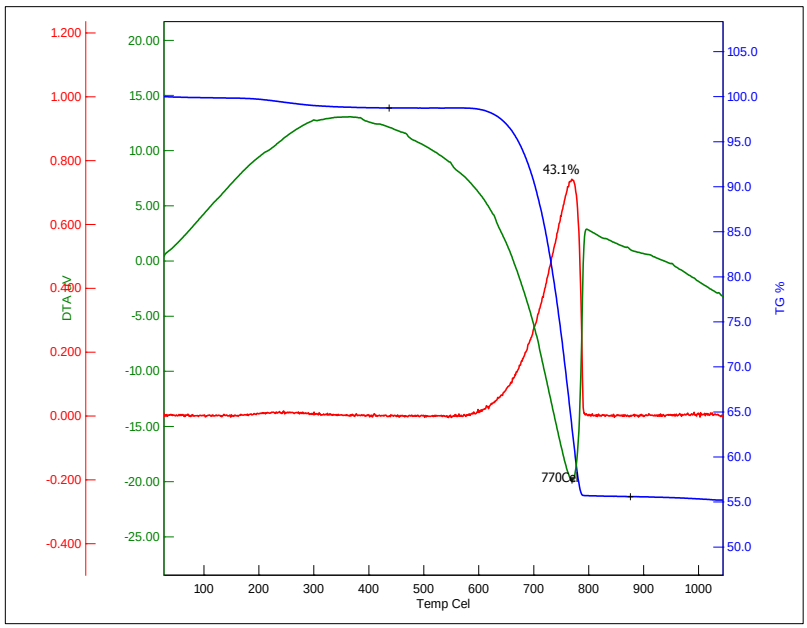

Figure 8.1 DTA analysis graphics of *Clinocardium ciliatum*

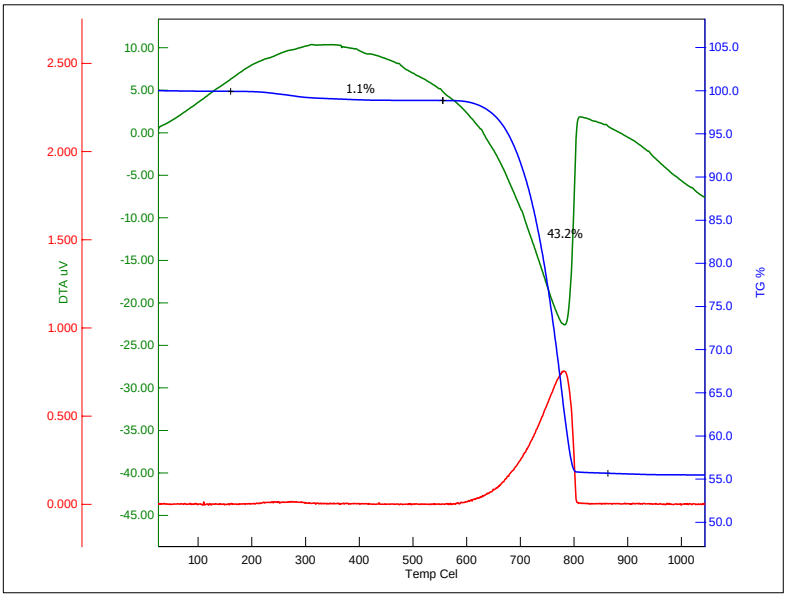

Figure 8.2 DTA analysis graphics of *Turritella terebra*

Table 8.1 Calcium contents of raw materials obtained from DTA analysis

Raw Material	Mass Loss (%)	Mass of CaO (%)	Moles of Ca in 2 g
Clinocardium ciliatum	43.1	56.9	0.02839
Turritella terebra	43.2	56.8	0.02834

Table 8.2 Phosphoric acid amounts used for bioceramic preparation

Origin	Moles of P	H_3PO_4 (µl/2g)
Clinocardium	0.017	822
Turritella terebra	0.01697	820.6

Mechanochemical synthesis method is used to obtain calcium phosphate materials with two different sintering temperatures; 1000 °C and 1200 °C. The mechanochemical process has the advantages of simplicity and reproducibility of a solid-state procedure to perform mass production and the basic characteristics of an ordinary wet reaction to

generate a powder with an acceptable microstructure. The samples were calculated as 2 grams and they were weighted after the reaction and sintering procedure. Amounts of bioceramic powders through the process for the samples were sintered at 1000 °C and 1200 °C are shown in the Table 8.3.

Table 8.3 Amounts of bioceramic powders through the process for the samples were sintered at 1000 °C and 1200 °C

Origin / Synthesis Method	Sintering Temperature(°C)	Initial Weight(g)	After the Reaction(g)	After the Sintering Process(g)
Clinocardium ciliatum	1000	2	2.05	1.77
	1200	2	2.13	1.95
Turritella terebra	1000	2	2.37	2.052
	1200	2	2.21	1.89

8.1 Fourier Transform Infrared Spectroscopy (FT-IR) Results of Samples

Figure 8.2 shows FT-IR spectrum of *Clinocardium ciliatum* and *Turritella terebra*. CO_3 bands can be seen at 858.32, 1093.63, 1454.33, and 1788.01. These bands can give an idea that the material is aragonite. Figure 8.3-8.4 shows FT-IR spectrum of samples at sintered 1000 °C and 1200 °C before and after SBF. In Figure 8.3A phosphate bands can be seen in 727.16, 875.68, 943.19, 970.19, 1001.06, and 1116.78. In Figure 8.3B phosphate bands present in 943.19, 970.19, 1001.06, 1078.21, 1116.78 and hydroxyl band present in the 3643.53. Figure 8.4A reveals HPO_4^{-2} vibration occurs at 725.23 which associated with Ca-deficient structure and in the range of 900-1300 phosphate stretches can be seen. Figure 4.4B displays hydroxyl band at 3568.31 and phosphate bands at 962.48, 1016.49, and 1085.92.

Moreover, the CO_3^{2-} group forms weak peaks as can be seen in all spectrums. As the process temperature increases, the intensities of the absorption bands for the PO_4^{3-} group become more distinctive and their characteristic peaks emerge more strongly.

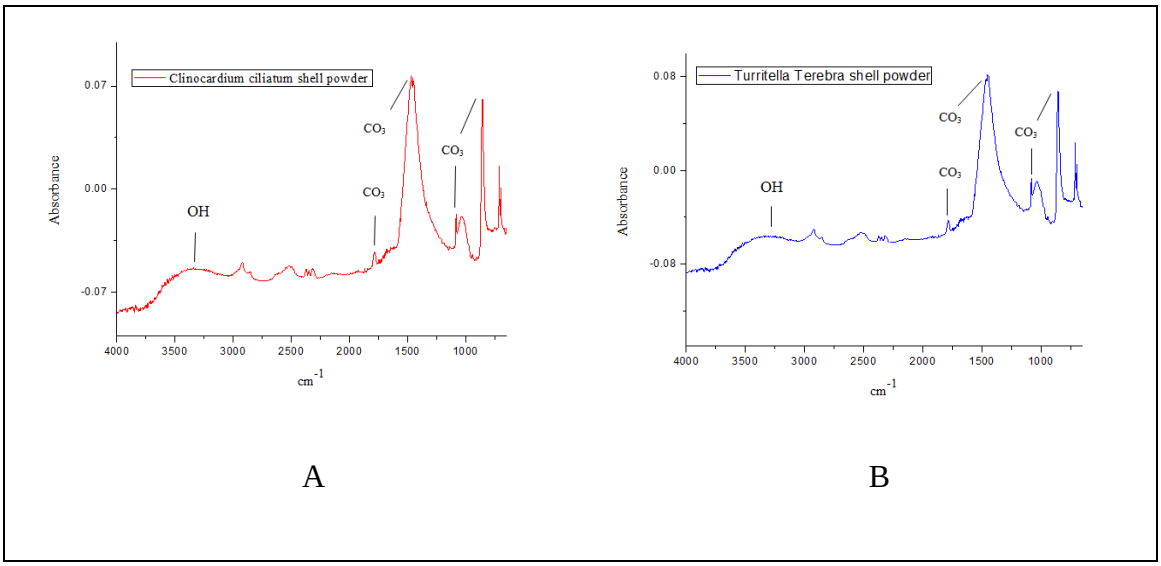

Figure 8.3 FT-IR spectra of A) *Clinocardium ciliatum* shell powder and B) *Turritella terebra* shell powder

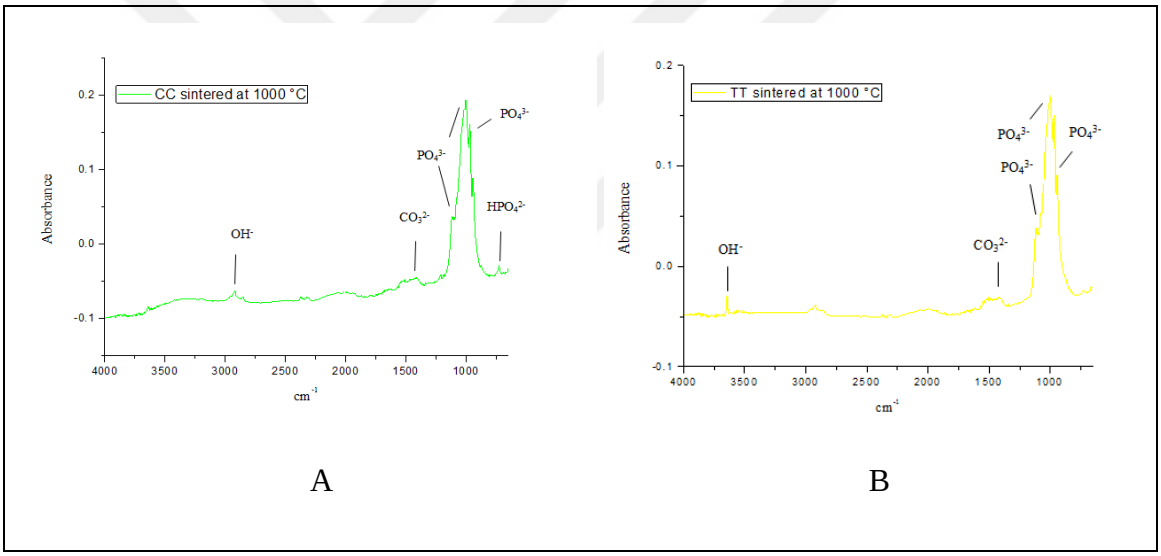

Figure 8.4 FT-IR spectra of sintered samples at 1000 °C A) produced from *Clinocardium ciliatum* B) produced from *Turritella terebra*

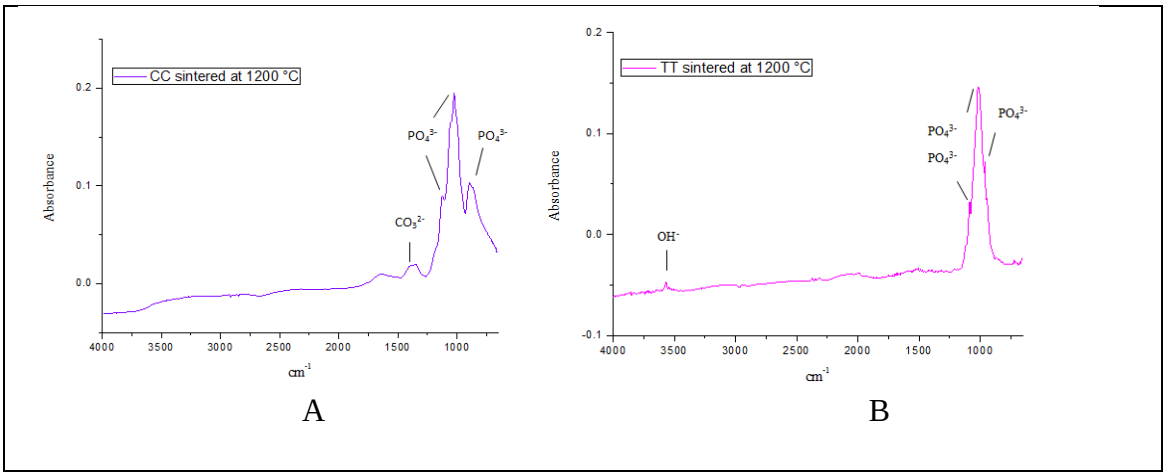

Figure 8.5 FT-IR spectra of sintered samples at 1200 °C A) produced from *Clinocardium ciliatum* B) *Turritella terebra*

8.2 X-Ray Diffraction (XRD)

As the produced samples were heated from 450 °C to 1200 °C, the peak height of the samples increases substantially, with an associated narrowing of the peak corresponding to increase in crystallinity. Figure 6 displays of aragonite which is naturally occurring $CaCO_3$ mineral. Figure 8.7A and 8.7B displays $Ca_2P_2O_7$. As it can be seen TCP occurred after the heating temperature had reached at least 850 °C. Figure 8.7A displays $Ca_2P_2O_7$ and 8.7B displays whitlockite. Figure 8.8A displays whitlockite and Figure 8.8B indicates β-tricalcium phosphate X-ray diffraction patterns. The term whitlockite was coined as a synonym for TCP identified by its X-ray diffraction in phosphate rocks. β -TCP is stable at room temperature and transforms at 1125 C to α –TCP. 2θ ranges 30.5 - 31.6, 37.0 - 38.5, 23.8 - 24.8, 5 38.5 - 59.0 can be attributed to β–TCP, and 2θ ranges 29.3 - 30.2, 30.5 - 31.6 can be attributed to α–TCP. In Figure 8.10B, HA showed its characteristic peaks at 25.87, 28.89, 31.73, 32.18, 32.86, 34.04 [109], [110]. Table 8.4 shows XRD results of the samples.

Table 8.4 XRD Results of the samples

	450 °C	850 °C	1000 °C	1200 °C
Clinocardium ciliatum(CC)	Calcium Phosphate	Whitlockite	Whitlockite	Whitlockite
Turritella terebra (TT)	Calcium Phosphate	Calcium Phosphate	TCP	Hydroxyapatite

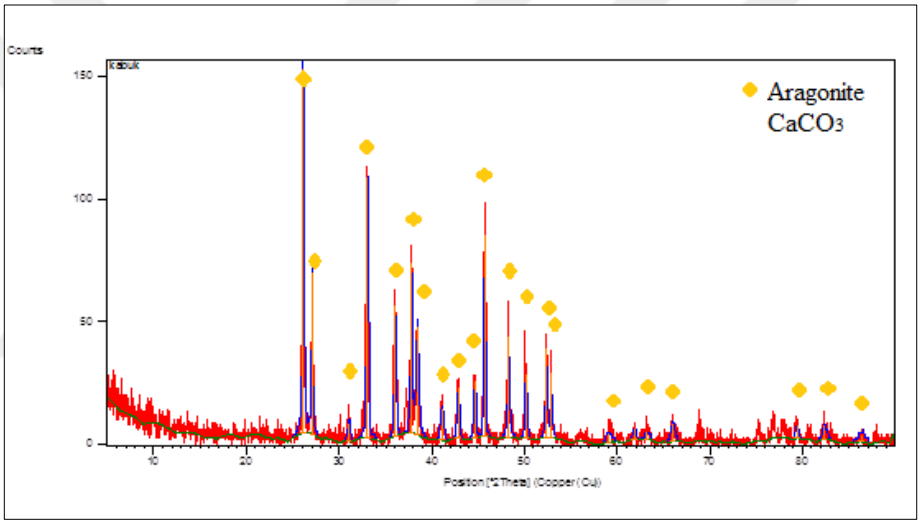

Figure 8.6 XRD patterns of sea shell *Clinocardium ciliatum*

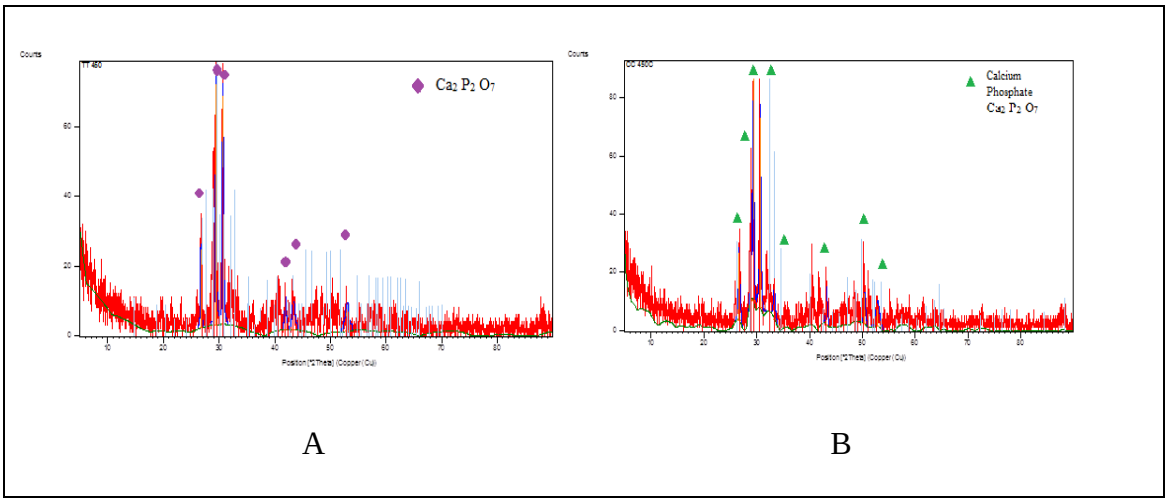

Figure 8.7 XRD patterns of sintered samples at 450 °C A) produced from *Clinocardium ciliatum* B) *Turritella terebra*

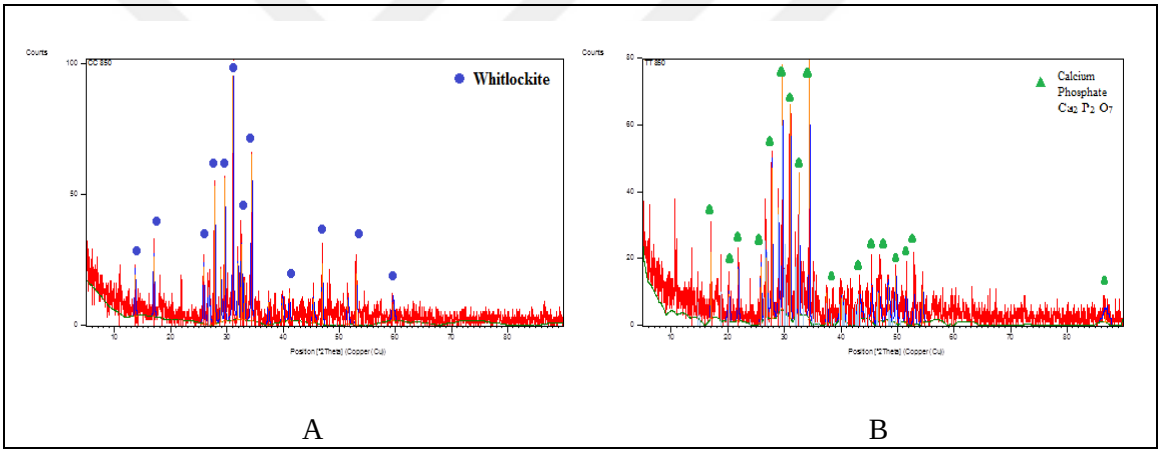

Figure 8.8 XRD patterns of sintered samples at 850 °C A) produced from *Clinocardium ciliatum* B) *Turritella terebra*

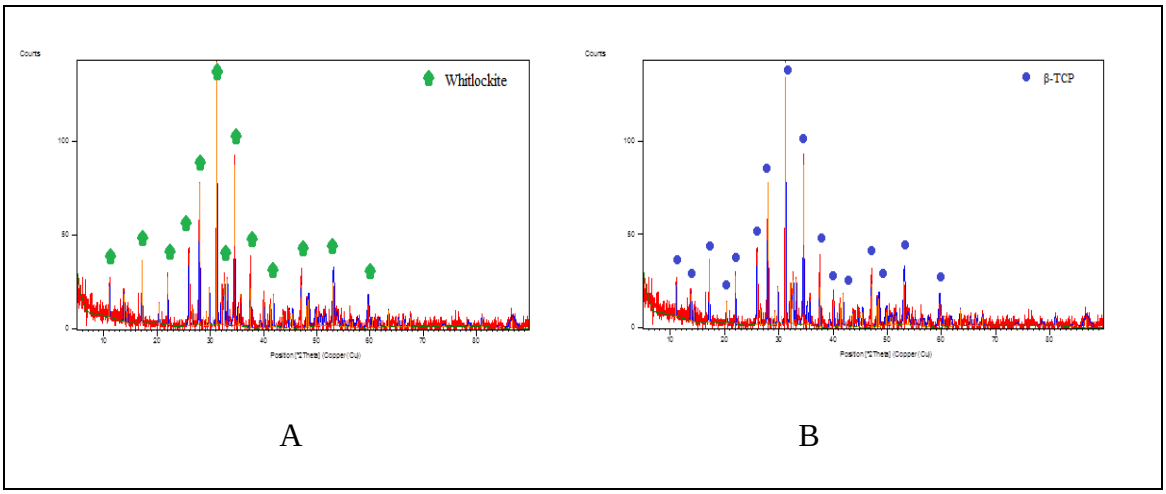

Figure 8.9 XRD patterns of sintered samples at 1000 °C A) produced from *Clinocardium ciliatum* B) *Turritella terebra*

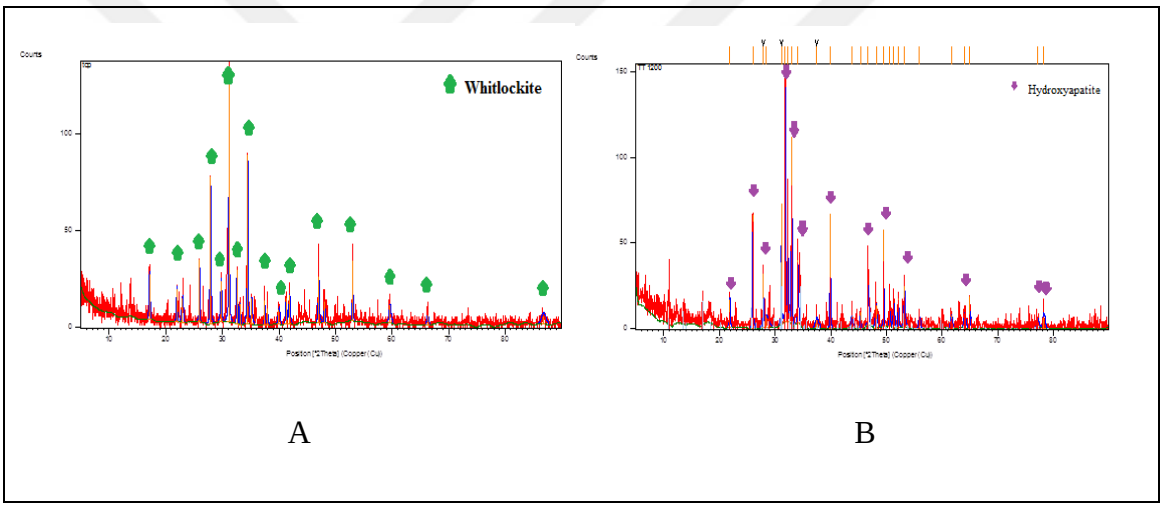

Figure 8.10 XRD patterns of sintered samples at 1200 °C A) produced from *Clinocardium ciliatum* B) *Turritella terebra*

8.3 BET Aanalysis of the Samples

Porous structure analysis was performed by adsorption - desorption gas analysis. Nitrogen was used in the analysis. Properties of nitrogen are known and it can be easily adsorbed on the surface of solids. The detailed parameters of the pores dispersed on the hydroxyapatite grains were measured by N_2 adsorption–desorption isotherms method. BET analysis results show that specific surface area and pore volume decreases with increasing sintering temperature.

Table 8.5 Specific surface area, pore volume and average pore diameter of samples

Origin	Sintering Temperature(°C)	Specific Surface Area(m^2/g)	Pore volume cm^3/g	Average Pore Diameter (4V/A by BET)
Clinocardium ciliatum	1000	0,9175	0,000878	3,82 nm
	1200	0,1475	0,000071	1,94 nm
Turritella terebra	1000	1,0925	0,001270	4,65 nm
	1200	0,4189	0,000057	0,54 nm

Average particle diameter was calculated in the following Eq. 8.1 and results are shown in the Table 8.2 :

$$d = \frac{6}{\left(BET\ surface\ Area\ in \frac{m^2}{g}\right) x \left(Density\ in \frac{g}{cm^3}\right)} \quad (8.1)$$

Table 8.6 Average particle diameter of samples

Origin	Sintering Temperature (°C)	Average particle diameter (m)
Clinocardium ciliatum	1000	$20.6x10^{-7}$
	1200	$126x10^{-7}$
Turritella terebra	1000	$17.4x10^{-7}$
	1200	$45.2x10^{-7}$

8.4 SEM/EDX of Samples

Morphology changes of the surfaces of the samples in SBF were determined using SEM. Samples before soaking in SBF and after soaking in SBF were visualized. Aggregation of HA was observed after soaking in SBF. After 7 days Ca/P ratio decreased for the samples were produced from *Clinocardium ciliatum* and sintered at

1000 °C and 1200 °C (CC 1000 and CC 1200). It can be attributed to Ca-deficient hydroxyapatite was obtained (Figure 8.11). On day 14^{th} and 21^{th} hydroxyapatite formation occurred. After 3 weeks, surface of the sample was produced from *Turritella terebra* and sintered at 1000 °C was covered with HA.

EDX analysis showed that there are measurable quantities of Cl^-, Na^+, and Mg^{2+} impurities on the surface of precipitated apatite. These impurities are ions that presented in simulated body fluid and bonded to apatite. Ca/P ratio of the samples before and after soaking in SBF can be seen in Table 8.2.

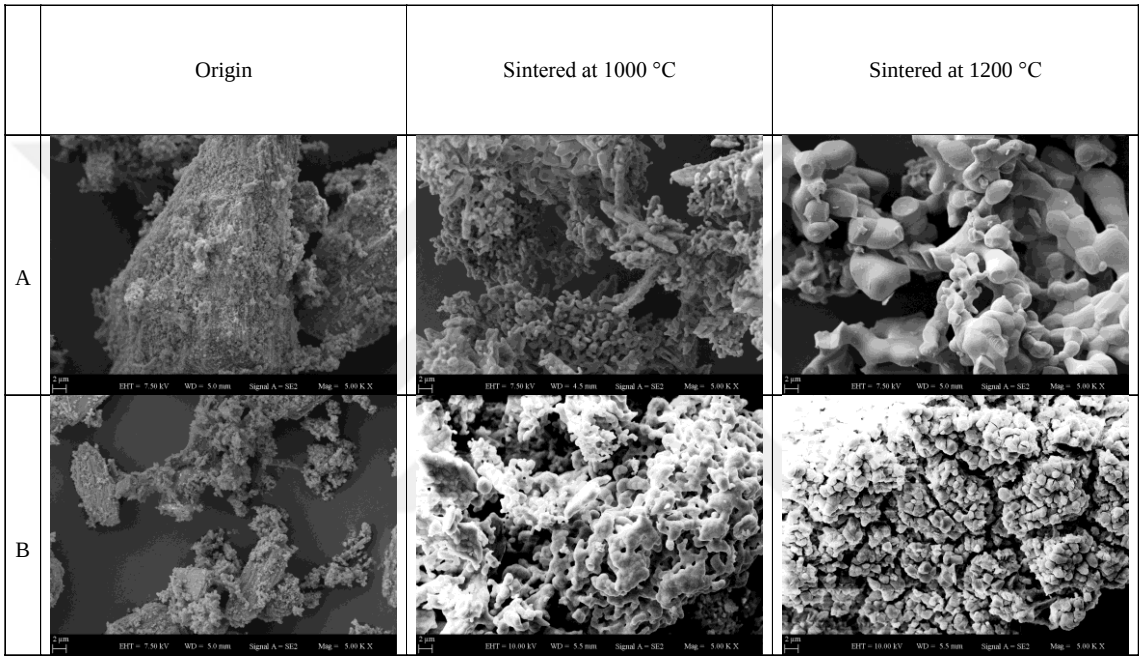

Figure 8.11 SEM images of samples produced from (A) sea shell *Clinocardium ciliatum* (B) sea snail *Turritella terebra* (5000x)

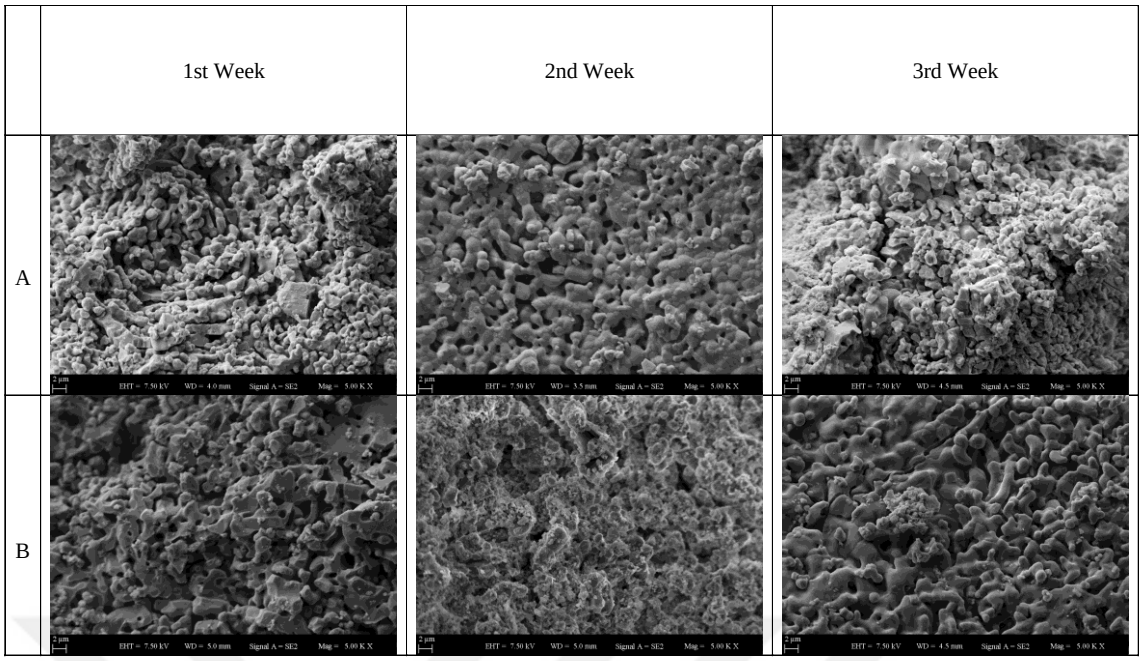

Figure 8.12 SEM images of samples produced from sea shell *Clinocardium ciliatum* (A) sintered at 1000 °C (B) 1200 °C after soaking in SBF (5000x)

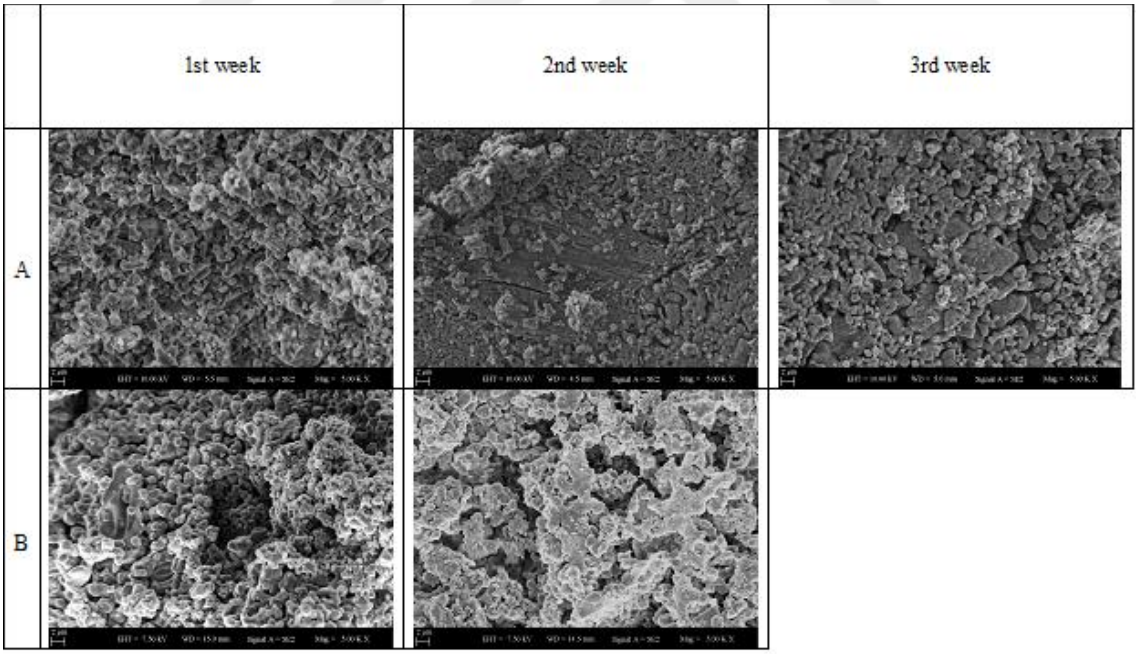

Figure 8.13 SEM images of samples produced from sea snail *Turritella terebra* (A) sintered at 1000 °C (B) 1200 °C (5000x)

Table 8.2 Ca/P ratio of the samples before and after soaking in SBF

Sample	Before soaking in SBF	Day 7th	Day 14 th	Day 21 th
β-TCP (CC1000)	2,05	1,43	2,10	1,93
α-TCP (CC 1200)	1,92	1,38	3.7	1,69
β-TCP (TT1000)	1,88	1,95	1,35	1,52
Hydroxyapatite (TT1200)	2.01	1,88	2,12	-

8.5 ICP-OES Analysis of SBF Solution

In simulated body fluid new solid phase transformation occurs; solid-phase forms from liquid phase and bone-like apatite grows on the surface of the calcium phosphate ceramics. This process consists two stages: nucleation and crystal growth. The apatite formation from the SBF solution usually is considered as a process of heterogeneous nucleation on calcium phosphate ceramics following the spontaneous growth of crystals. Heterogeneous nucleation process needs suitable nucleation sites on the sample and the enough supersaturability of Ca and P ion concentration in the solution. Thus this process is crucial to apatite formation. Parameters of SBF and experiment conditions have influence on the induction period for apatite nucleation. Normal SBF provide a medium for apatite formation; however it is not sufficient medium for spontaneous nucleation due to it does not provide required Ca and P ions concentration. There should be higher supersaturation of Ca and P ions for nucleation than for crystal growth in the SBF near the solid surface. The nucleation occurs when the Ca^{+2} ion concentration of the surface of the samples reaches to certain level. When Ca^{+2} and HPO_4^{2-}

concentrations increase in SBF apatite formation and the induction accelerates. In closed static solution, the nucleation formation is faster than in dynamic solution. If there are sufficient ions available in SBF, crystal nucleus grows to certain size and grows naturally. Apatite nuclei consumes Ca and P ions from surrounding fluid and it takes spherulitic shape.

The adhesion of ions to solid surface is relative to the pH of medium. When pH of the medium is higher than the isoelectric point of the surface, solid surface would be negative electrically, which exhibits strong adsorption to positive ions. The isoelectric point of CaP ceramic is lower than SBF; hence the surface of CaP ceramics is electrically negative in the SBF. Therefore, CaP ceramics exhibits strong adsorption to positive ions in the SBF solution when bone-like apatite formation occurs. Then, opposite ions, that is, negative ions, are attracted to the solid-liquid interface. Ca^{2+} first appeared on the surface of calcium phosphate ceramics and subsequently HPO_4^{2-} is attracted.

Concentration of Ca and P in the solution increases when the release of Ca^{2+}, HPO_4^{2-} and PO_4^{3-} form the surface of CaP ceramics. These ions, together with ions in SBF, react directly with the solid surface of the material through static electricity and finally result in adhesion of ions in solution to the solid surface. The second stage of bone-like apatite formation began after reaching a certain value of concentration of ions subsequently nucleation formation. After crystal nucleus forms, Ca and P in the solution decreases[111]. In dynamic solution, ions are driven to move by two different mechanisms transmission. The first is the concentration-gradient-driven ion dispersion. The second is the stress-gradient-driven ion transportation. The resultant ion movement in solution is called convective dispersion. The flowing rate caused by convection is in direct proportion to the flowing rate and ion concentration of the solution. In cycling SBF, ions dissolved from the sample surface can easily leave the sample surface to enter the SBF solution under the function of concentration-gradient-driven dispersion and stress-gradient-driven transportation. In cycling SBF, ions leave the sample surface and diffuse to SBF solution under the function of concentration-gradient-driven dispersion and stress-gradient-driven transportation. Ca and P ions on the sample surface can only be slightly higher than that in the solution and so, ions can not easily concentrate on the surface. The threshold for nucleation is difficult to reach. The SBF flowing may remove the excessive Ca and P ions from the sample surface and take away supersaturated Ca

and P come from the ceramic material, thus the nucleation on the surface will be avoided. Tang et al. reported that TCP dissolves faster that HA[112]. Reaction of the dissolution of TCP in aqueous solutions is:

$$3Ca_3(PO_4)_2\,(s) + H_2O \rightarrow 9Ca^{2+}\,(aq) + HPO_4^{\ 2}(aq) + 5PO_4^{\ 3}\,(aq) + OH^-\,(aq) \qquad (8.2)$$

Calcium-deficient hydroxyapatite (CDHA), $Ca_9(OH)(HPO_4)(PO_4)_5$ forms while β-TCP dissolves and the above aqueous ions incorporate together. CDHA can also combine with CO_3^{2-} ions and it is deficient of Ca^{2+} and OH^- in the unit cell of its crystal structure. CDHA yields the same XRD pattern with that of stoichiometric HA.

Precipitation increases with increasing surface area in contact with simulated body fluid which it promotes the dissolution of the sample. Powders that have high porosity would have high contact with fluid.

Perera et. al. studied effect of sintering conditions (temperature and time) on the microstructure (density and grain size) and mechanical properties. They produced β - TCP from Ca-deficient commercial powders and sintered at under the following conditions: temperatures of 1100, 1200, and 1300 °C, times of 1, 3, 5, and 7 h, air atmosphere and heating and cooling rates of 10 °C/min [69]. Optical performance was succeed in samples sintered at 1200 °C for 3 hours. They reported that microstructure refinement improves densification kinetics allowing TCP to be sintered at shorter times and/or lower temperatures.

Niakan et. al. obtained natural porous hydroxyapatite from bovine bone [113]. Bovine bone samples were sintered at different sintering temperatures from 600 °C to 1000 °C. Results exhibited that thermal stability of the HA matrix was not disrupted and they showed phase pure HA. It is determined that Ca/P ratio decreased with increasing sintering temperature and HA at 750 °C is optimum temperature to fabricate a well-defined porous HA.

Agnıeszka et. al. [114] examined *in vitro* (in SBF) behavior of hydroxyapatite (HA) obtained from pork bone sludge via different calcination methods with various temperatures from 650 °C to 950 °C with various holding times. Produced samples were soaked in SF for 62 days and they were analyzed by X-ray diffraction (XRD), FT-IR, SEM and EDX methods. It is been reported that different sintering temperatures has effect on behavior in SBF. Ca/P ratio decreased in all samples. pH was increased excessively at first days and continued to increase gradually in three weeks. Weight

increase was attributed to formation of the HPO^{2-}_4 -free HA in agglomerates on the surface of the samples and their pores.

Muralithran et. al. [115] studied effects of grain size on the relative density and hardness. They found that sintering behavior has impact on microstructure of hydroxyapatite. They sintered the samples at various temperatures from 1000 °C to 1450 °C with dwell time of 2 hours. It was seen that optimum sintering temperature is 1250 °C with a microstructure refinement and TCP was obtained at temperatures after 1400 °C.

Brazda et. al. [116], produced hydroxyapatite with ranging temperatures from 150 °C to 1200 °C. They examined the behaviors of samples in simulated body fluid and TRIS. They found that specific surface area decreased from 64.4 m^2/g at 150 °C to 0.17 m^2/g. Produced β-TCP dissolves in TRIS 2 times faster than in non-buffered water. It is been suggested that reaction of TRIS buffer solution with Ca^{2+} and Mg^{2+} ions to form a soluble complex compound and it leads to faster dissolution rate. Bioactivity of β-TCP and HA was confirmed in simulated body fluid by formation of HA. Dissolution rates were calculated from concentration changes. It is found that within 40–50 hours the dissolution process achieved the steady state.

Rocha et. al. [117] produced hydroxyapatite and TCP ceramics from cuttlefish bones at 200 °C and they examined their sintered behaviors at various temperatures between 1000 °C to 1400 °C (±5°C) with an interval of 50°with dwell time of 1 hour. Materials were in vitro behaviors were examined in simulated body fluid and cell culture. Results exhibited that sintering temperature effects the microstructure of the scaffolds. Refinement of grains was developed after sintering temperature of 1200 °C. Materials immersed in SBF for 1 and 2 weeks and their bioactivity was confirmed. MTT assay studies showed that increase of 24% of viability/proliferation in the presence of HA.

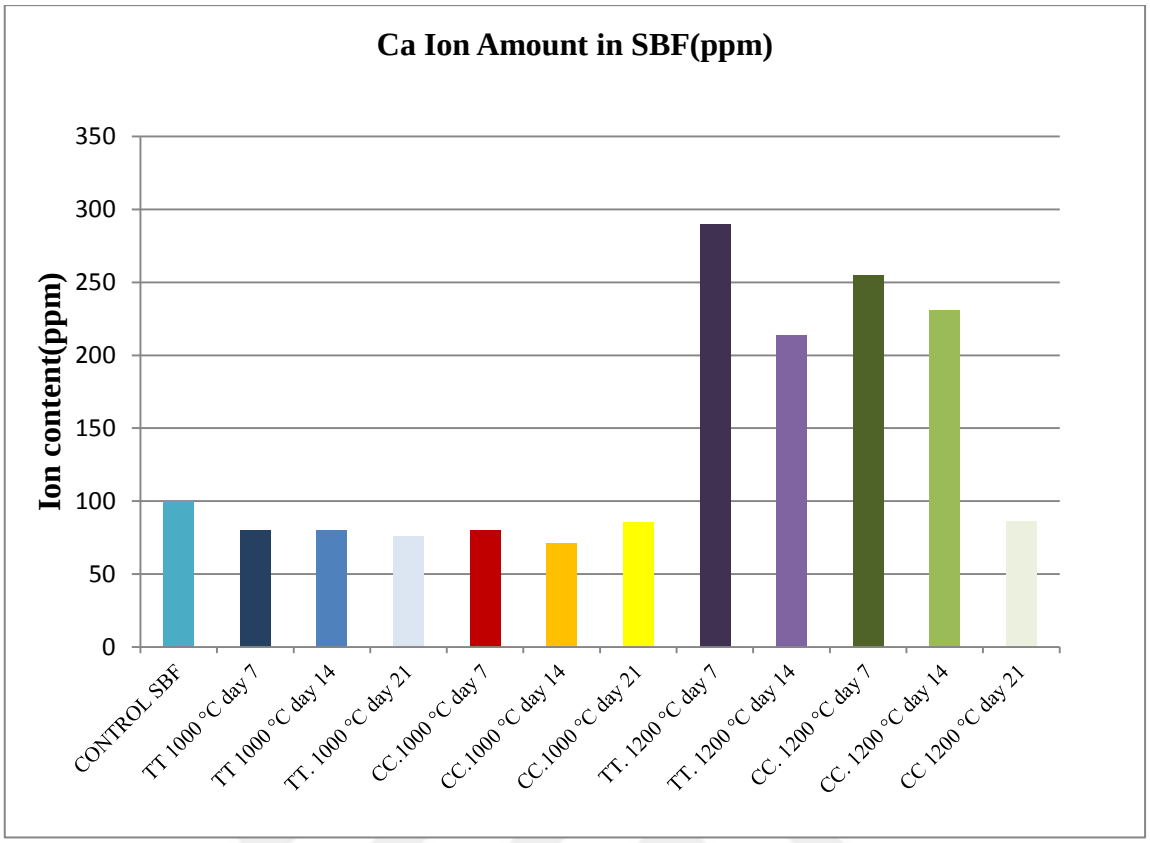

Figure 8.14 Ca ion content of samples in SBF

ICP-OES results show the Ca, P, Mg ion content of the samples. In Figure 8.14, it can be seen that Ca^{2+} ion contents decreased in samples that was sintered at 1000 °C, increased in samples that was sintered at 1200 °C. Samples were sintered at 1000 °C contains β-TCP. Ca^{2+} ions are consumed which it can be attributed to in formation of HCA (hydroxy carbonate apatite layer) which leads to HA formation. Ca^{2+} ion release decreased relatively in samples was sintered at 1200 °C which shows HCA formation increased by time. Ca^{2+} increase in the first week can be reason of Ca^{2+} dissolution from the sample.

Figure 8.15 shows P ion content of the samples in SBF in 7, 14, 21 days respectively. P ion content decreased in all samples compared to the sample before soaked in SBF which this shows Ca^{2+} ions were consumed to form HCA layer. Generally Ca^{2+} ion decreased by the time samples soaked in SBF. For samples was sintered in 1000 °C Ca^{2+} ions in SBF decreased comparing to samples were sintered in 1200 °C which Ca^{2+} consumption can be attributed that hydroxyapatite formation.

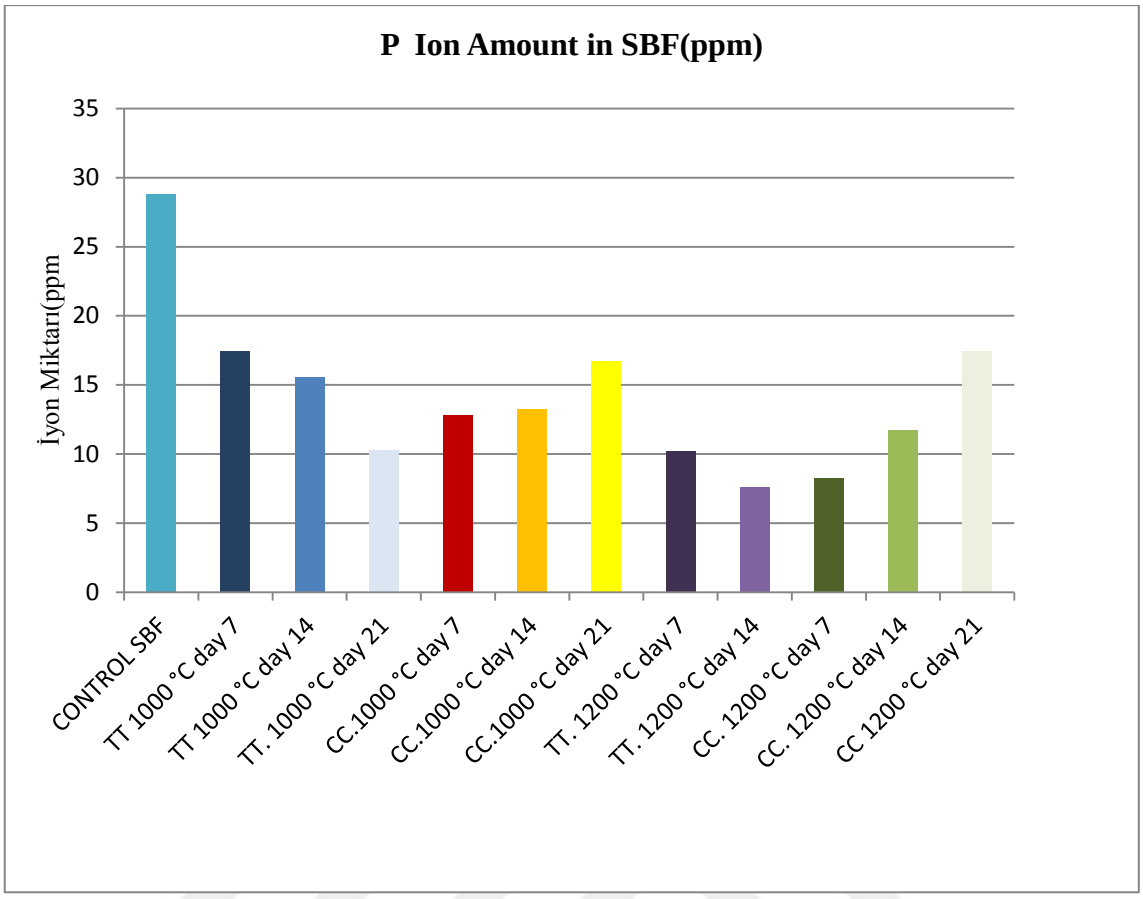

Figure 8.15 P ion content of samples in SBF

Figure 8.16 shows Mg content of samples before and after soaking in SBF. Mg ion did not change excessively comparing to before soaking SBF. Mg^{2+} content in SBF decreased after immersion in simulated body fluid, indicating that magnesium is incorporated into the hydrolysis product. The transformation from CDHA into HA is influenced by the presence of ions in the solution, especially Mg^{2+}. It is determined that in the presence of Mg^{2+} ions, the ACP phase field expanded at the expense of the CDHA field. It is reported that the presence of Mg^{2+} ions enhanced ACP formation and retarded the transformation of ACP into other calcium phosphates at a given degree of supersaturation [118].

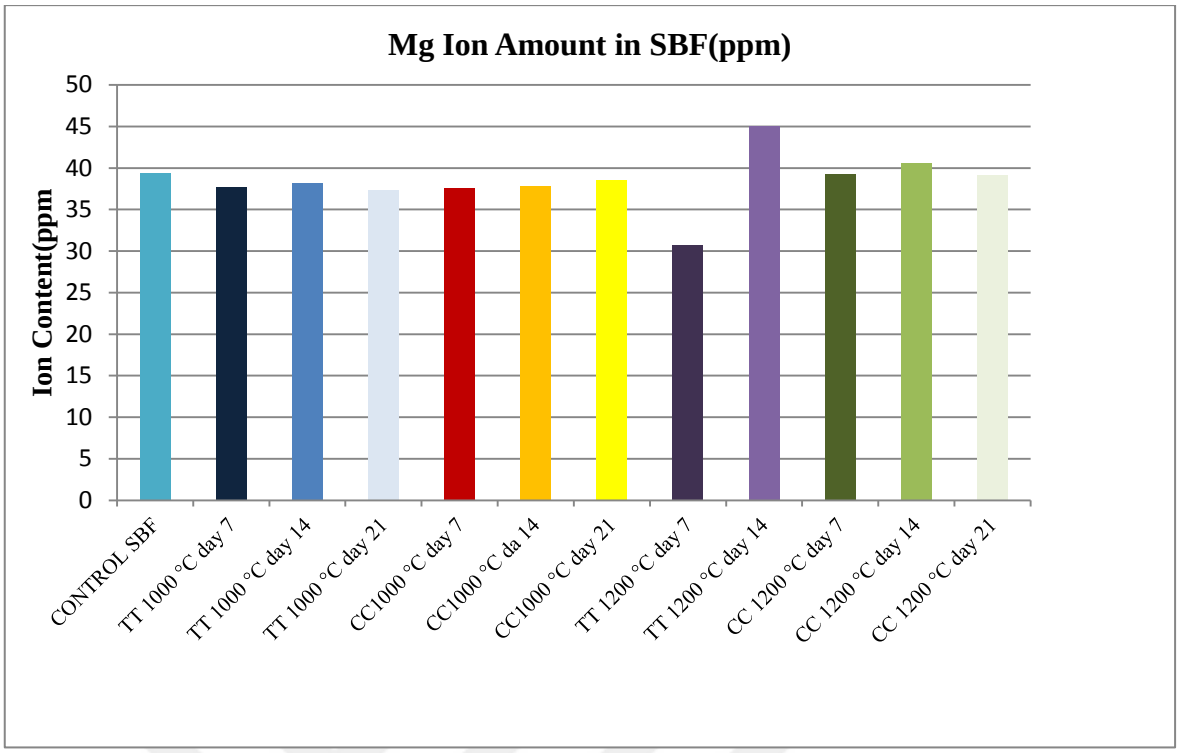

Figure 8.16 Mg ion content of samples in SBF

8.6 FT-IR Results of Samples in SBF

FT-IR analysis revealed the formation of carbonate bands after soaking in SBF. Also phosphate group's intensity increased and new phosphate peaks occurred after soaking in SBF. FT-IR data shows the presence of CO_3^{2-} around 1500 cm^{-1} and HPO_4^{2-} groups around 1000 cm^{-1} in all SBF soaked samples.

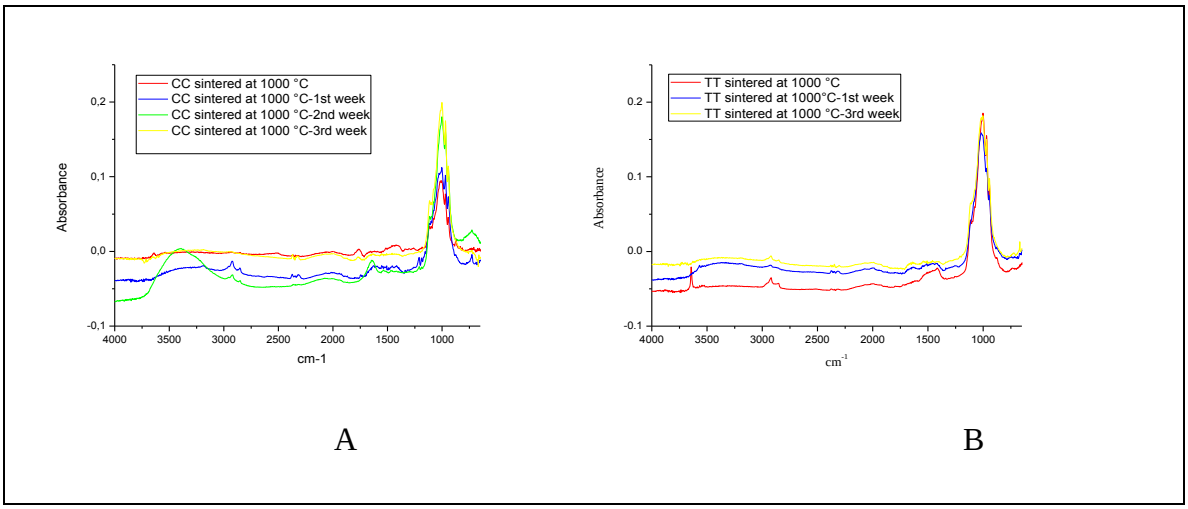

Figure 8.17 *Clinocardium ciliatum* (A) and *Turritella terebra* (B) that was sintered at 1000 °C: before and after soaking in SBF

Figure 8.17A shows CO_3^{2-} band intensity increased after 7 days immersion in SBF and P-O bands formed due to formation of HCA. Peak intensities decreased relatively by time which may be interpreted that HCA formation decreased over time. Figure 8.11B shows CO_3^{2-} and OH^- band intensities were increased after 7 days immersion in SBF. After 14 days of immersion in SBF peak intensities are relatively less comparing to 7 days of immersion in SBF.

It is been determined that superficially deposited layer of Ca-deficient HA, having HPO^{-}_4 incorporated is as given below:

$$(H^+ + PO^{3-}_4)_{solution} \rightarrow (HPO^{2-}_4)_{solid} \quad (8.3)$$

HA, precipitated from water solutions was Ca-deficient and contained internal hydrogen bonds between oxygen of adjacent orthophosphate groups, resulting in the presence of HPO^{2-}_4, not observed in the stoichiometric hydroxyapatite. Since then HPO^{2-}_4 ion has always been referred to as the absorption band in IR spectra in synthetic as well as in some biological apatites [114].

Figure 8.18 represents a typical FT–IR spectrum after discs were soaking in SBF, gave an evidence that HA containing HPO^{2-}_4 appeared.

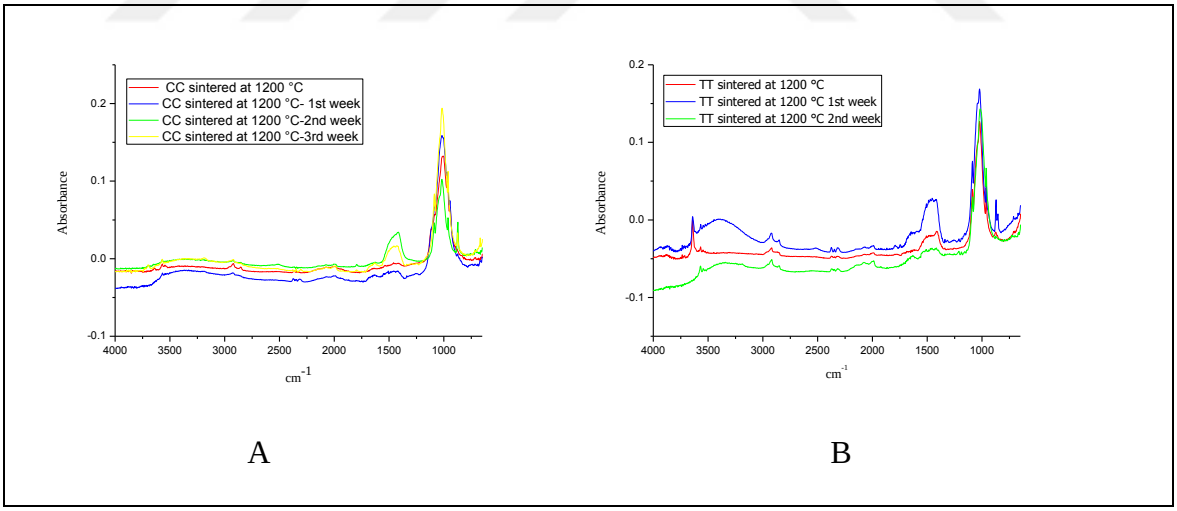

Figure 8.18 *Clinocardium ciliatum* (A) and *Turritella terebra* (B) that was sintered at 1200 °C: before and after soaking in SBF

8.7 pH Changes in SBF

pH changes of the pelleted samples are shown in Figure 8.19. pH of samples were sintered at 1200 °C increased excessively after 7 days. pH of the samples sintered at 1000 °C increased slightly in 7 days. Increase of the pH can be attributed to HPO_4

formation in SBF solution. After 7 days pH decreased and balances which means ions balanced in medium. pH changes give information about dissolution of the samples.

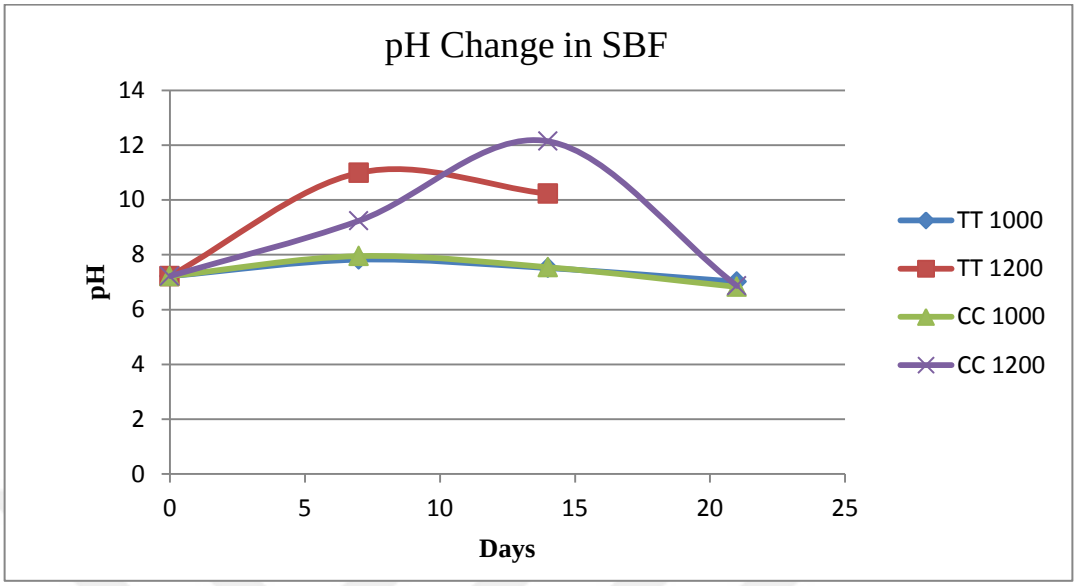

Figure 8.19 pH changes of the samples after soaking in SBF

8.8 pH Changes Occurs in the TRIS Solution

In vitro biodegradation behaviors were investigated in TRIS solution. Pelleted samples were soaked in TRIS solution for 7 days and pH changes were measured per day. Soaking calcium phosphate ceramics in their solutions cause loss of mass due to they release ions to solution. pH changes of samples gives information of their bioactivity a biodegradation due to release of Ca^{+2} and P ions.

It can be seen that pH of α-TCP produced from *Clinocardium ciliatum* and produced β-TCP from *Turritella terebra* increased excessively. This can be attributed that produced dissolution of α-TCP (CC1200) and β-TCP (TT1000) are very high (Figure 8.20).

pH of produced hydroxyapatite (TT1200) did not change which means it did not dissolved in high level. pH of produced β-TCP from *Clinocardium ciliatum* (CC1000) increased to 8.4 after 7 days. After 3^{th} day pH of the samples were balanced which can be attributed to Ca^{+2} ions are balanced in the medium.

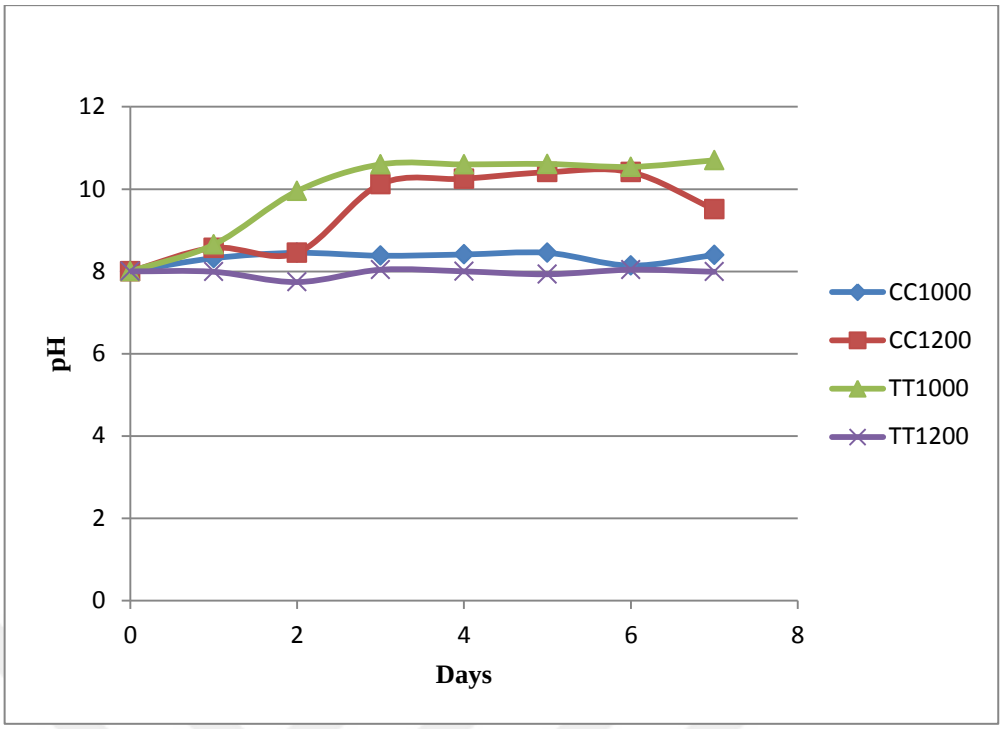

Figure 8.20 pH changes of samples in a TRIS solution in 7 days

8.6 Cell Studies

In cytotoxicity assay, different parameters are crucial to evaluate sample's compability. These parameters can be time of culture, biochemical assay type, cell lines, and controls. It is suggested to conduct a preliminary *in vitro* study to have more clear information in a biological medium.

The surface chemistry of sample defines the initial in vitro interactions of proteins, such as fibronectin with integrin cell-binding domains, which in turn arrange the cell adhesion process. Cell response to the CaP surfaces of this study can be regarded as the sum of their ability to attach, proliferate, and differentiate. In the attachment stage, cell filopodia search the substrate topography for the points to cell can adhere. Function of these filopodia is sensing the substrate and to extend over from the cell surface and find points for attachment.

In this study MTT was used as tetrazoliumformazan material. MTT is a positively charged compound that can be easily degraded in the cell by passing the membrane of the eukaryotic cells, but the degrading formazan is water-insoluble and thus precipitates in the form of crystals in the medium. The tetrazolium ring can only be broken by active mitochondria, so that the color reaction can only take place in living cells. The dead

cells lose their ability to reduce tetrazolium compounds and do not cause any color change. The amount of signal produced by the measurement is directly related to parameters such as tetrazolium salt concentration, cell type, number of viable cells and metabolic capacity, medium content, medium pH, plate-flask or well structure. The MTT compound is yellow and the formazan formed in purple. It is insoluble in water and should be dissolved in a suitable solvent to measure the absorbance. The use of dimethyl sulphoxide (DMSO) is suggested by Denizot and Lang (1986) to solve the formazan formed in the MTT test. As a solvent, the toxic effect of the generally preferred DMSO on cells is known, which reduces test reliability. Also damage to formazan crystals during pipetting to dissolve is another effect that reduces test sensitivity[119].

Samples were seeded to SAOS-2 osteoblast-like cells at concentrations of 20 μg / ml, 50 μg / ml, 100 μg / ml and 200 μg / ml for 24 hours and 7 days. Studies showed that samples do not have toxic affect on cells. Figure 8.21 and 8.23 show absorbance values of the samples. Figure 8.22 and 8.24 show cell viability of the samples at different concentrations.

Cell viability increased as the concentration increases in all samples in 24 hours. For samples were produced from *Clinocardium cilium* and sintered at 1000 °C highest cell viability is in concentration of 100 μm. For samples were sintered at 1200 °C highest cell viability is in concentration of 200 μm. For samples produced from *Turritella terebra* at 1000 °C concentration was increased gradually with amount of concentration.

For 7 days, cell viability increased gradually with concentration for samples produced from *Clinocardium cilium* at 1200 °C. Highest cell viability is in the concentration of 10 μm for samples were produced from *Cilinocardium cilium* and sintered at 1000 °C. Highest cell viability is in the concentration of 200 μm. for samples were produced from *Cilinocardium cilium* and sintered at 1200 °C. Highest cell viability is in the concentration of 200 μm for samples were produced from *Turritella terebra*.

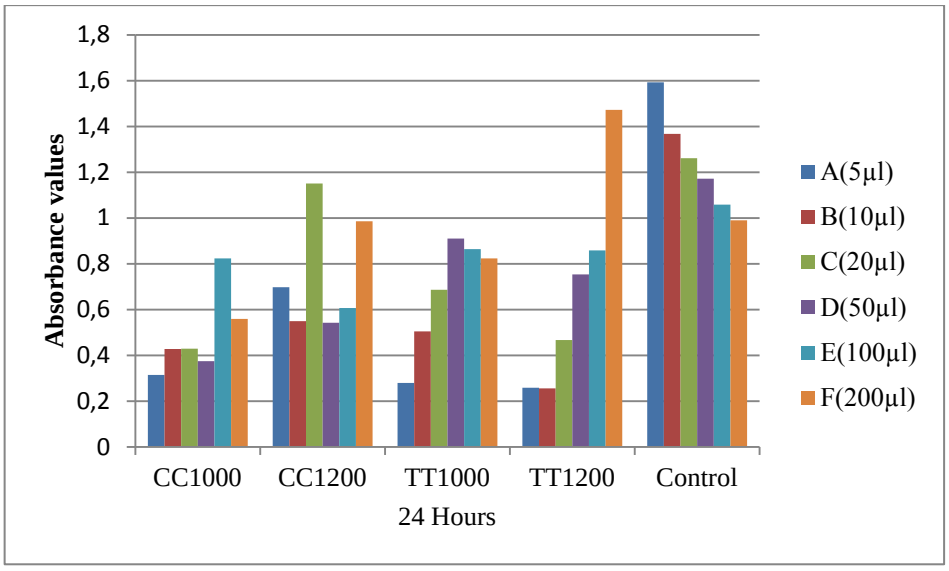

Figure 8.21 Absorbance values of samples after 24 hours

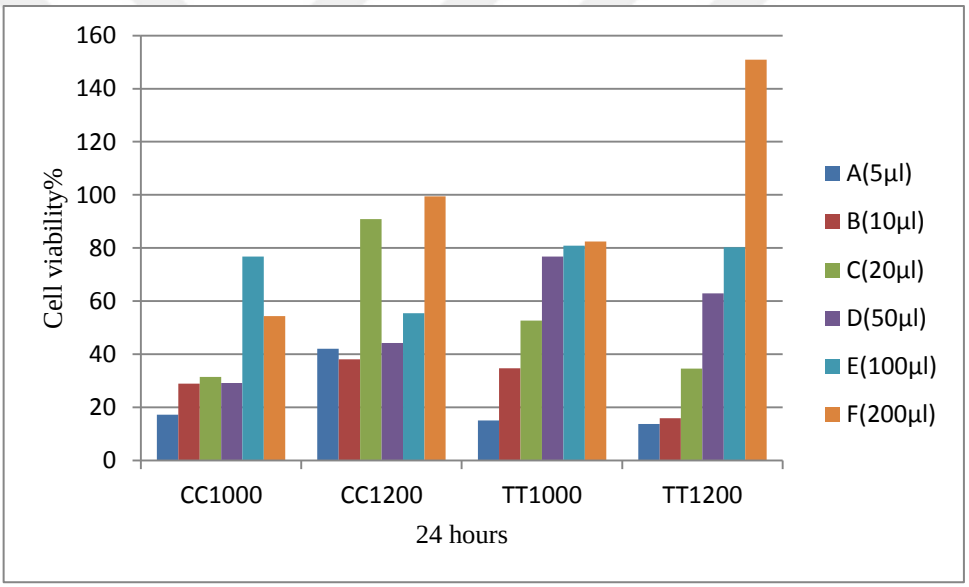

Figure 8.22 %Cell viability of samples after 24 hours

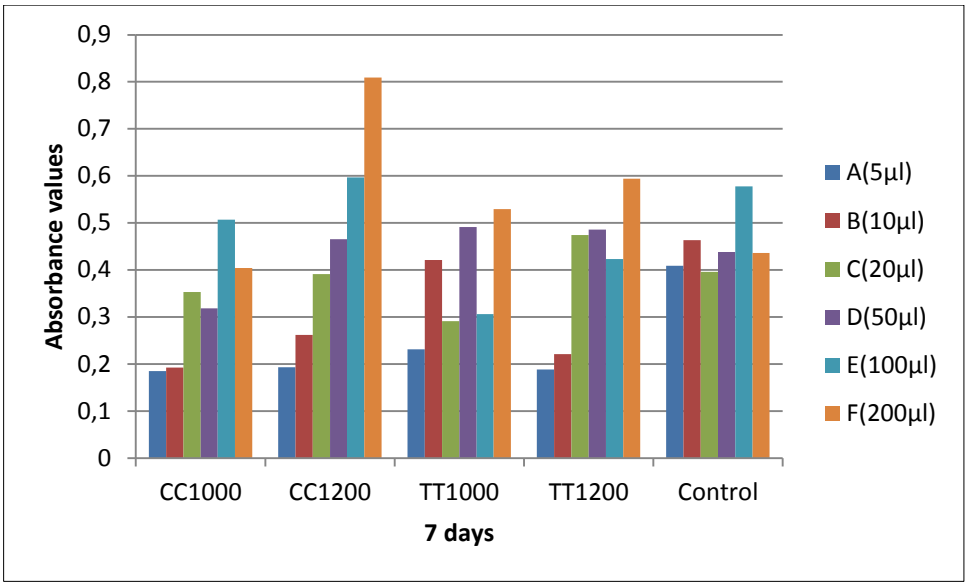

Figure 8.23 Absorbance values of samples after 7 days

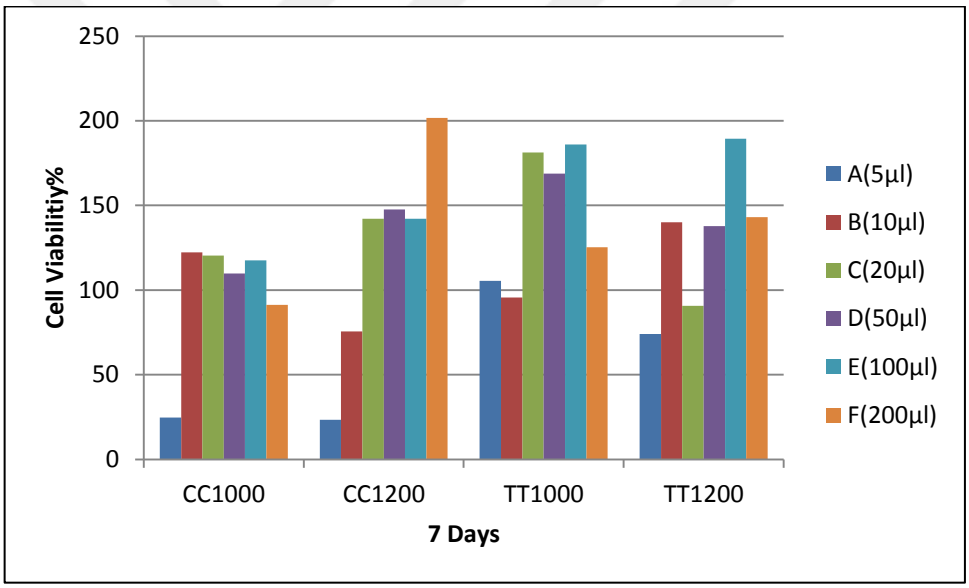

Figure 8.24 %Cell viability of samples after 7 days

CHAPTER 9

CONCLUSIONS AND RECOMMENDATIONS

In this study aragonite in *Clinocardium Cilium* and *Turritella terebra* were transformed to different bioceramics via mechanochemical method. The sintering behavior was examined in different temperatures which are 450 °C, 850 °C, 1000 °C and 1200 °C. It was observed that TCP was formed after 850 °C sintering temperature for *Clinocardium Cilium.* In-vitro bioactivity behaviors of produced samples were examined in simulated body fluid and cytotoxicity test was carried out. In vitro SBF behavior is related to in vivo bone bonding mechanism. The results showed that produced materials can be good candidate in field of orthopedic and dental appicalitions.

This study aims to offer an economical and easy method to obtain calcium phosphate apatites can be used in bone grafts, drug delivery, and bone regeneration. Following results have been obtained as a result of this study:

1. As the sintering temperature differs different calcium phosphate ceramics were produced. Increasing of sintering temperature enable to obtain materials with tight junctions.

2. FT-IR results showed HPO_4^{2-} and CO_3^{2-} intensity increases after samples were soaked in SBF. It indicates that aggregation of apatite occurred on the surface of the sample.

3. XRD results showed that in different sintering temperatures various CaP ceramics occurs. After 850 °C hydroxyapatite and tricalcium phosphate apatites appeared.

4. Materials behaviors in TRIS resulted of pH increase which it can be attributed to biodegradability. In 7 days, pH of the samples produced from *Clinocardium Cilium* and sintered at 1000 °C and 1200 °C increased to 9.48 and 9.51 relatively. pH of the

samples produced from *Turritella terebra* and sintered at 1000 °C and 1200 °C increased to 8.17 and 9.41 relatively.

5. MTT assay results showed for 24 hours cell viability was the highest for samples were produced from *Clinocardium Cilium* and sintered at 1200 °C in a concentration of 200 μm. For 7 days, cell viability was the highest for samples were produced from *Turritella terebra* and sintered at 1200 °C in a concentration of 200 μm.

It is recommended that simulated body fluid behaviors of the materials can be examined in XRD analysis to determine the crystal structure of the aggregation. Also, for further investigations materials can be utilized for composite graft to increase the abilities of the microstructure for bone treatment studies.

REFERENCES

[1] Curtis R. V., (2008). Dental biomaterials: imaging, testing and modelling. Boca Raton, Fla.: CRC Press [u.a.], London.

[2] Compact bone & spongy (Cancellous Bone), https://en.wikipedia.org/wiki/Bone#/media/File:Illu_compact_spongy_bone.jpg., 9 November 2017.

[3] Jang D.W., Franco R. A., Sarkar S. K., Lee B.T., (2014). "Fabrication of Porous Hydroxyapatite Scaffolds as Artificial Bone Preform and its Biocompatibility Evaluation" ASAIO J., 60:216–223.

[4] Cornell C. N., Lane, Seligson J. M., Henry D., Chapman S., Vincent M., Merkow K., Gustilo R., (1991). "Multicenter trial of Collagraft as bone graft substitute" J. Orthop. Trauma, 5:1–8.

[5] Kim Y.H., Lee B.T., (2011). "Novel Approach to The Fabrication of an Artificial Small Bone Using a Combination of Sponge Replica And Electrospinning Methods" Sci. Technol. Adv. Mater., 035002.

[6] Dee K. C., Puleo D. A., Bizios R., (2003). An Introduction to Tissue-Biomaterial Interactions., John Wiley & Sons, Hoboken, NJ

[7] León B., Jansen J., Eds., (2009). Thin Calcium Phosphate Coatings for Medical Implants. New York, NY: Springer New York.

[8] Parhi P., Ramanan A., Ray A. R., (2004). "A Convenient Route for the Synthesis of Hydroxyapatite Through a Novel Microwave-Mediated Metathesis Reaction" Mater. Lett., 58(27–28):3610–3612.

[9] Tathe A., Ghodke M., Nikalje A. P., (2010) A brief review: biomaterials and their application, Int. J. Pharm. Pharm. Sci., 2:19–23.

[10] Kulshrestha A. S., Mahapatro A., Henderson L. A., Eds., (2010). Biomaterials, Washington, DC: American Chemical Society, 1054.

[11] Naderi H., M. Matin M., Bahrami A. R., (2011). "Review paper: critical issues in tissue engineering: biomaterials, cell sources, angiogenesis, and drug delivery systems," J. Biomater. Appl., 26:383–417.

[12] Hill D., (1998). Design Engineering of Biomaterials for Medical Devices. Wiley.

[13] Black J., (1998). Handbook of Biomaterial Properties, First Edition, New York.

[14] Patel N. R., Gohil P. P., (2012). "A Review on Biomaterials: Scope, Applications & Human Anatomy Significance" Int. J. Emerg. Technol. Adv. Eng., 2:91–101.

[15] Zenz C. R., (2007). "Materials Used to Safely Replace or İnteract with Biological Systems", Conference on Biomaterials WS2008, Genomics and Bioinformatics.

[16] Okazaki Y., Gotoh E., (2005). "Comparison of Metal Release From Various Metallic Biomaterials in Vitro" Biomaterials, 26:11–21.

[17] Alvarado J., Maldonado R., Marxuach J., Otero R., (2003). "Biomechanics of Hip and Knee Prostheses", Appl. Eng. Mech. Med. GED–University P. R. Mayaguez.

[18] Pubns N., (1984). Contemporary Biomaterials - Material and Host Response, Clinical Applications, New Technology and Legal Aspects, Bethesda, Maryland.

[19] Geetha M., Singh A. K., Asokamani R., Gogia A. K., (2009). "Ti Based Biomaterials, the Ultimate Choice for Orthopaedic Implants – A review" Prog. Mater. Sci., 54:397–425.

[20] Au A. G., V. Raso J., Liggins A. B., and Amirfazli A., (2007). "Contribution of Loading Conditions and Material Properties to Stress Shielding Near the Tibial Component of Total Knee Replacements," J. Biomech., 40:1410–1416.

[21] Pasinli A., (2004). "Biyomedikal Uygulamalarda Kullanılan Biyomalzemeler" Makine Teknol. Elektron. Derg., 4:25–34.

[22] Heness G. L. and Ben-Nissan B., (2004). "Innovative Bioceramics", Materials Forum, 104-114.

[23] Hench L. L., (1998). Bioceramics, J. Am. Ceram. Soc., 81:1705–1728.

[24] Antoniac I. V., Ed., (2016). Handbook of Bioceramics and Biocomposites, Cham: Springer International Publishing, Romania.

[25] Hench L. L. and Wilson J., (1984). "Surface-active biomaterials," Science, vol. 226:630–636.

[26] Kokubo T., (1982). "KURENAI: Kyoto University Research Information Repository," Bull Inst Chem Res Kyoto Univ, vol. 60:3–4.

[27] Kostorz G., (2016). High-Tech Ceramics: Viewpoints and Perspectives, First Edition, Zurich.

[28] Bonfield W., Grynpas M. D., Tully A. E., Bowman J., Abram J., (1981). "Hydroxyapatite Reinforced Polyethylene Mechanically Compatible Implant Material for Bone Replacement" Biomaterials, 2:185–186.

[29] Schneiders W., Reinstorf A., Pompe W., Grass R., Biewner A., Holch M., Zwipp H., Rammelt S., (2007). "Effect of modification of hydroxyapatite/collagen composites with sodium citrate, phosphoserine, phosphoserine/RGD-peptide and calcium carbonate on bone remodelling," Bone, 40(4):1048–1059.

[30] Kikuchi M., (2013). "Hydroxyapatite/collagen Bone-like Nanocomposite," Biol. Pharm. Bull., 36:1666–1669.

[31] Murugan R. and Ramakrishna S., (2004). "Bioresorbable composite Bone Paste Using Polysaccharide Based Nano Hydroxyapatite," Biomaterials, 25:3829–3835.

[32] Hong Z., Zhang P., Liu A., Chen L., Chen X., and Jing X., (2007). "Composites of Poly(lactide-Co-Glycolide) and the Surface Modified Carbonated Hydroxyapatite Nanoparticles", J. Biomed. Mater. Res. A, 81:515-522.

[33] Petricca S. E., Marra K. G., and Kumta P. N., (2006). "Chemical Synthesis of Poly(Lactic-Co-Glycolic Acid)/Hydroxyapatite Composites for Orthopaedic Applications," Acta Biomater., 2:277–286.

[34] Sato T., Kawamura M., Sato K., Iwata H., Miura T., (1991). "Bone Morphogenesis of Rabbit Bone Morphogenetic Protein-Bound Hydroxyapatite-Fibrin Composite", Clin. Orthop., 254–262.

[35] Sun D., Yuhui C., Tran R., Song X., Denghui X., Chunhong J., Ying G., Zhongmin Z., Jinshan G., Jian Y., Dadi J., Xiaochun B., (2014). "Citric Acid-based Hydroxyapatite Composite Scaffolds Enhance", (2014), Calvarial Regeneration," Sci. Rep., 4(4):6912.

[36] Knabe C., Koch C., Rack A., Stiller M., (2008). "Effect of β-tricalcium phosphate Particles with Varying Porosity on Osteogenesis After Sinus Floor Augmentation in Humans" Biomaterials, 29:2249–2258.

[37] Bioceramic, https://en.wikipedia.org/wiki/Bioceramic, 9 November 2017

[38] Salinas A. J., Vallet-Regí M., (2013). "Bioactive Ceramics: From Bone Grafts To Tissue Engineering" RSC Adv., 3:11116.

[39] Piconi C. Porporati A. A., (2016). "Bioinert Ceramics: Zirconia and Alumina," in Handbook of Bioceramics and Biocomposites, I. V. Antoniac, Ed. Springer International Publishing, 59–89.

[40] Kim H.M., Himeno T., Kokubo T., Nakamura T., (2005). "Process and Kinetics of Bonelike Apatite Formation on Sintered Hydroxyapatite in a Simulated Body Fluid," Biomaterials, 26:4366–4373.

[41] Kokubo T., (1990). "Surface Chemistry of Bioactive Glass-ceramics," J. Non-Cryst. Solids, 120:138–151.

[42] Vallet-Regí M., Salinas A. J., Ramírez-Castellanos J., González-Calbet J. M., (2005). "Nanostructure of Bioactive Sol−Gel Glasses and Organic−Inorganic Hybrids", Chem. Mater., 17:1874–1879.

[43] Vallet-Regí M., González-Calbet J. M., (2004). "Calcium Phosphates as Substitution of Bone Tissues," Prog. Solid State Chem., 32:1–31.

[44] López-Noriega A., Arcos D., Izquierdo-Barba I., Sakamoto Y., Terasaki O., Vallet-Regí M., (2006). "Ordered Mesoporous Bioactive Glasses for Bone Tissue Regeneration," Chem. Mater., 18:3137–3144.

[45] Cacciotti I., Lombardi M., Bianco A., Ravaglioli A., Montanaro L., (2012). "Sol–gel derived 45S5 Bioglass: Synthesis, Microstructural Evolution and Thermal Behaviour", J. Mater. Sci. Mater. Med., 23:1849–1866.

[46] Ambrosio L., (2010). Ed., Biomedical composites. Boca Raton, Fla.: CRC Press.

[47] Sheikh Z., Najeeb S., Khurshid Z., Verma V., Rashid H., Glogauer M., (2015). "Biodegradable Materials for Bone Repair and Tissue Engineering Applications", Materials, 8,(9):5744–5794.

[48] Tan L., Yu X., Wan P., Yang K., (2013). "Biodegradable Materials for Bone Repairs: A Review," J. Mater. Sci. Technol., 29(6)503–513.

[49] Zhang M., Wang K., Shi Z., Yang H., Dang X., Wang W., (2010). "Osteogenesis of the Construct Combined BMSCs with β-TCP in Rat," J. Plast. Reconstr. Aesthet. Surg., 63:227–232.

[50] Cutright D. E., Bhaskar S. N., Brady J. M., Getter L., Posey W. R., (1972). "Reaction of Bone to Tricalcium phosphate Ceramic Pellets," Oral Surg. Oral Med. Oral Pathol., 33:850–856.

[51] Cameron H. U., Pilliar R. MacNab M., I., (1973). "The Effect of Movement on the Bonding of Porous Metal to Bone", J. Biomed. Mater. Res., 7:301–311.

[52] Bohner M., (2001). "Physical and Chemical Aspects of Calcium Phosphates Used in Spinal Surgery", Eur. Spine J. Off. Publ. Eur. Spine Soc. Eur. Spinal Deform. Soc. Eur. Sect. Cerv. Spine Res. Soc., 10(2):S114-121.

[53] Ong K. L., Lovald S., Black J., (2014). Orthopaedic Biomaterials in Research and Practice, Second Edition, CRC Press.

[54] Dorozhkin S. V., (2016). Calcium Orthophosphate-Based Bioceramics and Biocomposites., Moscow

[55] K. J., R. John F., H. John M., (2002). Phosphates: Geochemical, Geobiological, and Materials Importance, USA.

[56] Benaqqa C., Chevalier J., Saädaoui M., Fantozzi G., (2005). "Slow Crack Growth Behaviour Of Hydroxyapatite Ceramics", Biomaterials, 26:6106–6112.

[57] Wang L., Nancollas G. H., (2008). "Calcium Orthophosphates: Crystallization and Dissolution," Chem. Rev., 108:4628–4669.

[58] Ozeki K., Fukui Y., Aoki H., (2007). "Influence of the Calcium Phosphate Content of the Target on the Phase Composition and Deposition Rate of Sputtered Films", Appl. Surf. Sci., 253:5040–5044.

[59] Oshida Y., (2015). Hydroxyapatite: Synthesis and Applications, New York.

[60] Santhosh S. and Balasivanandha Prabu S., (2013). "Thermal Stability of Nano Hydroxyapatite Synthesized From Sea Shells Through Wet Chemical Synthesis" Mater. Lett., 97:121–124.

[61] Okuda T., Ioku K, Yonezawa I, Minagi H, Kawachi G, Gonda Y, Murayama H, Shibata Y, Minami S, Kamihira S, Kurosawa H, Ikeda T., (2007). "The Effect of the Microstructure of β-Tricalcium Phosphate on the Metabolism of Subsequently Formed Bone Tissue", Biomaterials, 28:2612–2621.

[62] Zhou J., Zhang X., Chen J., Zeng S., Groot K., (1993). "High temperature characteristics of synthetic hydroxyapatite," J. Mater. Sci. Mater. Med., 4:83–85.

[63] Yu-Peng L., Yi-Zhong S., Rui Fu Z., Mu S. L., and Ting Q. L., (2002). "Factors Influcing Phase Compositions and Structure of Plasma Sprayed Hydroxyapatite Coatings During Heat Treatment", Appl. Surf. Sci., 345–354.

[64] Wang J., Shaw L. L., (2010). "Grain-Size Dependence of the Hardness of Submicrometer and Nanometer Hydroxyapatite," J. Am. Ceram. Soc., 93:601–604.

[65] Bertazzo S., Zambuzzi W. F., Campos D. D. P., Ogeda T. L., Ferreira C. V., Bertran C. A., (2010). "Hydroxyapatite Surface Solubility and Effect on Cell Adhesion", Colloids Surf. B Biointerfaces, 78:177–184.

[66] Chen C.C. and Boskey A. L., (1985). "Mechanisms of Proteoglycan Inhibition of Hydroxyapatite Growth," Calcif. Tissue Int., 37:395–400.

[67] Chen C.C., Boskey A. L., Rosenberg L. C., (1984). "The Inhibitory Effect of Cartilage Proteoglycans on Hydroxyapatite Growth," Calcif. Tissue Int., 36:285–290.

[68] He L.H., Standard O. C., Huang T. T. Y., Latella B. A., Swain M. V., (2008). "Mechanical Behaviour of Porous Hydroxyapatite," Acta Biomater., 4:577–586.

[69] Perera F. H., Martínez-Vázquez F. Miranda J., P., Ortiz A. L., Pajares A., (2010). "Clarifying the Effect of Sintering Conditions on the Microstructure and Mechanical Properties of β-tricalcium Phosphate," Ceram. Int., 36:1929–1935.

[70] Dorozhkin S. V., (2012). "Calcium Orthophosphates: Applications in Nature, Biology, and Medicine." CRC Press, Moscow.

[71] Kim H.W., Kim H.E., (2006). "Nanofiber Generation of Hydroxyapatite and Fluor-Hydroxyapatite Bioceramics", J. Biomed. Mater. Res. B Appl. Biomater., 77B: 323–328.

[72] Akram M., Ahmed R., Shakir I., Ibrahim W. A. W., Hussain R., (2014). "Extracting Hydroxyapatite and Its Precursors from Natural Resources," J. Mater. Sci., 49(4):1461–1475.

[73] Bahrololoom M. E., Javidi M., Javadpour S., Ma J., (2009). "Characterisation of Natural Hydroxyapatite Extracted From Bovine Cortical Bone Ash" J. Ceram. Process. Res., 10:129–138.

[74] Paul W. and Sharma C. P., (1999). "Development of Porous Spherical Hydroxyapatite Granules: Application Towards Protein Delivery" J. Mater. Sci. Mater. Med., 10:383–388.

[75] Ravaglioli A. and Krajewski A., (1992). "Bioceramics and the Human Body", Springer, Netherlands.

[76] Sadat-Shojai M., Khorasani M.T., Dinpanah-Khoshdargi E., Jamshidi A., (2013). "Synthesis methods for nanosized hydroxyapatite with diverse structures," Acta Biomater., 9(8):7591–7621.

[77] Okada M. and Furuzono T., (2012). "Hydroxylapatite Nanoparticles: Fabrication Methods And Medical Applications", Sci. Technol. Adv. Mater., 13:064103.

[78] Ferraz M. P., F. J., Manuel C. M., (2004). "Hydroxyapatite Nanoparticles: A Review of Preparation Methodologies", J. Appl. Biomater. Biomech. JABB, 2:74–80.

[79] Liu C., Huang Y., Shen W., Cui J., (2001). "Kinetics of Hydroxyapatite Precipitation at pH 10 to 11," Biomaterials, 22:301–306.

[80] Bayraktar D. and Taş A. C., (2000). "Biomimetic preparation of HA Powders at 37 C in urea-and Enzyme Urease-Containing Synthetic Body Fluids," Turk. J. Med. Sci., 30:235–246.

[81] Matijevic E., (1986). "Monodispersed Colloids: Art and Science," Langmuir, 2:12–20.

[82] Ishikawa K. and Eanes E. D., (1993). "The Hydrolysis of Anhydrous Dicalcium Phosphate into Hydroxyapatite," J. Dent. Res., 72:474–480.

[83] Onuma K., (2006). "Recent Research on Pseudobiological Hydroxyapatite Crystal Growth and Phase Transition Mechanisms", Prog. Cryst. Growth Charact. Mater., 52:223–245.

[84] Suzuki O., Kamakura S., Katagiri T., Nakamura M., Zhao B., Honda Y., Kamijo R., (2006). "Bone Formation Enhanced By Implanted Octacalcium Phosphate Involving Conversion Into Ca-Deficient Hydroxyapatite", Biomaterials, 27:2671–2681.

[85] Jinawath S., Polchai D., Yoshimura M., (2002). "Low-temperature, Hydrothermal Transformation of Aragonite to Hydroxyapatite", Mater. Sci. Eng. C, 22:35–39.

[86] Sunouchi K., Tsuru K, Maruta M, Kawachi G, Matsuya S, Terada Y, Ishikawa K. (2012). "Fabrication of Solid and Hollow Carbonate Apatite Microspheres as Bone Substitutes Using Calcite Microspheres as A Precursor", Dent. Mater. J., 31:549–557.

[87] Furuta S., Katsuki H., and Komarneni S., (1998). "Porous Hydroxyapatite Monoliths from Gypsum Waste," J. Mater. Chem., 8:2803–2806.

[88] Ishikawa K., (2010). "Bone Substitute Fabrication Based on Dissolution-Precipitation Reactions," Materials, 3:1138–1155.

[89] Kokubo T. and Takadama H., (2006). "How Useful is SBF in Predicting in Vivo Bone Bioactivity?," Biomaterials, 27:2907–2915.

[90] Gunduz O., Sahin Y. M., Agathopoulos S., Ben-Nissan B., Oktar F. N., (2014). "A New Method for Fabrication of Nanohydroxyapatite and TCP from the Sea Snail Cerithium vulgatum," J. Nanomater., 2014:1–6

[91] Sahin Y. M., Gunduz O., Ficai A., Ekren N., Tuna A., Inan A.T., Oktar F.N. (2016). "Can European Sea Bass (*Dicentrarchus labrax*) Scale Be a Good Candidate for Nano-Bioceramics Production?", Key Eng. Mater., 696:60–65.

[92] Piccirillo C., Pullar R. C., Costa E., Santos-Silva A., M. Pintado M. E., Castro P. M. L., (2015). "Hydroxyapatite-based Materials of Marine Origin: A Bioactivity and Sintering Study," Mater. Sci. Eng. C, 51:309–315.

[93] Roy D. M. and Linnehan S. K., (1974). "Hydroxyapatite Formed from Coral Skeletal Carbonate by Hydrothermal Exchange," Nature, 247:220–222.

[94] Sivakumar M., T. Kumar S., Shantha K. L., Rao K. P., (1996). "Development of hydroxyapatite derived from Indian coral," Biomaterials, 17:1709–1714.

[95] Peña J., LeGeros R. Z., Rohanizadeh R., LeGeros J. P., (2001). "$CaCO_3$/Ca-P Biphasic Materials Prepared by Microwave Processing of Natural Aragonite and Calcite," Key Eng. Mater., 192–195:267–270.

[96] Hu J., Russell J. J., Ben-Nissan B., Vago R., (2001). "Production and Analysis of Hydroxyapatite From Australian Corals via Hydrothermal Process," J. Mater. Sci. Lett., 20:85–87.

[97] Chou J., Samur R., Ozyegin L. S., Ben-Nissan B., Oktar F. N., Macha I., (2012). "An Alternative Synthesis Method For Di Calcium Phosphate (Monetite) Powders From Mediterranean Mussel (Mytilus galloprovincialis) Shells", Journal of the Australian Ceramic Society, 122 - 128.

[98] Şahin Y. M., Gündüz O. , Bulut B. , Özyeğin L. , Gökçe H. , Ağaoğulları D. , Chou J. , Kayalı E. , Ben-Nissan B. , Oktar F. , (2015). "Nano-Bioceramic Synthesis from Tropical Sea Snail Shells (Tiger Cowrie - Cypraea Tigris) with Simple Chemical Treatment" Acta Phys. Pol. A, 127:1055–1058.

[99] Ağaoğullari D., Kel D., Gökçe H., Duman I., Övençoğlu M.L., Akarsubaşı A.T., Bilgiç D., Oktar F.N., (2012). "Bioceramic Production from Sea Urchins" Acta Phys. Pol. A, 121:23–25.

[100] Gunduz O., Sahin Y.M. , Agathopoulos S. , Ağaoğulları D. , Gökçe H. , Kayali E.S. , Aktas C. , Ben-Nissan B. , Oktar F.N. (2013). "Nano Calcium Phosphate Powder Production through Chemical Agitation from Atlantic Deer Cowrie Shells (*Cypraea cervus Linnaeus)*", Key Eng. Mater., 587:80–85.

[101] Tămăşan M., Ozyegin L. S., Oktar F. N., Simon V., (2013). "Characterization of Calcium Phosphate Powders Originating from Phyllacanthus Imperialis and Trochidae Infundibulum Concavus Marine Shells," Mater. Sci. Eng. C, 33(5):2569–2577.

[102] Lemos A. F., Rocha J.H.G., Quaresma S.S.F, Kannan S., Oktar F. N., Agathopoulos S., Ferreira J.M.F, (2006). "Hydroxyapatite Nano-Powders Produced Hydrothermally From Nacreous Material", J. Eur. Ceram. Soc., 26:3639–3646.

[103] *Clinocardium_ciliatum*, https://en.wikipedia.org/wiki/Clinocardium_ciliatum, 9 November 2017.

[104] *Clinocardium_ciliatum*, http://eol.org/pages/402747/overview, 9 November 2017.

[105] Habitats of *Clinocardium_ciliatum* , http://www.discoverlife.org/mp/20m?map=Clinocardium+ciliatum, 9 November 2017.

[106] *Turritella terebra*, http://www.sealifebase.org/summary/Turritella-terebra.html, 9 November 2017

[107] *Turritella terebra*, http://eol.org/pages/4876617/overview, 9 November 2017.

[108] Habitats of *Turritella terebra*, http://www.discoverlife.org/mp/20m?map=Turritella+terebra, 9 November 2017.

[109] Prevéy P. S., (2000). "X-ray Diffraction Characterization of Crystallinity and Phase Composition in Plasma-Sprayed Hydroxyapatite Coatings", J. Therm. Spray Technol., 9:369–376.

[110] Jolliff B. L., Hughes J. M., Freeman J. J., Zeigler R. A., (2006). "Crystal Chemistry of Lunar Merrillite and Comparison to Other Meteoritic and Planetary Suites of Whitlockite and Merrillite", Am. Mineral., 91:1583–1595.

[111] Duan Y. R., Zhang Z. R., Wang C. Y., Chen J. Y., Zhang X. D., (2005). "Dynamic Study of Calcium Phosphate Formation on Porous HA/TCP Ceramics", J. Mater. Sci. Mater. Med., 16:795–801.

[112] Tang R., Hass M., Wu W., Gulde S., Nancollas G. H., (2003). "Constant Composition Dissolution of Mixed Phases. II. Selective Dissolution of Calcium Phosphates", J. Colloid Interface Sci., 260:379–384.

[113] Niakan A., Ramesh S., Ganesan P., Tan C.Y. Purbolaksono, Chandran H., Ramesh S., Teng W.D., (2015). "Sintering Behaviour of Natural Porous Hydroxyapatite Derived From Bovine Bone", Ceram. Int., 41:3024–3029.

[114] Sobczak-Kupiec A., Wzorek Z., Kijkowska R., Kowalski Z., (2013). "Effect of Calcination Conditions of Pork Bone Sludge on Behaviour of Hydroxyapatite in Simulated Body Fluid", Bull. Mater. Sci., 36:755–764.

[115] Kutty M. and Singh R., (2000). "The Effects of Sintering Temperature on the Properties of Hydroxyapatite," Ceram. Int., 26:221–230.

[116] Brazda L., Rohanova D., Helebrant A., (2008). "Kinetics of Dissolution of Calcium Phosphate (Ca-P) Bioceramics", Process. Appl. Ceram., 2:57–62.

[117] Rocha J. H. G., Lemos A.F., Agathopoulos S., Valério P., Kannan S., Oktar F. N., Ferreira J.M.F. (2005). "Scaffolds for Bone Restoration From Cuttlefish" Bone, 37:850–857.

[118] Wei X., Ugurlu O., Akinc M., (2007). "Hydrolysis of α-Tricalcium Phosphate in Simulated Body Fluid and Dehydration Behavior During the Drying Process," J. Am. Ceram. Soc., 90:2315–2321.

[119] Jalota S., Bhaduri S. B., Tas A. C., (2006). "In Vitro Testing of Calcium Phosphate (HA, TCP, And Biphasic HA-TCP) Whiskers", J. Biomed. Mater. Res. A, 78:481–490.

APPENDIX-A

SEM Images of the Products

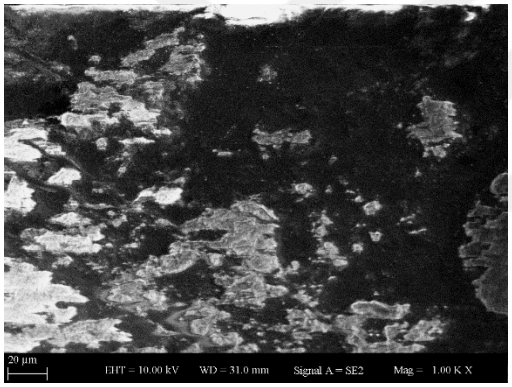

A

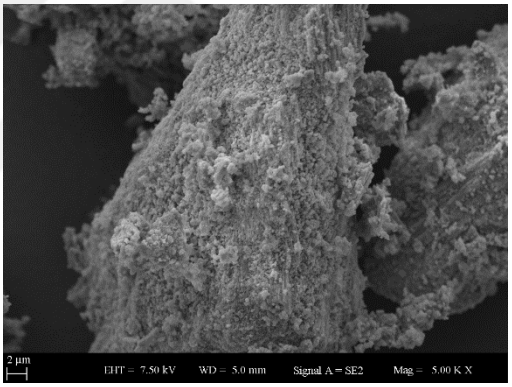

B

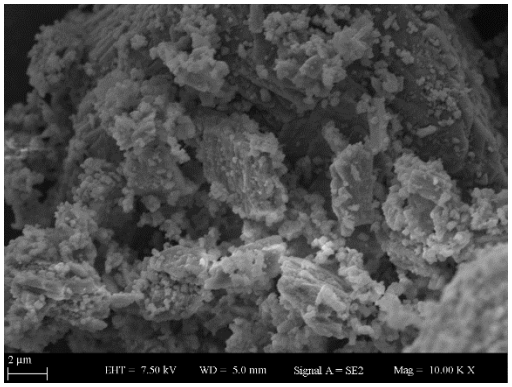

C

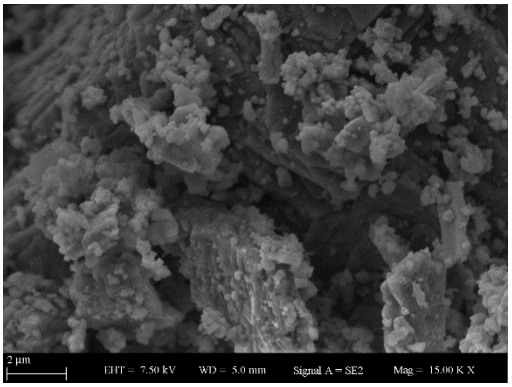

D

Figure A.1 SEM images of sea shell *Clinocardium ciliatum* A) 1000x B) 5000x C) 10000x D) 15000x

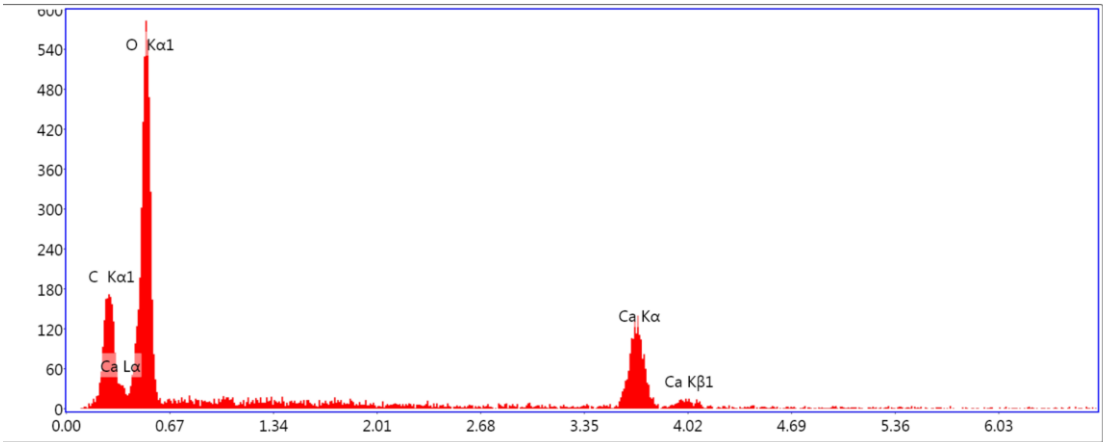

Figure A.2 EDX spectrum of sea shell *Clinocardium ciliatum*

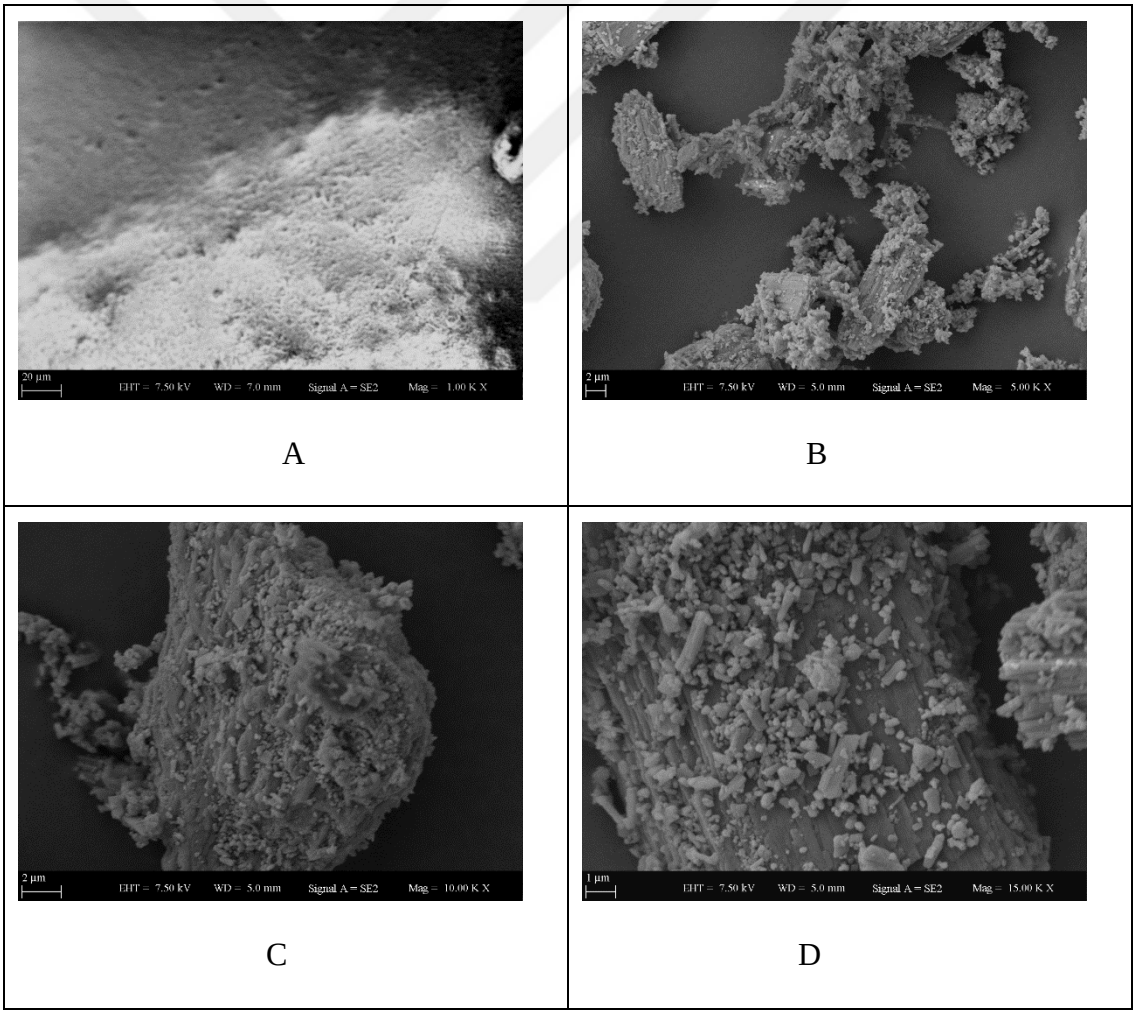

Figure A.3 SEM images of sea snail *Turritella terebra* A) 1000x B) 5000x C) 10000x D) 15000x

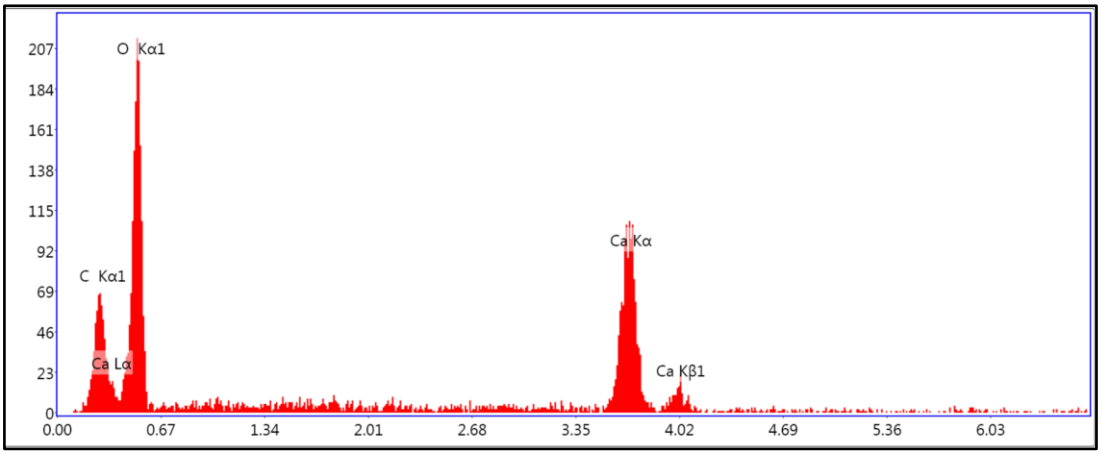

Figure A.4 EDX spectrum of sea snail *Turritella terebra*

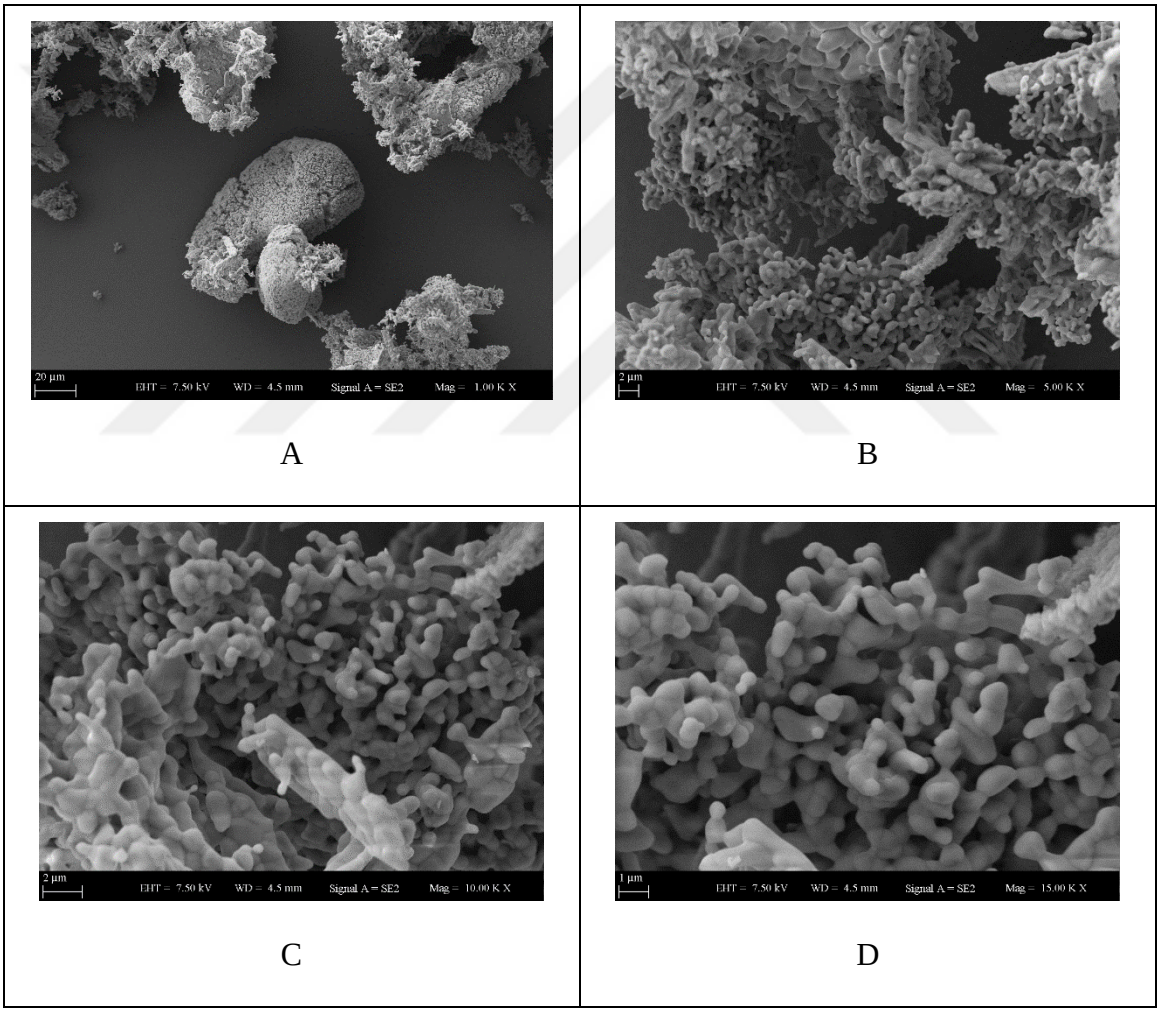

Figure A.5 SEM images of sintered samples produced from *Clinocardium ciliatum* at 1000 °C before soaking in SBF A) 1000x B) 5000x C) 10000x D) 15000x

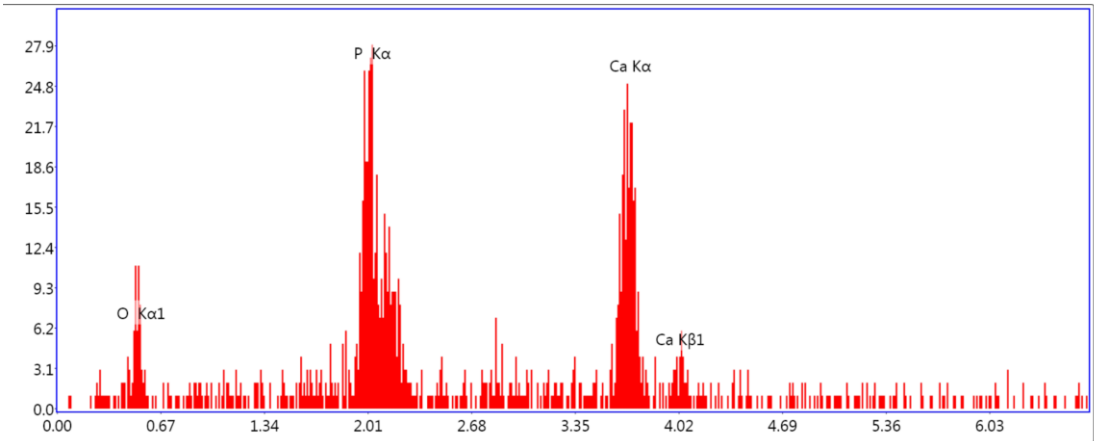

Figure A.6 EDX spectrum of sintered samples produced from *Clinocardium ciliatum* at 1000 °C before soaking in SBF

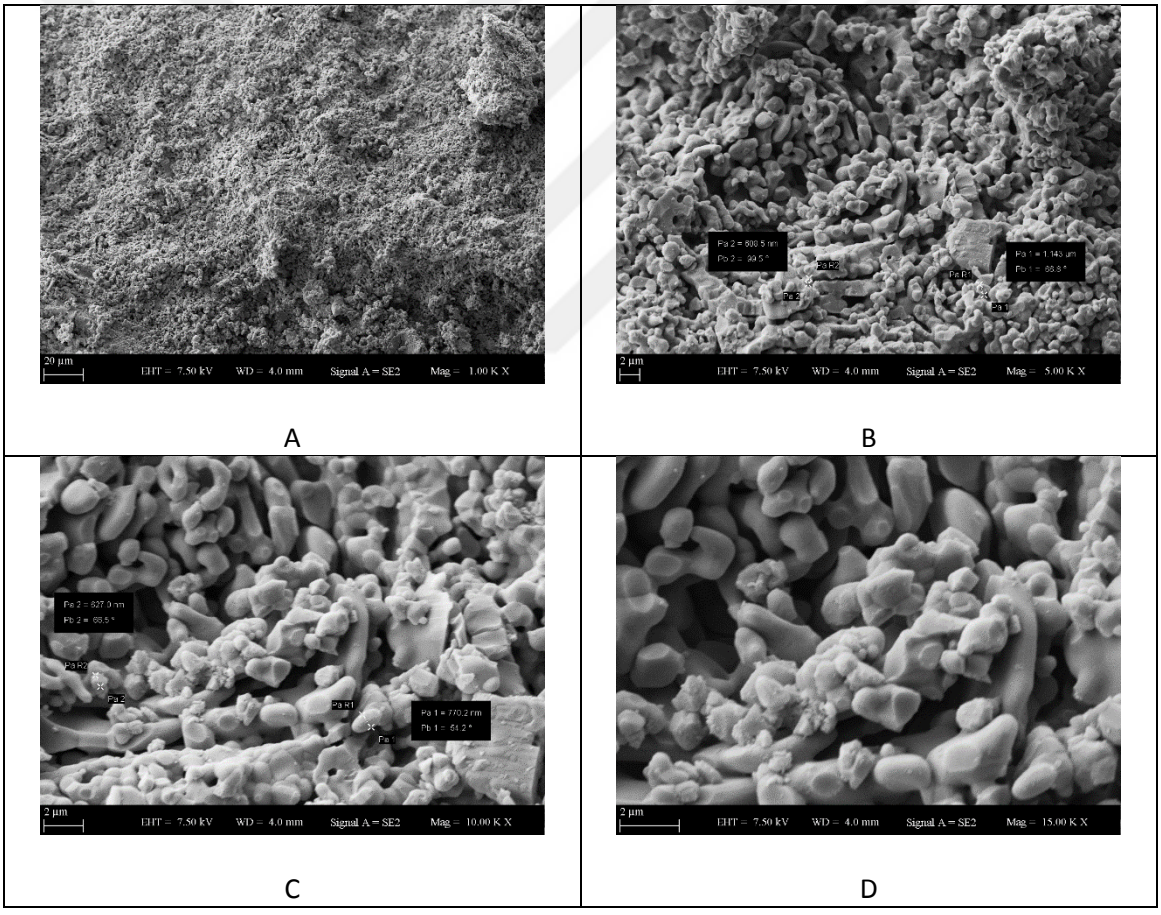

Figure A.7 SEM images of sintered samples produced from *Clinocardium ciliatum* at 1000 °C after soaking in SBF for a week A) 1000x B) 5000x C) 10000x D) 15000x

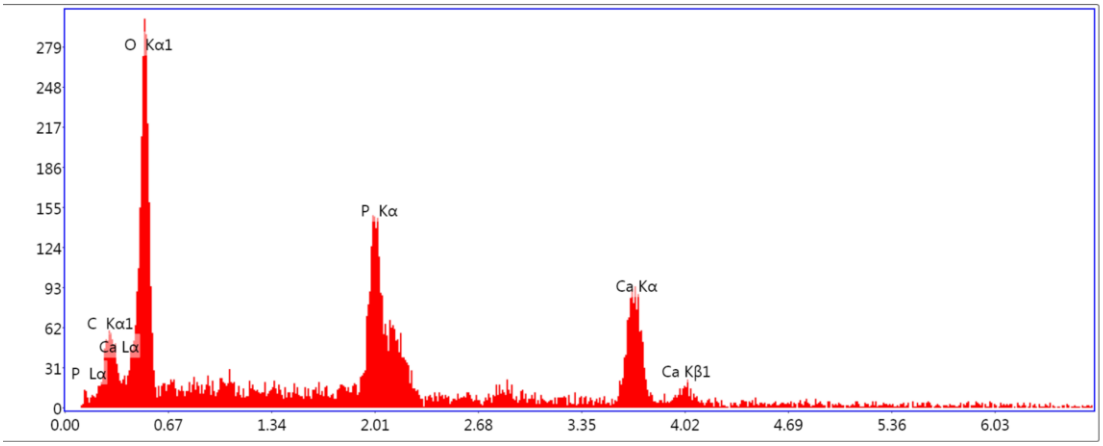

Figure A.8 EDX spectrum of sintered samples produced from *Clinocardium ciliatum* at 1000 °C after soaking in SBF for a week

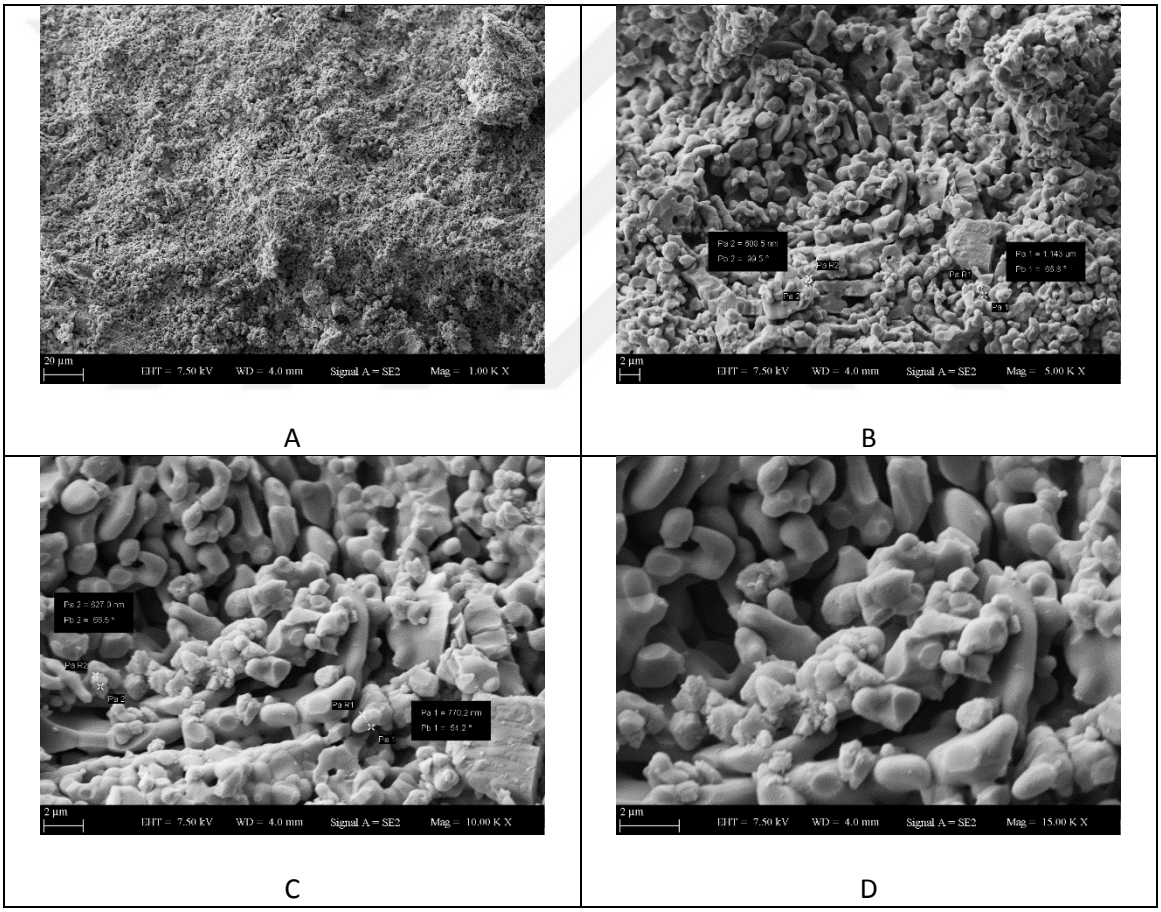

Figure A.9 SEM images of sintered samples produced from *Clinocardium ciliatum* at 1000 °C after soaking in SBF for 2 weeks A) 1000x B) 5000x C) 10000x D) 15000x

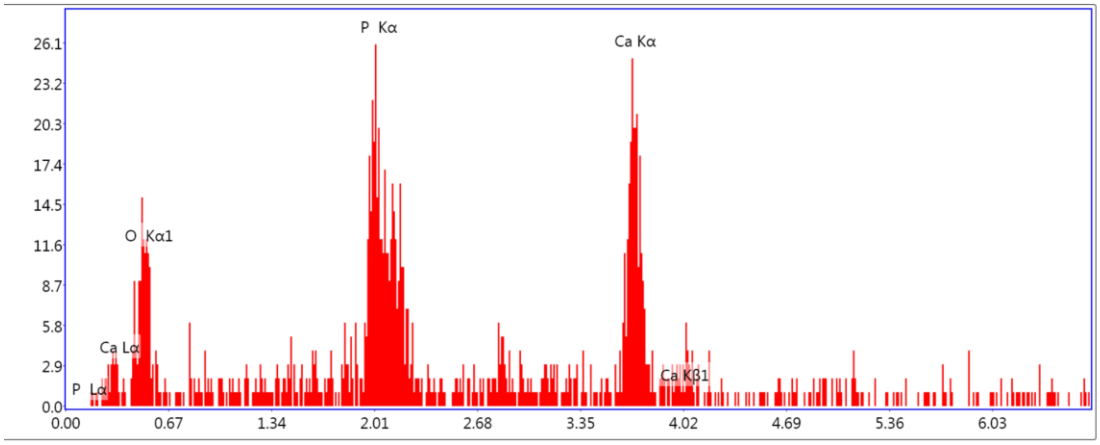

Figure A.10 EDX spectrum of sintered samples produced from *Clinocardium ciliatum* at 1000 °C after soaking in SBF for 2 weeks

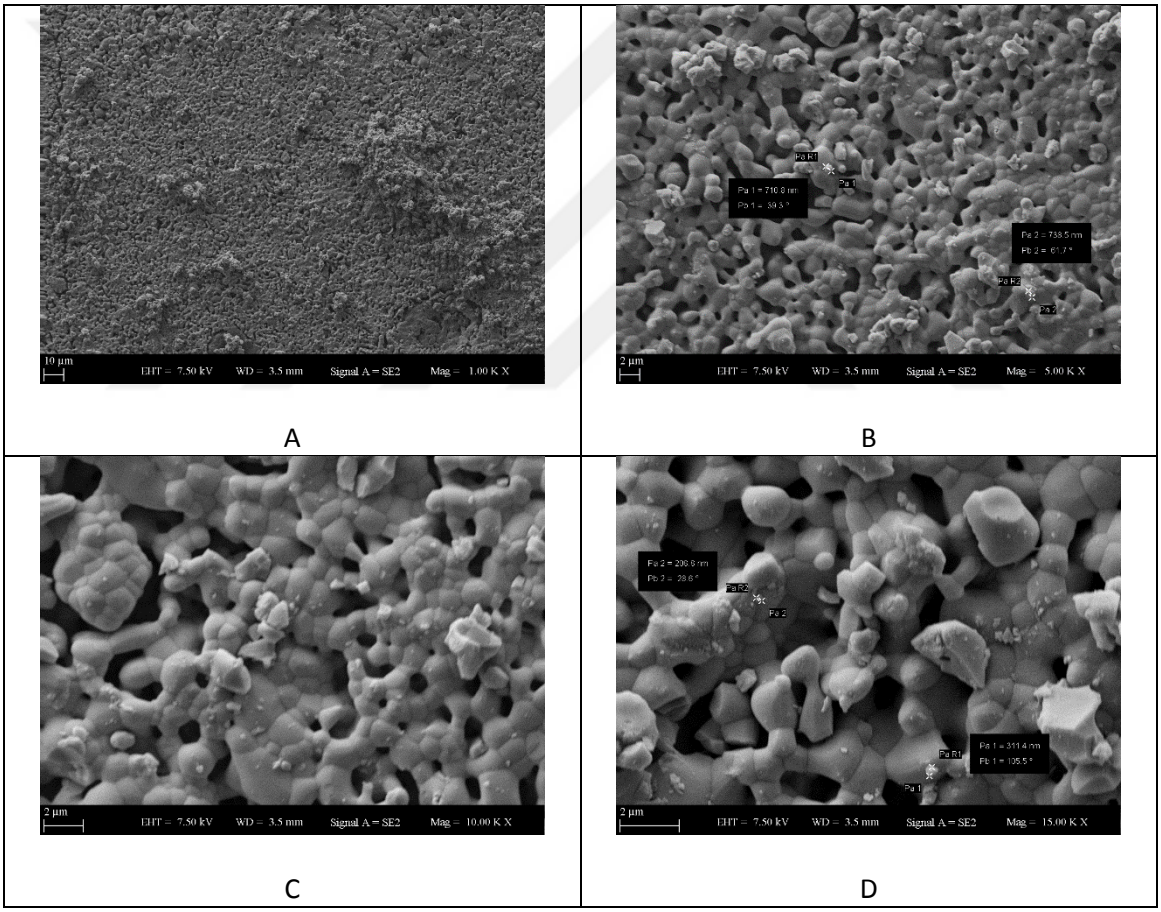

Figure A.11 SEM images of sintered samples produced from *Clinocardium ciliatum* at 1000 °C after soaking in SBF for 3 weeks A) 1000x B) 5000x C) 5000x D) 15000x

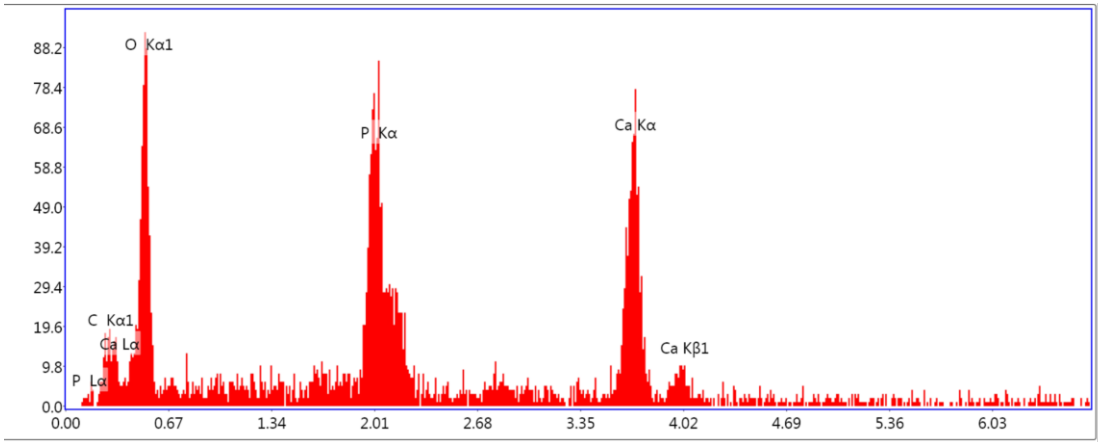

Figure A.12 EDX spectrum of sintered samples produced from *Clinocardium ciliatum* at 1000 °C after soaking in SBF for 3 weeks

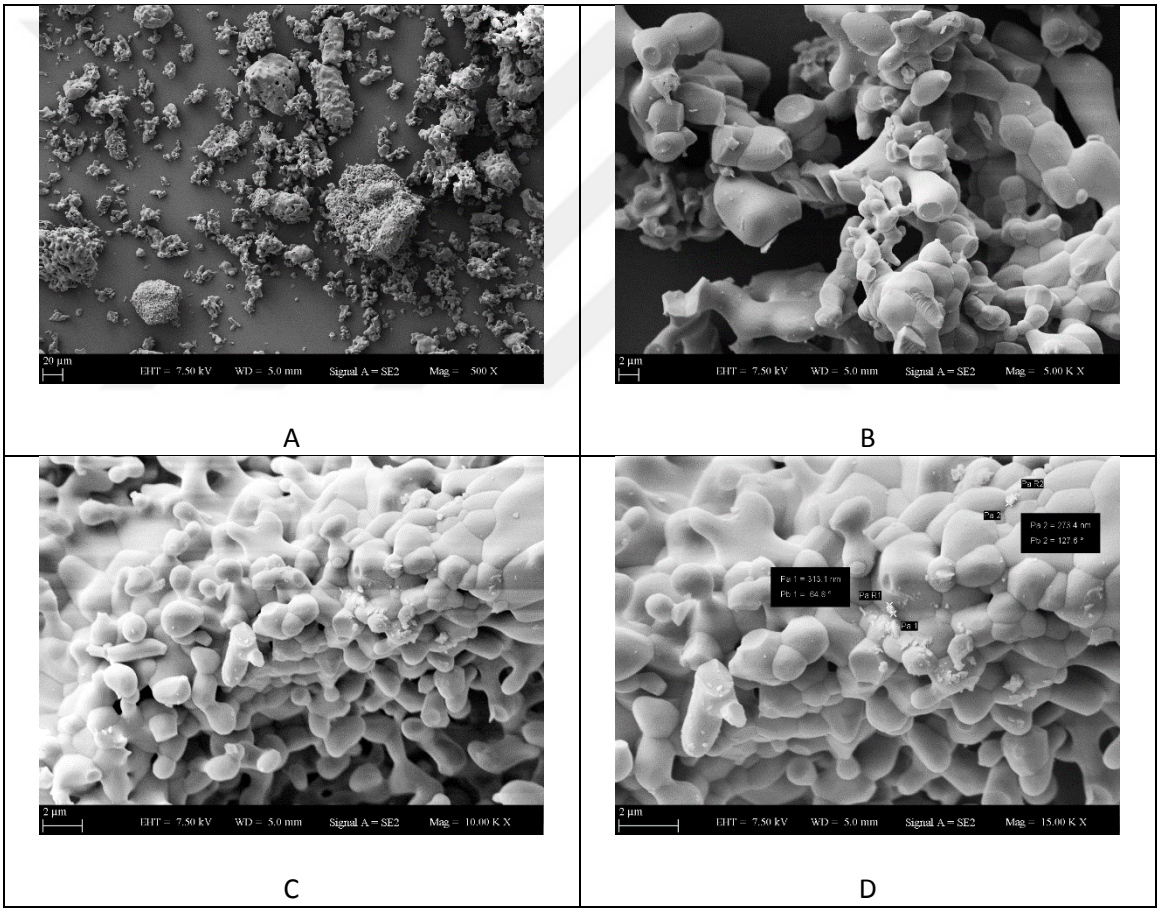

Figure A.13 SEM images of sintered samples produced from *Clinocardium ciliatum* at 1200 °C A) 500x B) 5000x C) 10000x D) 15000x

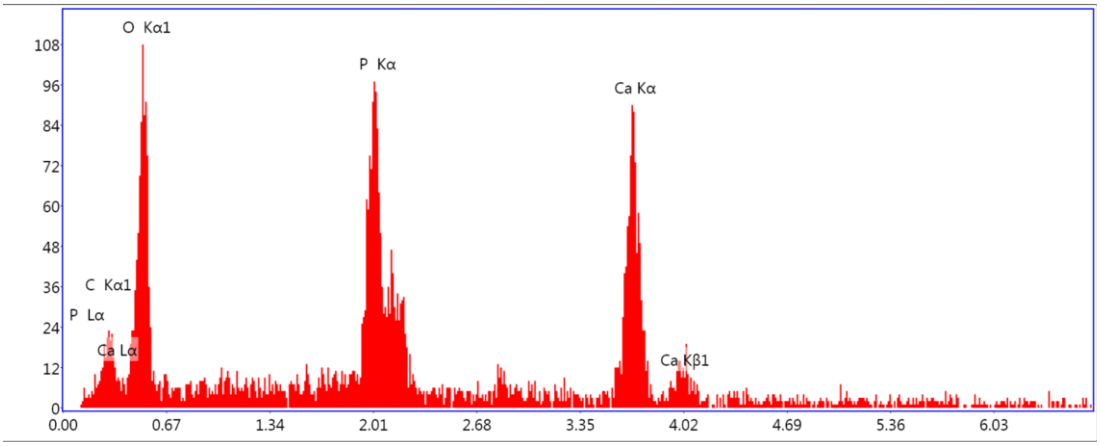

Figure A.14 EDX spectrum of sintered samples produced from *Clinocardium ciliatum* at 1200 °C

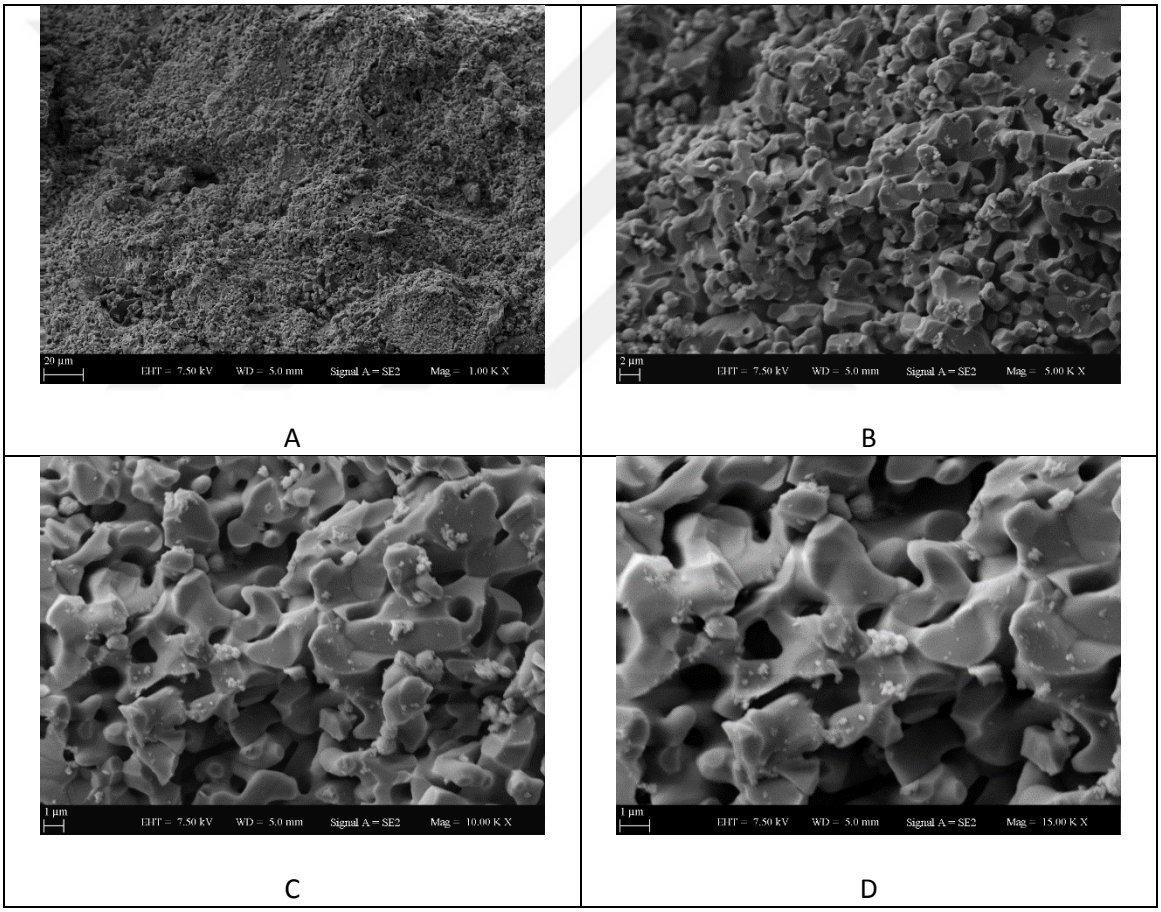

Figure A.15 SEM images of sintered samples produced from *Clinocardium ciliatum* at 1200 °C after a week A) 1000x B) 5000x C) 10000x D) 15000x

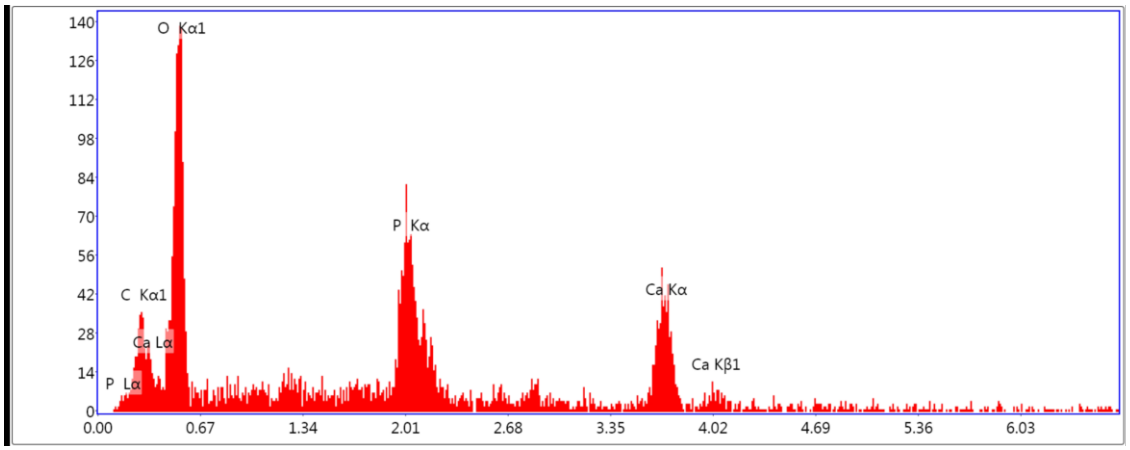

Figure A.16 EDX spectrum of sintered samples produced from *Clinocardium ciliatum* at 1200 °C after a week

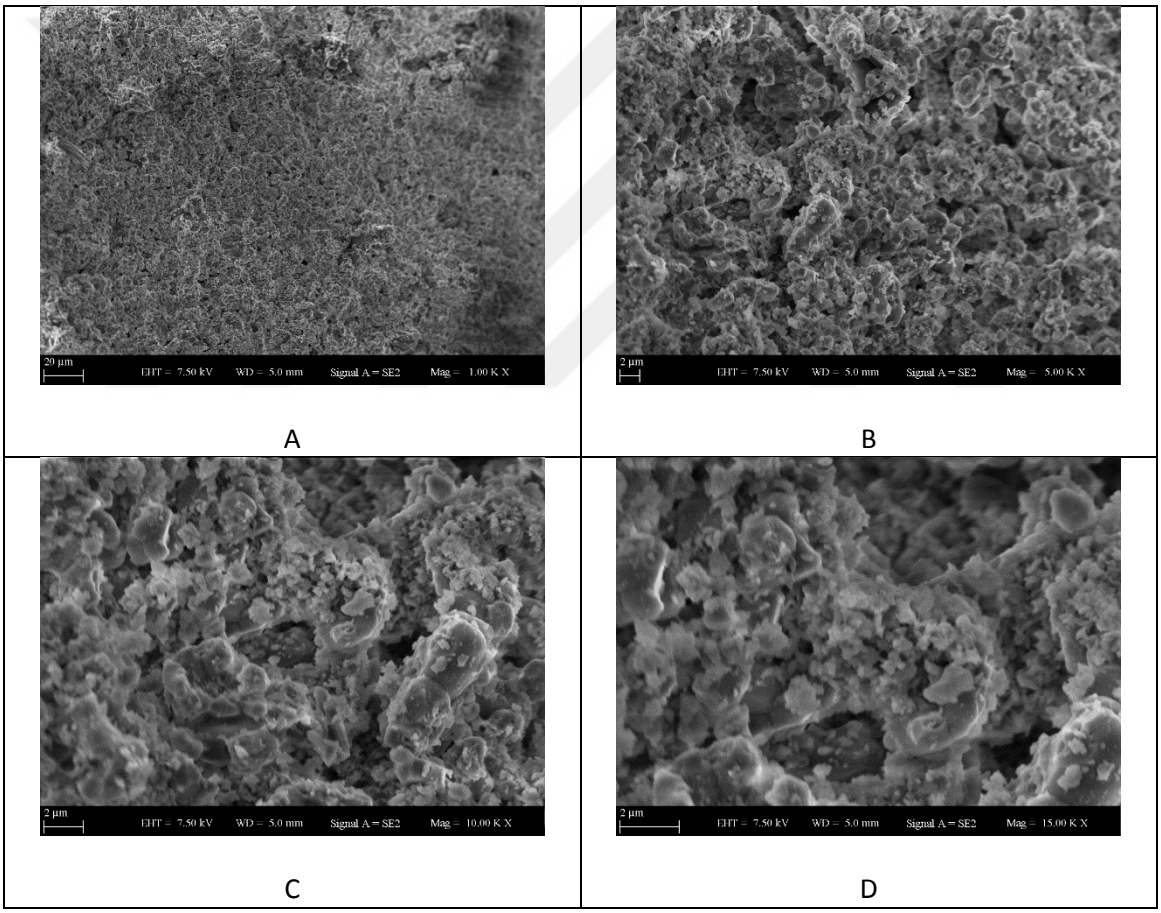

Figure A.17 SEM images of sintered samples produced from *Clinocardium ciliatum* at 1200 °C after two weeks A) 1000x B) 5000x C) 10000x D) 15000x

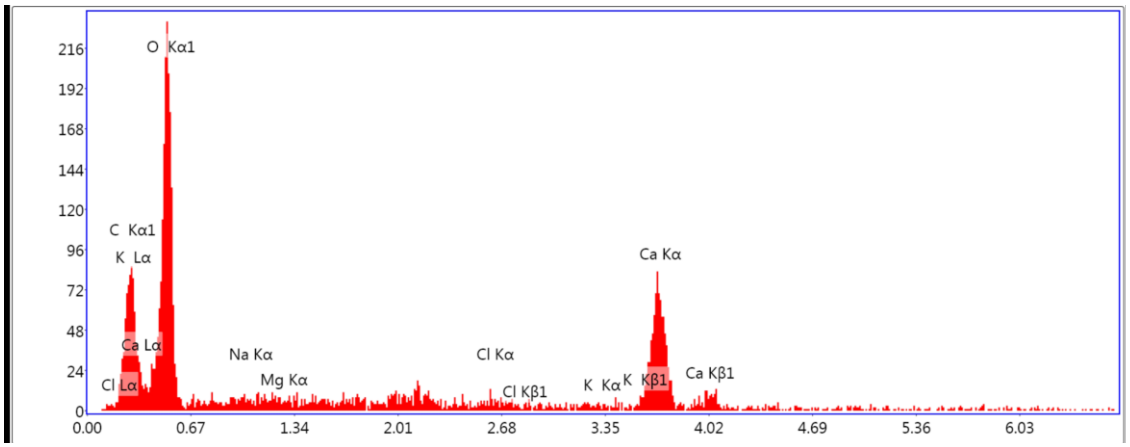

Figure A.19 EDX spectrum of sintered samples produced from *Clinocardium ciliatum* at 1200 °C after two weeks

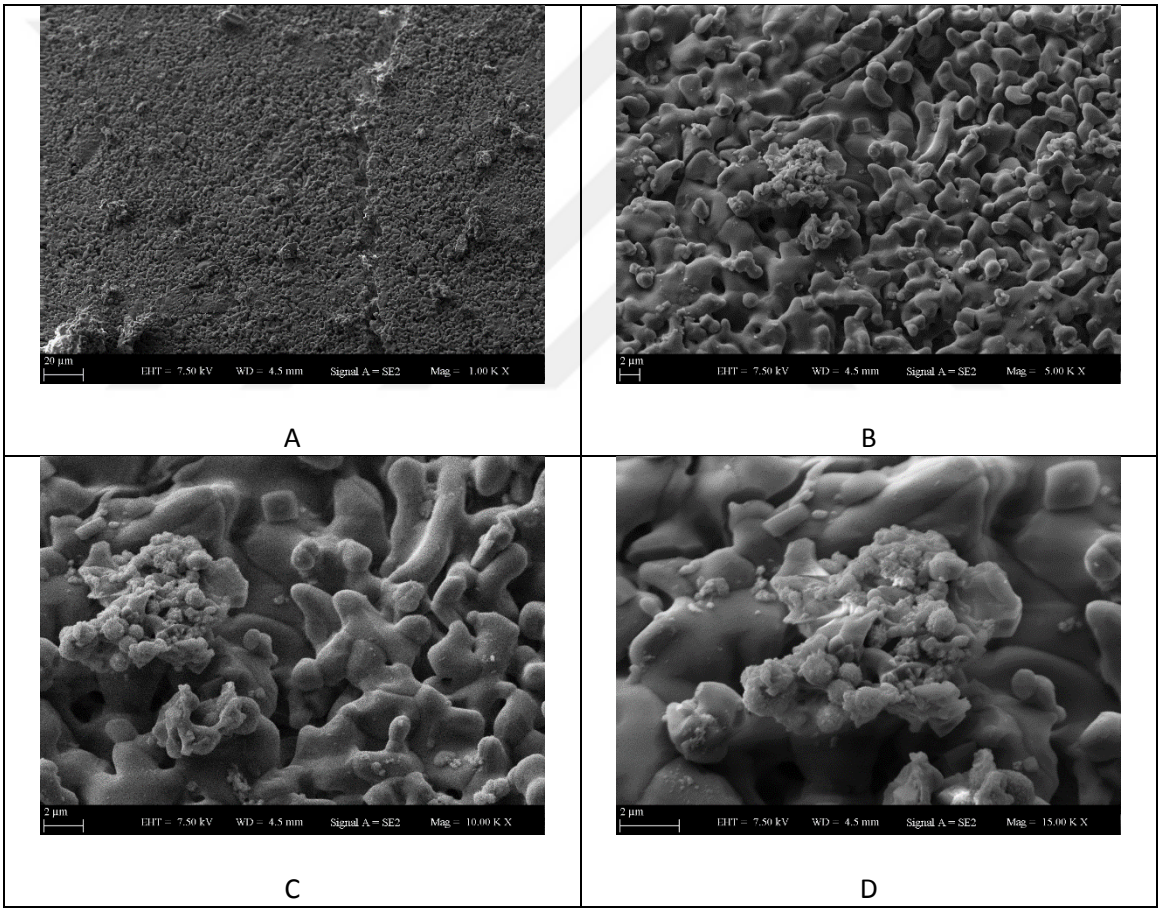

Figure A.20 SEM images of sintered samples produced from *Clinocardium ciliatum* at 1200 °C after three weeks A) 1000x B) 5000x C) 10000x D) 15000x

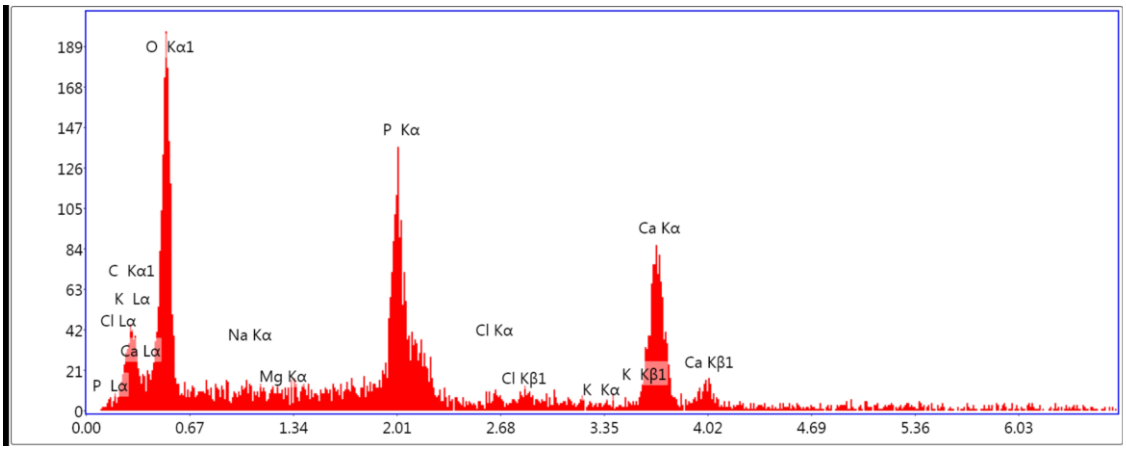

Figure A.21 EDX spectrum of sintered samples produced from *Clinocardium ciliatum* at 1200 °C after three weeks

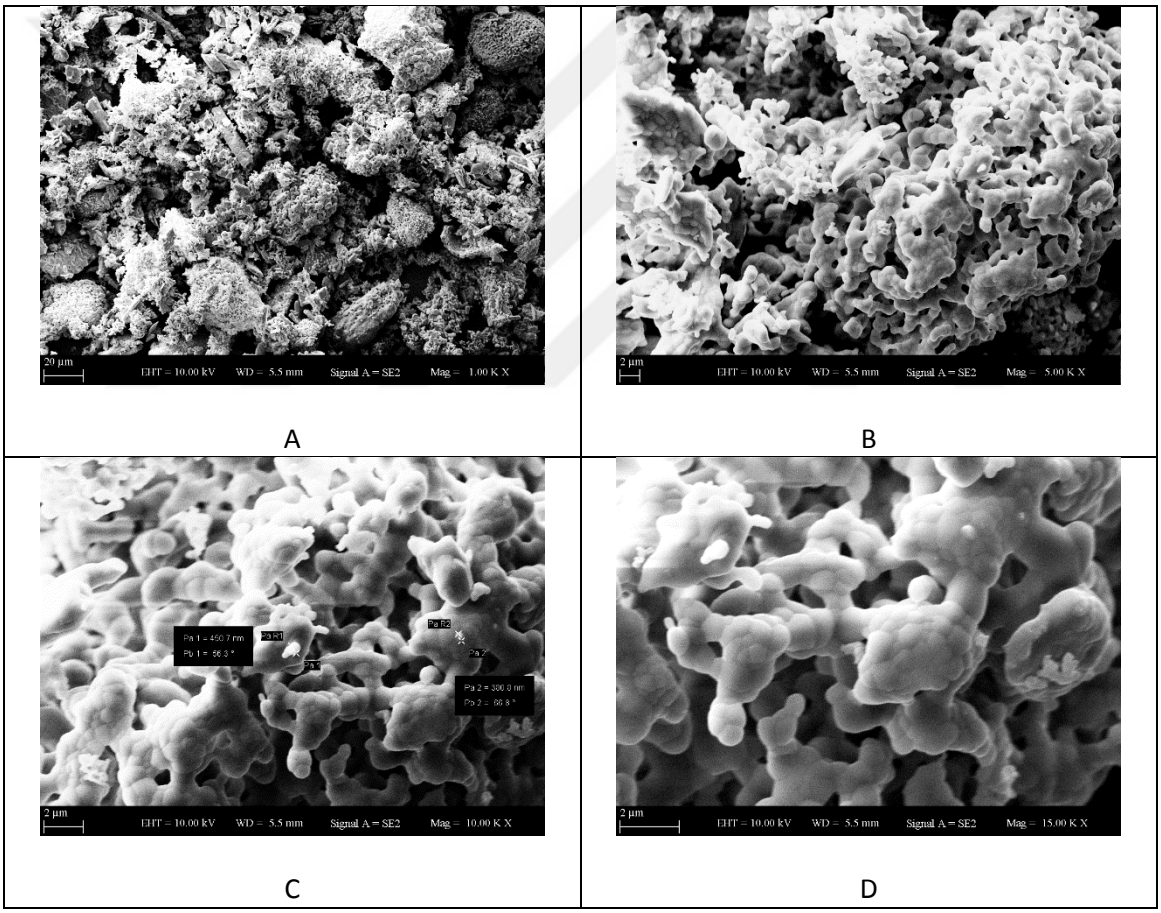

Figure A.22 SEM images of sintered samples produced from *Turritella terebra* at 1000 °C before soaking in SBF A) 1000x B) 5000x C) 10000x D) 15000x

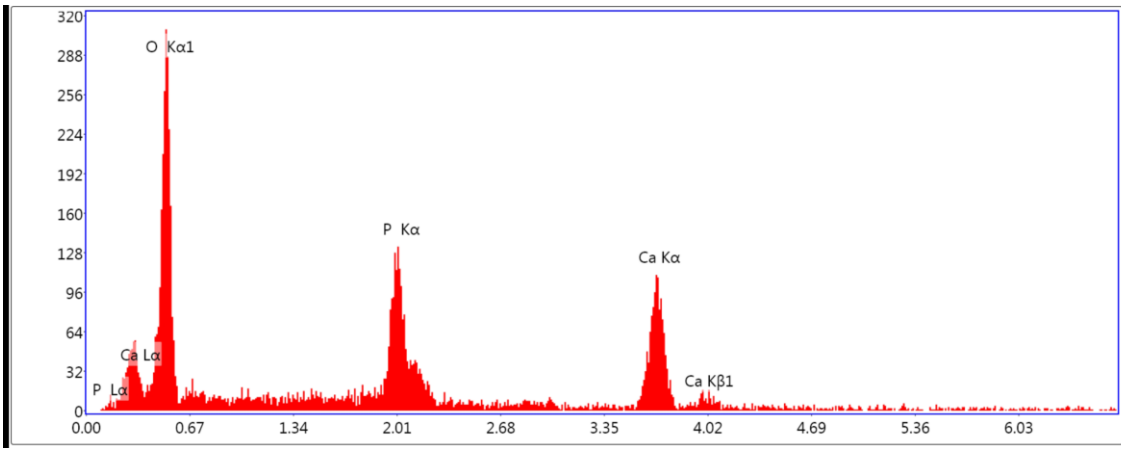

Figure A.23 EDX spectrum of sintered samples produced from *Turritella terebra* at 1000 °C before soaking in SBF

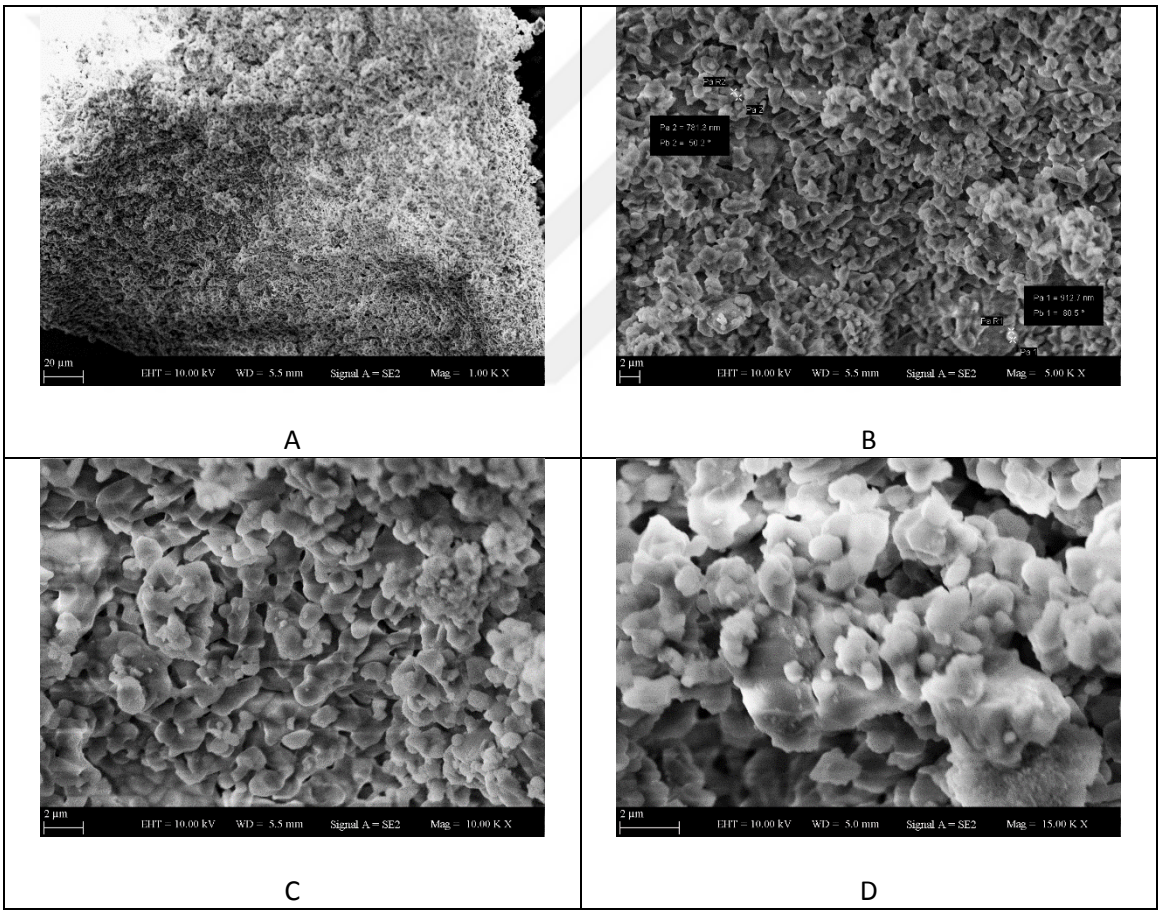

Figure A.24 SEM images of sintered samples produced from *Turritella terebra* at 1000 °C after soaking in SBF for a week A) 1000x B) 5000x C) 10000x D) 15000x

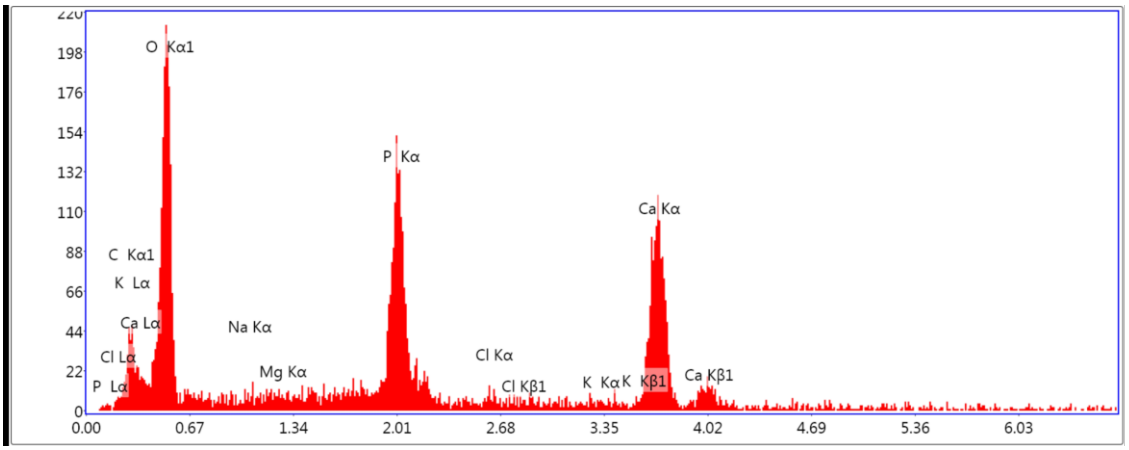

Figure A.25 EDX spectrum of sintered samples produced from *Turritella terebra* at 1000 °C after soaking in SBF for a week

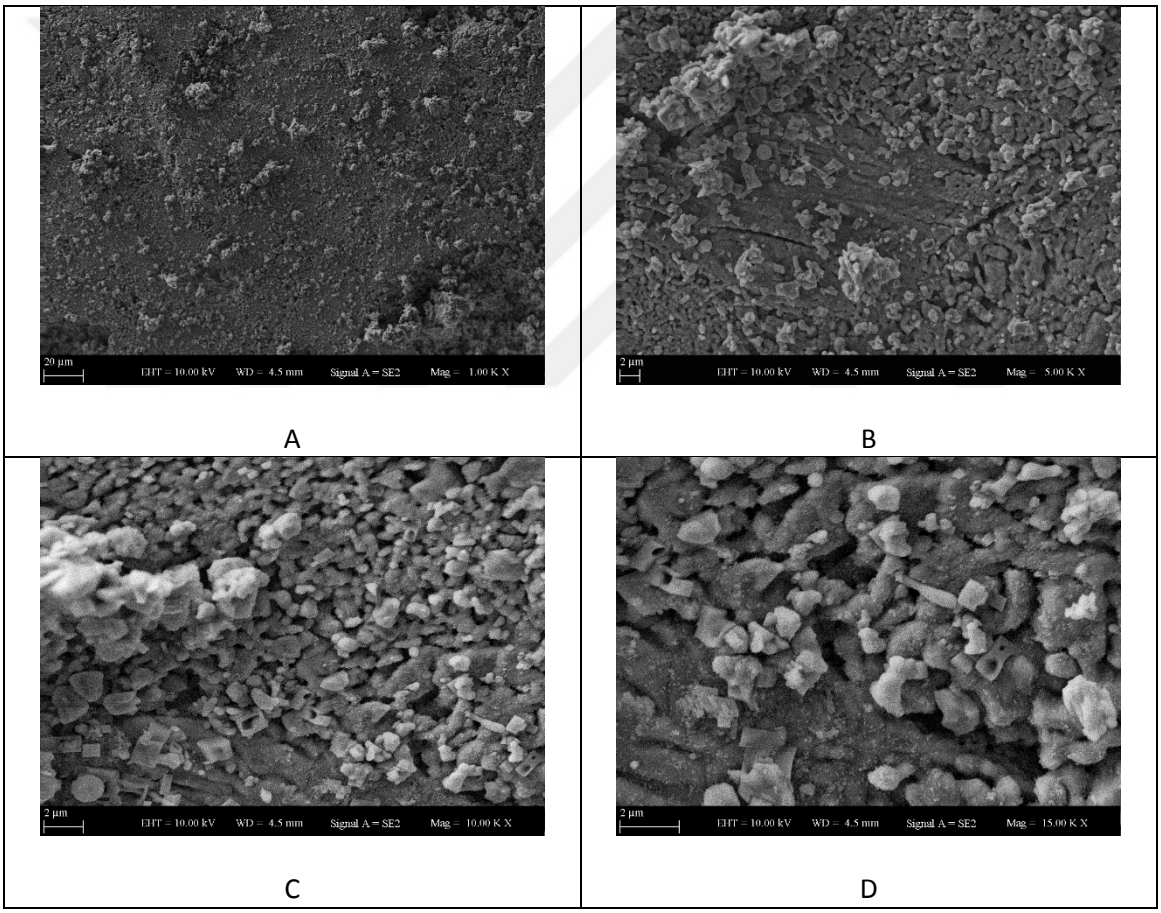

Figure A.26 SEM images of sintered samples produced from *Turritella terebra* at 1000 °C after soaking in SBF for two weeks A) 1000x B) 5000x C) 10000x D) 15000x

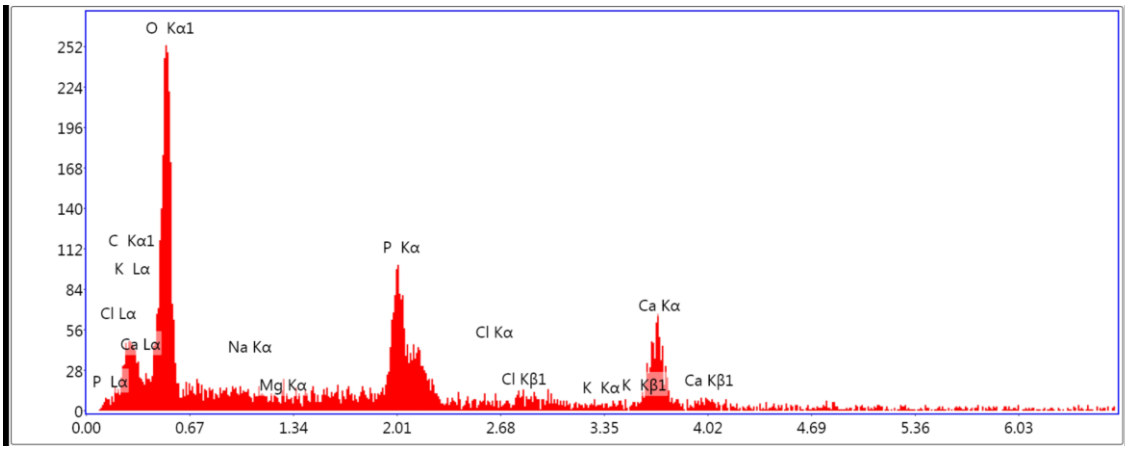

Figure A.27 EDX spectrum of sintered samples produced from *Turritella terebra* at 1000 °C after soaking in SBF for two weeks

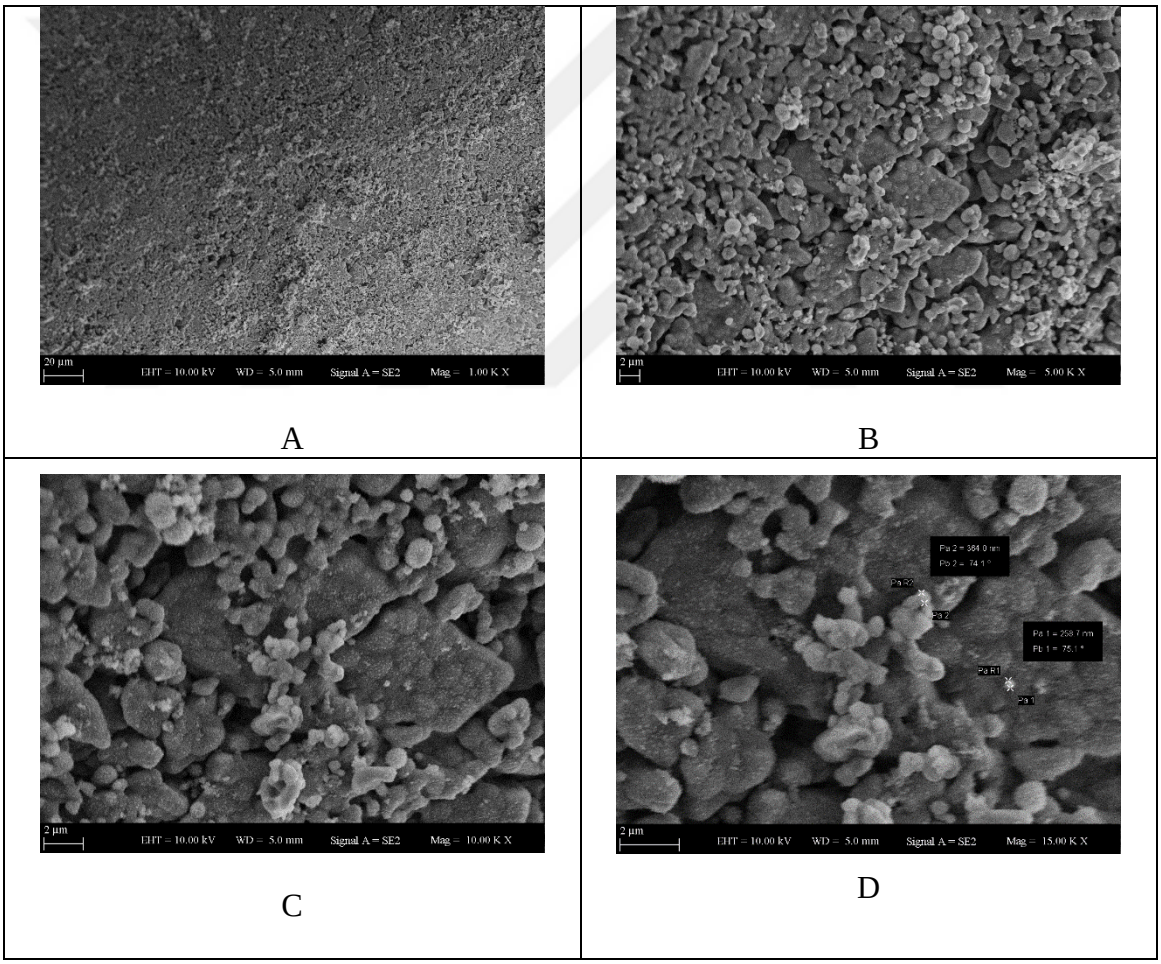

Figure A.28 SEM images of sintered samples produced from *Turritella terebra* at 1000 °C after soaking in SBF for three weeks A) 1000x B) 5000x C) 10000x D) 15000x

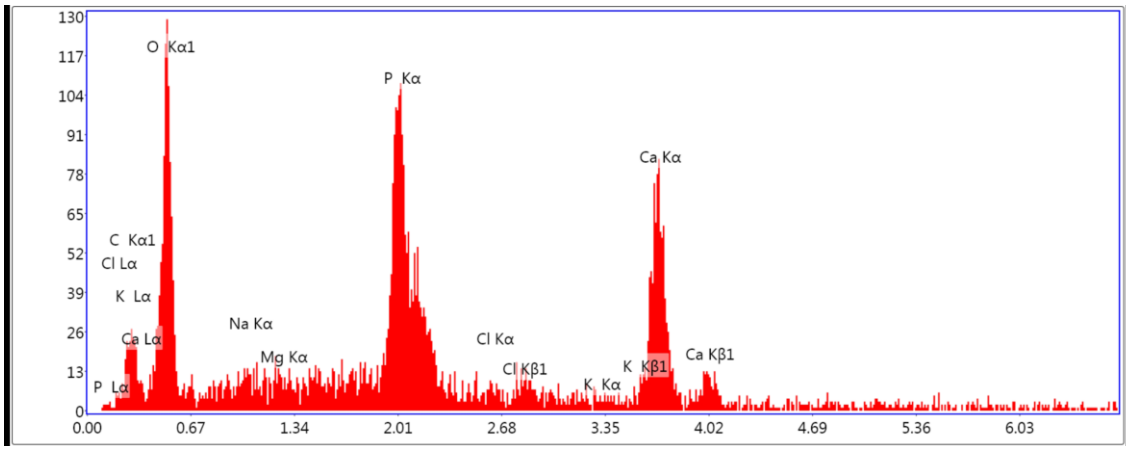

Figure A.29 EDX spectrum of sintered samples produced from *Turritella terebra* at 1000 °C after soaking in SBF for three weeks

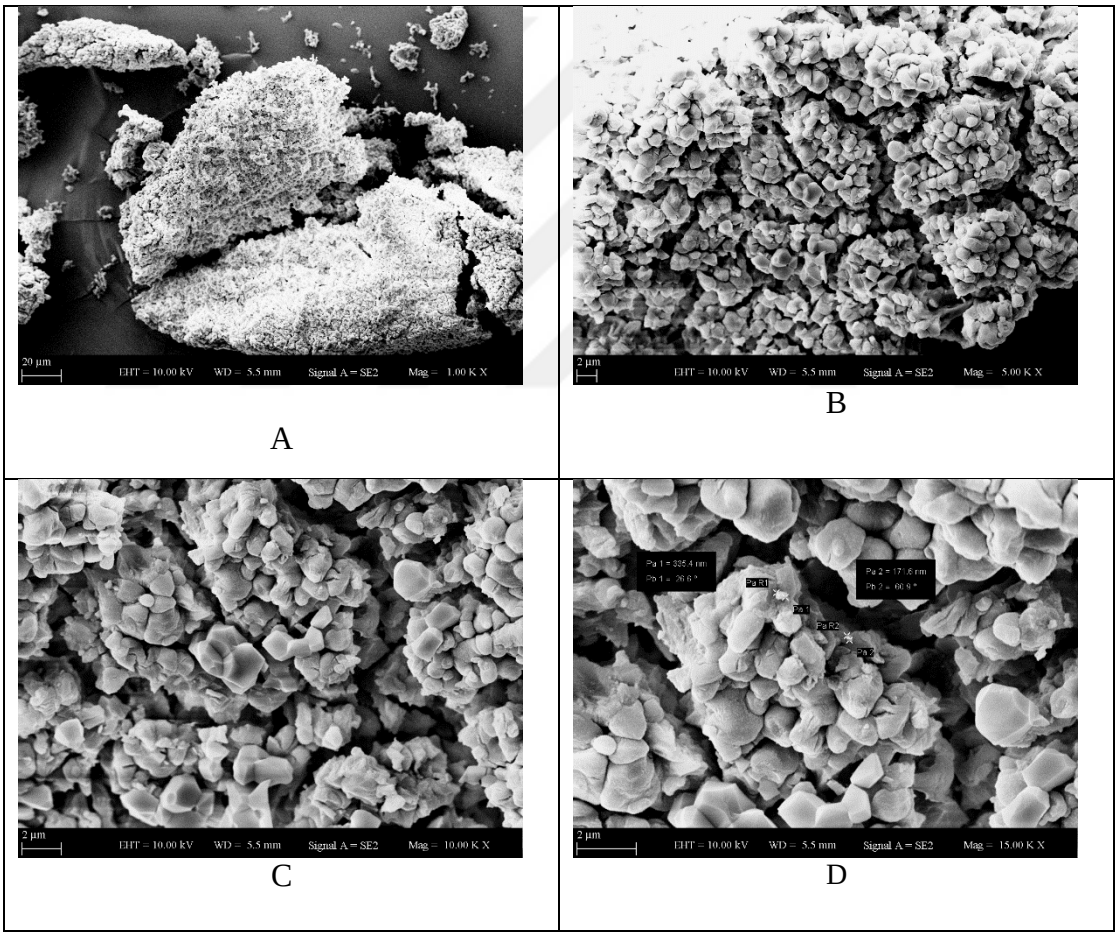

Figure A.30 SEM images of sintered samples produced from *Turritella terebra* at 1200 °C before soaking in SBF A) 1000x B) 5000x C) 10000x D) 15000x

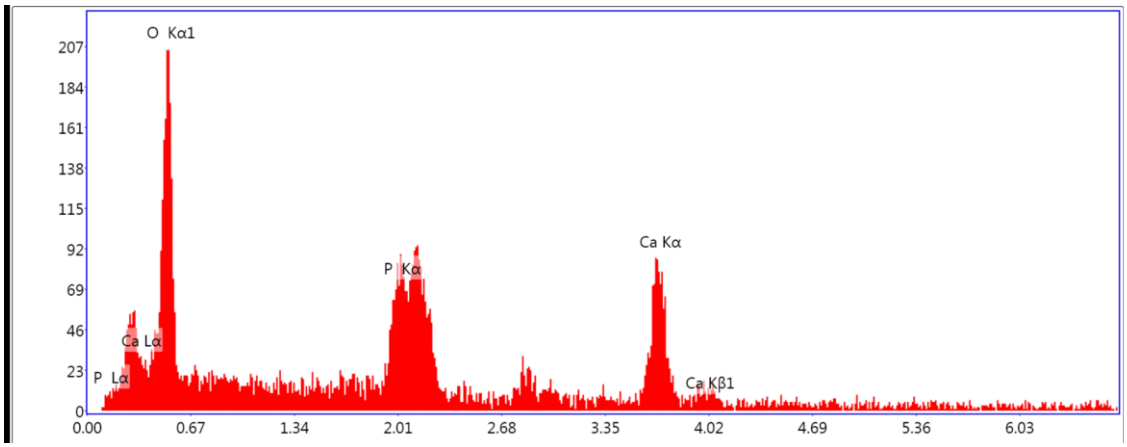

Figure A.31 EDX spectrum of sintered samples produced from *Turritella terebra* at 1200 °C before soaking in SBF

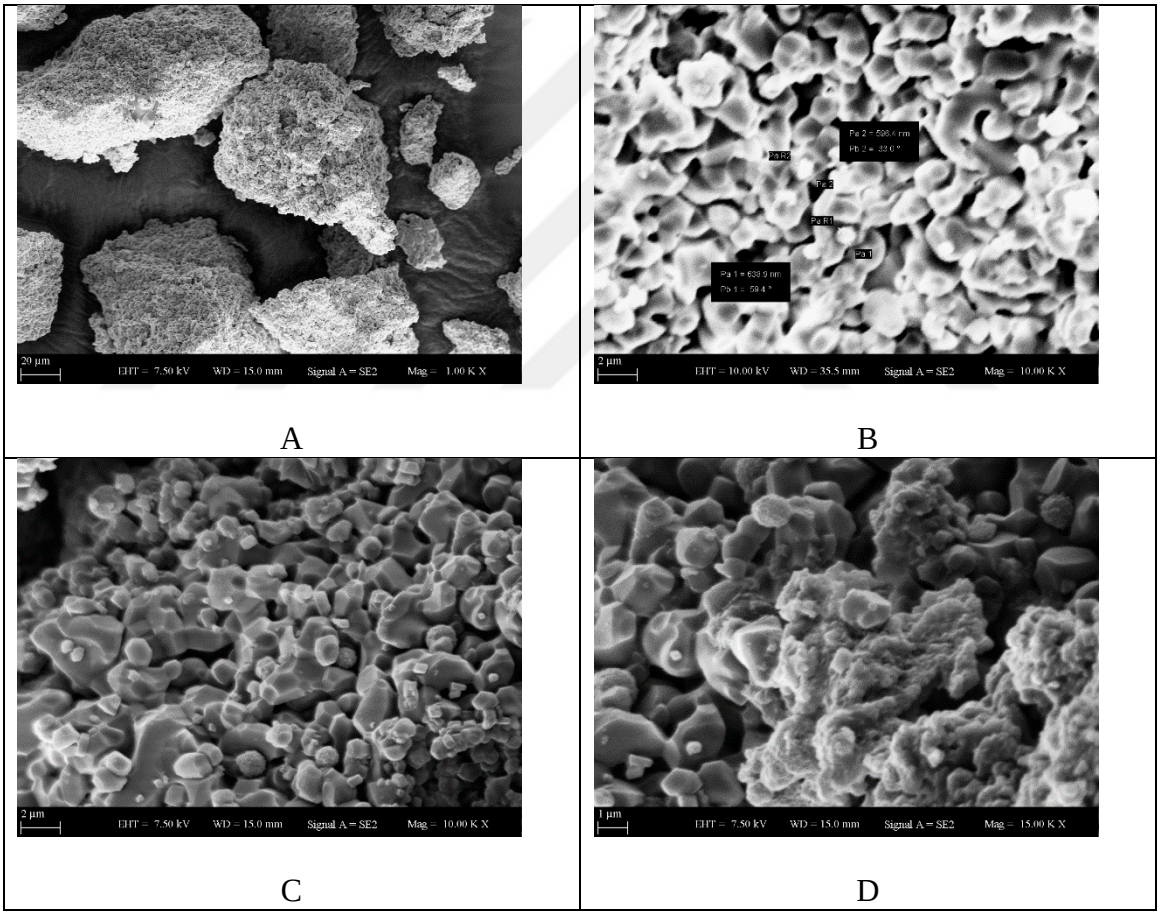

Figure A.32 SEM images of sintered samples produced from *Turritella terebra* at 1200 °C after soaking in SBF for a week A) 1000x B) 5000x C) 10000x D) 15000x

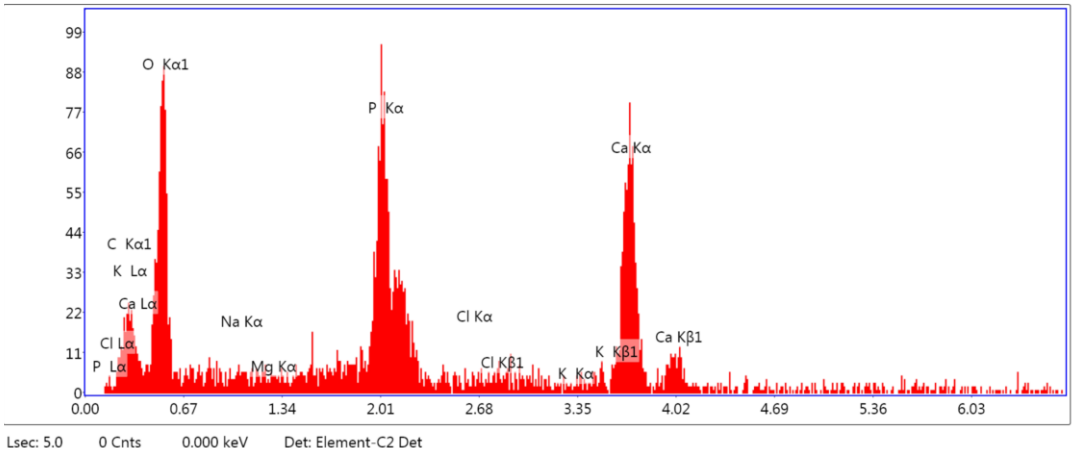

Figure A.33 EDX spectrum of sintered samples produced from *Turritella terebra* at 1200 °C after soaking in SBF for a week

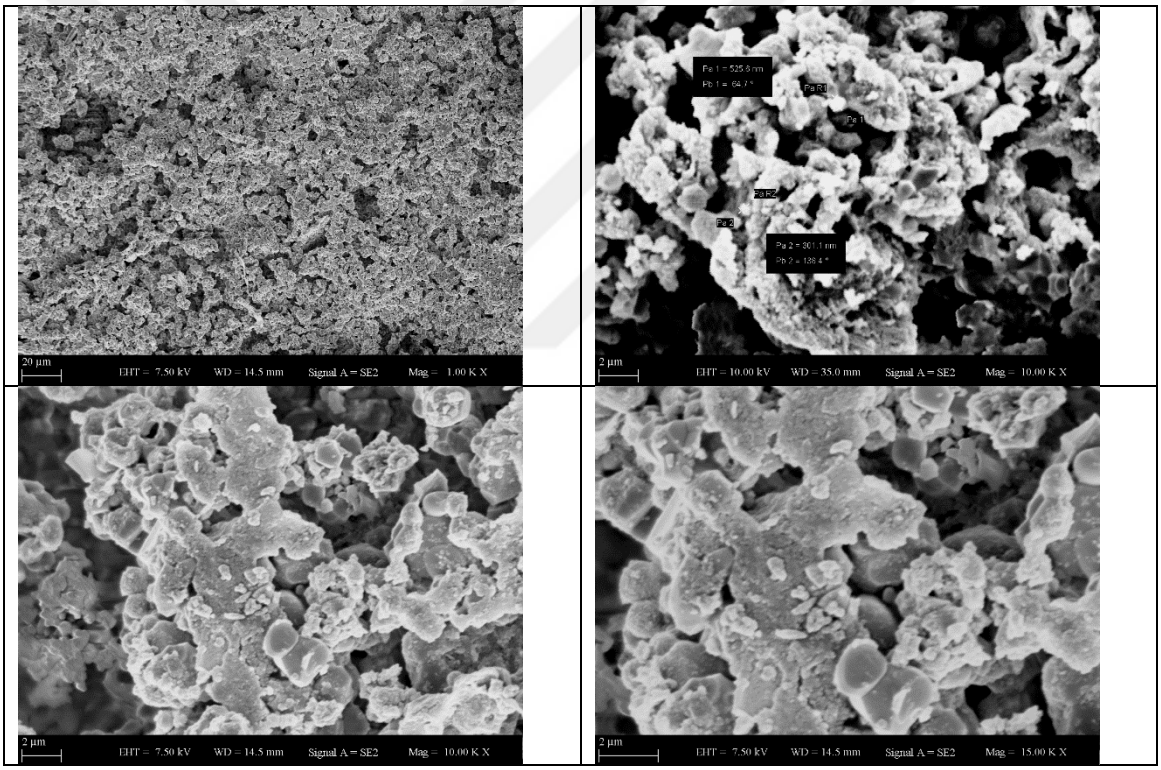

Figure A.34 SEM images of sintered samples produced from *Turritella terebra* at 1200 °C after soaking in SBF for two weeks A) 1000x B) 5000x C) 10000x D) 15000x

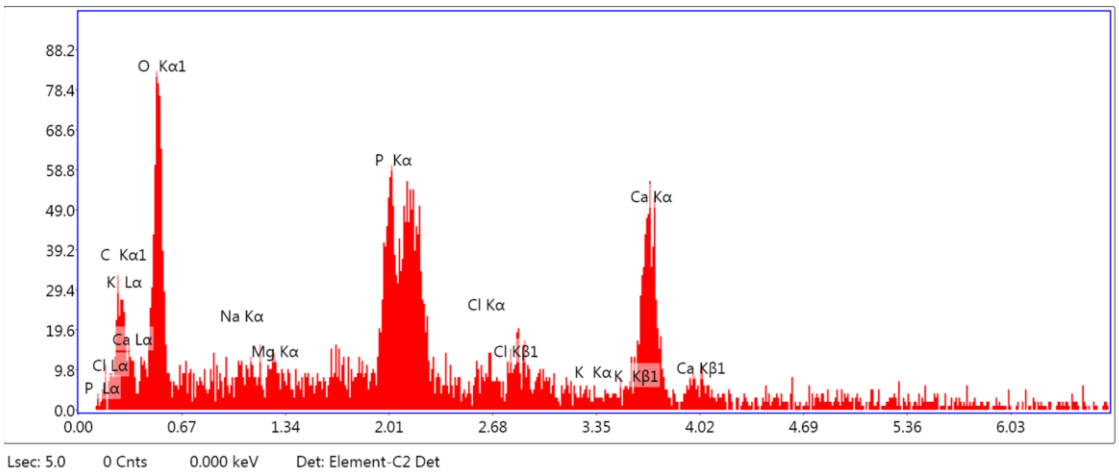

Figure A.35 EDX spectrum of sintered samples produced from *Turritella terebra* at 1200 °C after soaking in SBF for two weeks

CURRICULUM VITAE

PERSONAL INFORMATION

Name Surname : Zeynep ORMAN

Date of birth and place :12.09.1993, Bursa

Foreign Languages :English

E-mail :zeorman23@gmail.com

EDUCATION

Degree	**Department**	**University**	**Date of Graduation**
Master	Bioengineering	Yildiz Technical University	2017
Bachelor of Science	Chemical Engineering	Yildiz Technical University	2015
High School	Applied Science	Rafet Kahraman Anatolian High School	2011

PUBLISHMENTS

Conference Papers

1. Orman Z., Erden İ., Kılıçarslan F. A., Gürbüz O., (2016). "The Synthesis of D-π-A Derivate 4,5-Diazafluorenone for Dye-Sensitized Solar Cell, Investigation of Spectroscopic and Electrical Properties", 2nd International Conference on Organic Electronic Material Technologies (OEMT2016), Çanakkale.

2. Orman Z., Yucel S., Sahin Y. M., Gunduz O., Oktar F. N. (2017). "Production and Characterization of Bioceramic Powders of Biological Origin", 2nd Annual Conference and Expo on Biomaterials, Madrid.

Projects

1. Scholar at TUBITAK project 113z910